2005-08-01

A Simple Electronic Speckle Pattern Interferometry System using Holographic Optical Elements

Guntaka Tulasi Sridhar Reddy
Technological University Dublin

A simple electronic speckle pattern interferometry system using holographic optical elements

By

Guntaka Tulasi Sridhar Reddy

MSc (Tech)

A thesis submitted to the Dublin Institute of Technology for the degree of Doctor of Philosophy PhD

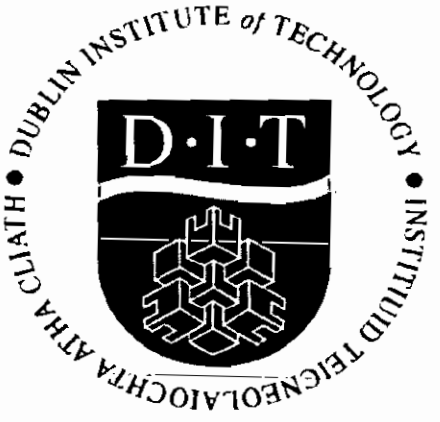

Supervisors: Dr Vincent Toal, Dr Suzanne Martin

Centre for Industrial & Engineering Optics

School of Physics

Dublin Institute of Technology

August 2005

Abstract

The aim of the work reported in this thesis is to develop a simple electronic speckle pattern interferometry (ESPI) system by combining holographic optical element technology with speckle interferometry. A holographic optical element is used in an ESPI system instead of the lenses, mirrors, beam splitters and beam combiners which are usually required in a conventional system. The final ESPI system consists only of a single holographic element, laser and CCD camera. Many currently available systems are complicated and consist of expensive optics that can be difficult to align. Even the simplest require several conventional optical elements to manipulate the laser light and provide the necessary object and reference beams. In this thesis holographic optical element technology is combined with speckle interferometry in order to make a simple, compact and low cost ESPI system. A compact ESPI system is built by incorporating a single holographic optical element, which generates a speckled reference beam and combines this with the object wavefront as it approaches the camera.

In addition, a dual interferometer was constructed with a facility to test an object using both ESPI and holographic interferometry. In this way the advantages of high quality interference fringes in holographic interferometry, speed and convenience of ESPI can be exploited. Firstly, the use of a self developing holographic recording material allowed live holographic interferometry to be carried out, and viewed with a CCD camera. It was then shown that the recorded hologram could be used, with no further adjustment, to provide a speckle reference beam to the camera, so that ESPI could be performed in the same optical set up. The out of plane deformation of the object was studied with the two techniques in one interferometer and results were presented. The self developing acrylamide based photopolymer used was a holographic

recording material formulated and prepared at the Centre for Industrial & Engineering Optics (IEO). Initially silver halide emulsions (including the HP series silver halide emulsions produced in the Central Laboratory for Optical Storage and Processing of Information, Bulgarian Academy of Sciences, Sofia, Bulgaria) were used to fabricate some of the holographic optical elements because they allowed the recording of reflection format HOEs essential to the compact final ESPI system design. However, as improved formulations of IEO's own photopolymer became available, reflection holographic optical elements were also recorded in the photopolymer.

Full field displacement maps of object deformations were obtained by implementing phase shifting techniques using a laser diode in which the drive current was modulated to produce a path length change by varying the wavelength.

The final compact ESPI system using a reflection holographic optical element was also used to study vibration mode patterns. Amplitude and phase of the modes were mapped using phase shifting techniques and the results are presented.

For the first time, reflection holographic optical elements recorded in acrylamide based photopolymer material were used in a single optical element interferometer. This system was also used to study the vibration mode pattern of the object.

Declaration

I certify that this thesis which I now submit for examination for the award of PhD, is entirely my own work and has not been taken from the work of others save and to the extent that such work has been cited and acknowledged within the text of my work.

This thesis was prepared according to the regulations for postgraduate studies by research of the Dublin Institute of Technology and has not been submitted in whole or in part for an award in any other Institute or University.

The Institute has permission to keep, or lend or to copy this thesis in whole or in part, on condition that any such use of the material or the thesis be duly acknowledged.

Signature GTSridharReddy Date 16/12/2005

Acknowledgements

There are a lot of people I have to thank for different reasons. Firstly I would like to thank my supervisor, Dr Vincent Toal, Head School of Physics. I haven't expected any better mentor than him. His guidance is an example to follow. His excellent knowledge of research work, continuous support and never failing optimism helped me a lot. I never forget the way he encourages and clarifies the technical questions.

My sincere thanks belong to Dr Suzanne Martin, Manager IEO for continuous support and encouragement.

I want to thank Dr Hugh Byrne for the help and suggestions he has provided to me.

I would like to thank staff & colleagues at IEO, Dr Emilia Mihaylova, Dr Izabela Naydenova, Dr Brian Bowe, Fiona Coyle, Michel O'Hora, Martin Somers, and Hosam Sherif for their help and suggestions.

It is my pleasure to thank Prof V. Sainov, Director, CLOSPI, Sofia for allowing me to work in their laboratory on a short term scientific mission (STSM, COST-P8). Also I would like to thank the staff and members of the group. I would like to sincerely acknowledge Joseph Keogh for the constant help and encouragement.

I will never forget the support I received from Mr and Mrs Raghavendra.

I would like to thank the School of Physics for giving me an opportunity to pursue the Doctoral Degree. FOCAS is greatly acknowledged for providing the excellent and state of the art research facilities.

Finally I would like to thank my family members for their ever green support.

I would like to say thanks to Vivek, Shiva, Varma, Sateesh and Ramesh.

Contents

List of Figures

Summary

In Chapter 1 the aim of the work is presented. An overview of different types of non-destructive evaluation techniques is presented. Both non-optical and optical techniques are described. Holographic interferometry (HI) and Electronic speckle pattern interferometry (ESPI) are discussed along with other optical techniques.

Chapter 2 introduces the basics of holography. In-line and off-axis holography are explained. Factors which affect the quality of the hologram are also discussed in detail. Types of holograms and their recording are explained.

Chapter 3 gives a comprehensive description of the different recording materials available for holographic applications. Photopolymer material holographic characteristics and physical properties are discussed because of this material's frequent use in the HI and Holographic Optical Element fabrication in the work reported here. Photochemical reactions which take place during hologram formation in the photopolymer are described.

Chapter 4 explains different types of interferometers. The interferometers described in this chapter are standard and well-known but are limited in use because they are limited to objects with optical quality surfaces and simple shapes.

In Chapter 5 holographic interferometry is introduced as a means of studying non-optical quality surfaces. An out-of-plane sensitive system was constructed and used to measure the radial strain of a thick poly vinyl chloride (PVC) pipe.

In Chapter 6 an ESPI system including a HOE recorded on photopolymer material is presented as an alternative to the HI approach. The main advantage is the fact that a new hologram is not needed each time a new set of measurements is taken. The possibility of using the same optical system for ESPI and HI is demonstrated. The PVC pipe which was tested using HI was again tested using the HOE based ESPI system. A phase shifting HOE based ESPI system using a near infra red laser diode is also demonstrated and results obtained from phase shifting are presented.

Chapter 7 describes the experimental work using reflection HOEs recorded in silver halide emulsions. A much simpler ESPI system was built using a reflection HOE. The system was used to measure the deformation of an object.

Chapter 8 explains the use of reflection HOEs recorded in photopolymer material. Vibration mode patterns of loud speaker obtained using the ESPI system are presented.

1. Introduction

1.1 Theme of work

The aim of the work reported in this thesis was to develop simple electronic speckle pattern interferometers incorporating holographic optical elements (HOEs). The performance of the final system should be the same as that of conventional electronic speckle pattern interferometers. A self developing photopolymer recording material formulated and produced at the Centre for Industrial & Engineering Optics was available for recording the HOEs. The self developing property makes it advantageous to use the material in live fringe holographic interferometry as well and an additional aim of this work was to exploit this in a dual system and compare the results.

The use of a reflection holographic optical element reduces the number of components to a minimum, and therefore was an important aim of the work. Reflection holograms were recorded first in silver halide and later in photopolymer. It was important to be able to use the HOEs at visible and near infra red wavelengths in order to facilitate quantitative analysis through the use of phase shifting. The project worked towards the ultimate aim of a HOE based system with the minimum optical components and a compact CCD camera, capable of providing quantitative results through digital phase shifting techniques, by modulating the current of a compact near infra red laser.

In this thesis two optical Non-Destructive Evaluation (NDE) techniques, holographic interferometry and ESPI are used.

NDE techniques deal with the inspection or testing of a material, component or assembly. NDE techniques can be divided into two categories; non-optical and optical techniques. Many of the non-optical techniques involve contact with the test specimen during the test, whereas the optical techniques do not involve contact with the test specimen.

1.2. Non-optical NDE techniques

The non-optical techniques are radiography, acoustic and magnetic techniques. Radiographic techniques use x-ray, gamma ray and neutron and proton radiation for testing. Acoustic techniques include ultrasonic testing and acoustic emission. Magnetic techniques include eddy current, flux leakage and magnetic particle inspection.

1.2.1 Radiography

Radiography [1] is one of the oldest NDE techniques. X-rays, gamma rays are widely used in radiography. A schematic of a radiographic imaging technique is shown in Figure 1.1.

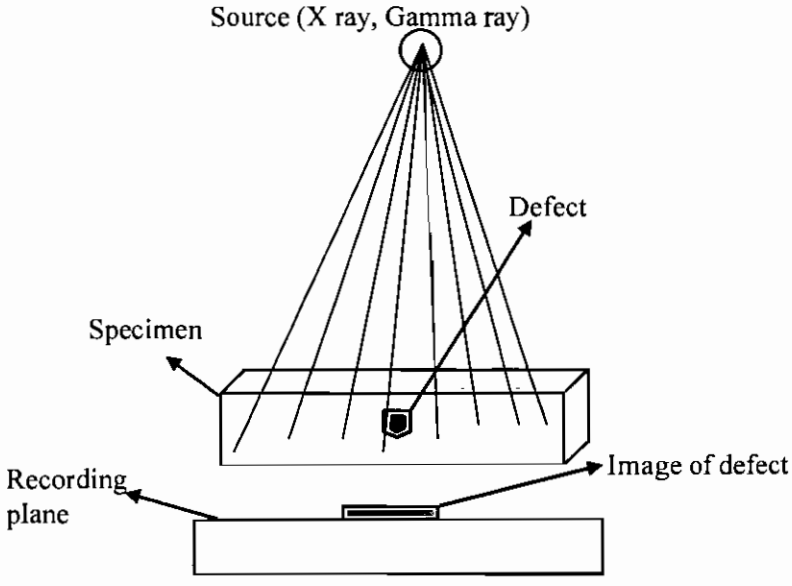

Figure 1.1 Radiographic imaging

1.2.1.1 X-Radiography

X-rays are high energy electromagnetic radiation that lies beyond the ultraviolet end of spectrum. Upon incident on a test specimen x-ray radiation is absorbed by the specimen. A differential absorbance is created due to the discontinuities in the specimen such as flaws and voids. A variation of the intensity distribution is created, which is imaged onto a photographic film held on the other side of the test specimen. The latent

image is formed on the film. The developed image reveals the defects in the specimen. Xeroradiography is an alternative technique in which the photographic film is replaced by a selenium-coated aluminium plate which is electrically charged, under dark-room conditions and placed in a light-tight cassette [2].

1.2.1.2 Gamma Radiography

Gamma ray radiographic technique is identical to x-ray radiography, except with a difference in the use of the radiation source. Gamma rays are produced by a radioactive source. Commonly used isotopes for gamma ray production are ^{60}Co, ^{137}Cs, and ^{192}Ir. Gamma rays with energies ranging from 0.54 MeV to 1.33 MeV can be produced, with corresponding penetration depths ranging from 13 to 230 mm in materials such as lead. Gamma ray production does not require an electrical resource and hence they can be well adapted for use in remote locations. It also has the advantage that it is rapid when compared with x-radiography. Disadvantages of gamma radiography include safety and heavy shielding requirements [3].

1.2.1.3 Neutron & Proton Radiography

Neutrons are used as the radiation source in neutron radiography. They are produced by nuclear reactors as a part of the fission process or by nuclear generators such as cyclotrons. The radiographic shadow image of the test specimen is produced in a way similar to x-ray and gamma ray radiography. Materials such as oils, plastics and heavy metals such as tungsten and lead, which are practically opaque to x-rays or gamma rays, can be tested using neutron radiography. The major difference between x-radiography and neutron radiography is that the attenuation coefficients for x-rays increases approximately with increasing atomic number, whereas for neutrons the attenuation coefficients vary randomly with atomic number. As a result of this feature it is possible to detect the presence of low density materials [4]. Neutron radiography is a

complimentary technique to x-radiography but not a rival [5, 6]. Radiography can also be carried out using protons (monoenergetic positively charged fundamental particles). Some sources of proton radiation include frequency-modulated cyclotrons and radio isotopes sources such as ^{210}Po. The total amount of radiation to produce a proton radiograph is less than that required to produce an X radiograph. Proton radiography has higher resolution than x-radiography; this is due to the high signal to noise ratio offered by the protons [7].

Radiographic techniques are used to measure the thickness of a material ranging from a few millimeters to centimeters. Objects with complex shapes can be tested. Real time viewing of radiographic images is possible with a large number of viewing angles. These techniques have some disadvantages: access to both sides of the test object is always required and they are expensive to use and hazardous to health.

1.2.2 Acoustic techniques

Acoustic NDE techniques include Ultrasonic and Acoustic emission testing.

1.2.2.1 Ultrasonic testing

Ultrasonic technology [3, 8, 9] is widely used and more associated with NDE. The applications of ultrasonic technology have received significant attention for research and development. Ultrasonic waves are vibrational waves with frequencies ranging from 100 kHz to 2 MHz. The waves are generated using a piezoelectric transducer. The ultrasonic pulse generated from a transducer is coupled to the test object either by a physical contact or through a column or layer of liquid. The waves travel through the test object and are reflected, refracted or diffracted by the discontinuities or interfaces. A separate receiving transducer is used to detect the echo signal coming from the discontinuity. The size and position of the defect or discontinuity are estimated with considerable accuracy by measuring the velocity of the returned signal and the elapsed

time between the transmitted and received signals. The choice of ultrasonic frequency is determined by the resolution required and the type of test specimen. Higher frequencies enable a more detailed examination of the test object with greater resolution, but scattering and attenuation effects will increase.

The advantages of using ultrasonic NDE techniques are: internal discontinuities in opaque materials are visually presented, detailed information about the flaw size, orientation and location within an object is obtained, operational costs are low and flaws in metallic and non-metallic materials are detected. Internal thermal and stress patterns can also be detected and imaged.

This technique has the following disadvantages: Flaw imaging equipment is expensive and complex. Inspection of complex shapes is impractical. 360° access to the test sample is not always possible.

1.2.2.2 Acoustic Emission

Many materials when subjected to stress will emit acoustic waves. Acoustic wave emission (AE) is also called stress wave emission [10]. Stress waves are generated due to the rapid release of energy from localized sources within the material. If the material contains defects, cracks might occur at the heavily stressed spots. Analyzing the emitted signal gives information about the defect in the test specimen. The signals can be analyzed in various ways; spectral analysis of each pulse, counting the number of pulses and rate of the emission of the pulses. The best example of AE is an earthquake, which happens due to the generation of stress waves from the inner layers of the earth's crust. AE technique is a passive technique and it does not require an excitation signal for detection. It is a method of detecting the occurrence of defect growth rather than detecting for the presence of defects in a sample [11]. Typical areas of application of AE techniques are: the process control industry, structural integrity assessments of

engineering structures, detection of corrosion attack on metals [12] and leak testing of the underground gas pipelines.

AE techniques have the following advantages: the signal emitted by a defect in the material provides a path to the monitoring sensor and testing in hostile environments is possible by means of remote monitoring. AE technique has the following disadvantages: it will not measure the size of the defect or crack. Identification of the signal when testing complex shapes is difficult due to multiple travel paths from the source and quantitative analysis of the defect or crack has to be done by some other NDE technique.

1.2.3 Magnetic methods

Magnetic methods of NDE include eddy current testing, magnetic flux leakage and magnetic particle inspection.

1.2.3.1 Eddy current testing

If a coil carrying an alternating current is brought close to the surface of an electrically conducting surface, an eddy current will be induced in the specimen [13]. The current generated is proportional to the electrical conductivity of the material. The eddy currents flowing in the test specimen induce electromotive force (emf) in the coil. The phase and amplitude of the induced emf are related to the characteristics of the test specimen and to the presence or absence of defects in it. The defects are analyzed using the phase and amplitude of the emf.

Typical applications of eddy current inspection are summarized below in Table 1.1

Table 1.1 Applications of eddy current technique

Thickness measurement	Flaw detection	Material property determination	Flow or position measurement
• Sheet metal • Paints • Thin insulation • Rocket motor linings	• Foil, wire • Tube testing • Bolt hole inspection • Weld inspection	• Heat treatment evaluation • Fire damage estimation • Impurity content determination • Hardness measurement	• Small motion • Flow of liquid in pipe • Liquid level monitoring in tanks

The characteristics of the eddy current techniques make them the right choice for many inspection tasks in NDE. There is no need for a mechanical contact with the test specimen. Eddy current penetration depth, the inspection depth, is controlled by the frequency of the energizing current. Its sensitivity is high for small discontinuities.

The drawbacks associated with eddy current testing are: testing is limited to electrically conductive materials, material and instrumentation parameters affecting the eddy current flow complicate the interpretation of the test results, increase of inspection signal frequency decreases the penetration depth.

1.2.3.2 Magnetic flux leakage

If a magnetic field is applied to a ferromagnetic specimen, magnetic flux develops permanently within the material. The presence of a defect on the surface of a material distorts the magnetic field. Magnetic flux leakage [13] occurs around the defect. The leakage field is measured by placing a detector near the surface of the test object. The magnetic field can be applied to the material by the use of a permanent magnet, or electro magnet, or by passing a large electric current through the specimen. The limitations of the technique are that it is only applicable to test ferromagnetic materials and testing of objects with irregular shapes is not possible.

1.2.3.3 Magnetic particle inspection (MPI)

Magnetic particle inspection techniques are one of the oldest and most widely used magnetic techniques in NDE [2]. If the surface of a magnetized specimen is covered with very fine iron powder, the iron particles are attracted towards the region where the magnetic field emerging from the surface is strongest. The particles will build up at the vicinity of a crack on the test surface. The particles are seen with the eye. It is only possible to get information about the length of the crack but not the depth of the crack; for this reason it is used only for rapid detection of cracks.

The limitations of the technique are that detection is limited to ferromagnetic materials and only cracks located on the surface of a material are detected.

1.3 Optical techniques

Optical inspection techniques have a reputation for extreme precision, and they generate the results pictorially. Most of the optical techniques used for NDE use the phenomenon of interference. The experiments of Thomas Young [14] first illustrated the phenomenon of interference and the wave nature of light. Interference is defined as the distribution of the intensity variation when two or more light waves emitted from the same source are combined [14]. The resultant amplitude is the algebraic sum of the amplitudes of the individual waves. The variation in intensity appears as a pattern of bright and dark regions, called interference fringes. Michelson used this phenomenon for optical measurements in the Michelson interferometer [14]. It is the most widely known optical interferometer used for applications such as measurement of distance with a precision of the order of the wavelength of light, measuring the wavelength of spectral lines and measuring the optical thickness of transparent objects.

Optical techniques such as holographic interferometry, electronic speckle pattern interferometry, electronic speckle shear interferometry, moiré techniques and

photoelasticity are important techniques useful for non-destructive evaluation. Holographic and electronic speckle pattern interferometry work using the phenomenon of interference.

1.3.1 Holographic interferometry

Holography was invented by Gabor [15]. It is the technique of recording both phase and amplitude of the light waves scattered from the object, on a photosensitive medium. Recording the phase information of the object wavefront preserves the 3 dimensionality of the final image. The holographic recording on a photosensitive medium is due to the interference between the light waves scattered from the object and a reference wave. A schematic of hologram recording and reconstruction is shown in Figure 1.2. Laser light is split into two beams using a beam splitter. One beam falls onto the photosensitive medium and second beam falls on the object. The light waves scattered from the object (object beam) are incident on the photosensitive medium. Interference occurs between the object and reference beams at the photosensitive medium. The photosensitive medium used to record holograms must have a high resolution because it has to resolve the finely spaced interference fringes formed between the object and reference waves. During reconstruction a developed hologram is illuminated with the reference beam. The reference beam regenerates the object wavefront through diffraction by the hologram. The reconstructed wavefront resembles exactly the original object wavefront. Thus a 3 dimensional image of the object can be seen.

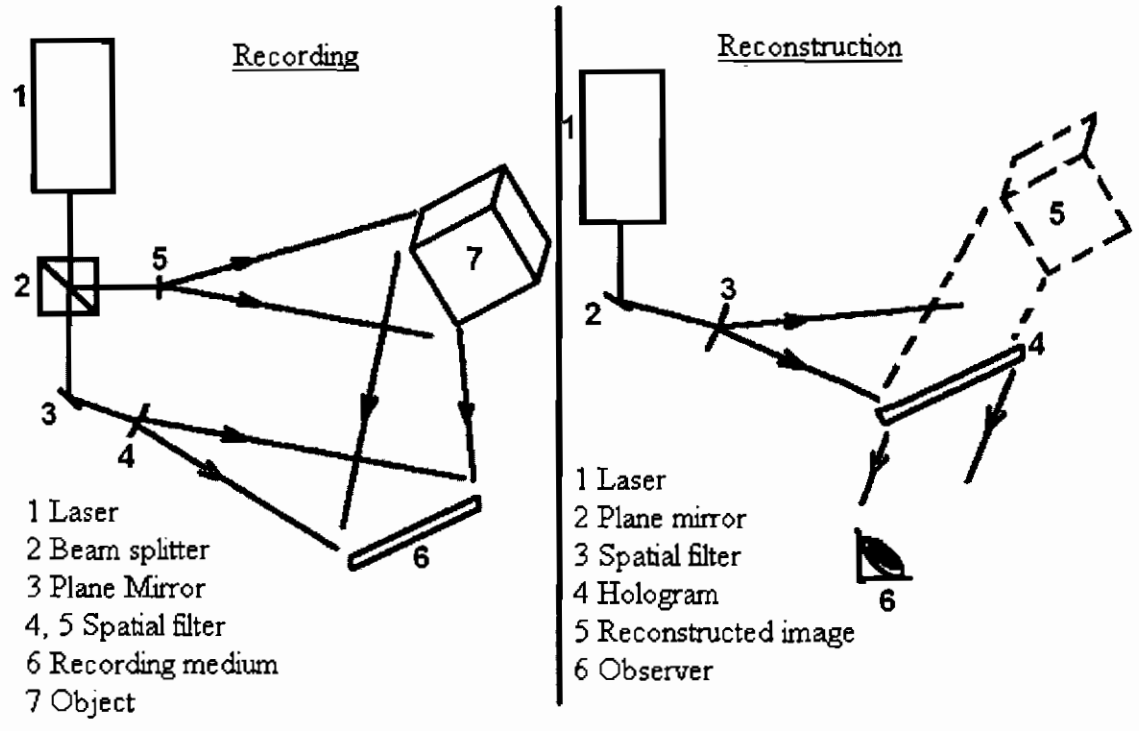

Figure 1.2 Hologram recording & reconstruction

Generating an exact replica of an object wavefront is a useful phenomenon in non-destructive evaluation. This is used in holographic interferometry [16]. In holographic interferometry two holograms of an object in its undisplaced and displaced state are recorded. The composite record is called a holographic interferogram. When the interferogram is illuminated with the reference beam, two object wavefronts are reproduced and interfere with each other resulting in interference fringes whose characteristics are determined by the displacement of the object.

1.3.2 Electronic speckle pattern interferometry

1.3.2.1 Speckle formation

Electronic speckle pattern interferometry (ESPI) is an optical measurement technique [17]. It utilizes the speckle effect. When a rough surface is illuminated with laser light, the speckle is formed interferometrically by the combination of light amplitude vectors from a large number of scattering centers on the surface. The speckle

effect is observed only when the surface roughness is of the order of, or greater than, the wavelength of illuminating light. The speckle effect is not observed when the surface is illuminated with normal white light source due to the lack of coherence. Objective and subjective speckle are two types of speckle.

Objective speckle

When a rough surface is illuminated over an area of cross section D with a laser light, a speckle pattern is observed on a screen S at a distance Z from the object (Figure 1.3).

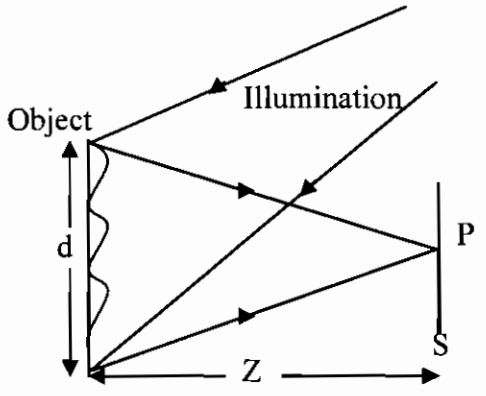

Figure 1.3 Formation of objective speckle

An arbitrary point on the screen S receives light from all the points on the scattering surface. The speckle pattern at a point P is the superposition of the light amplitude vectors from all points on the scatter surface. From the Young's double slit experiment, [17] any two points separated by a distance "d" will give rise to fringes with frequency $f = \frac{d}{\lambda z}$. The fringes with highest spatial frequency will be formed by the two edge points on the scatter surface, for those points spatial frequency f_{max} is given by [17]

$$f_{max} = \frac{d}{\lambda Z} \quad \text{.....1.1}$$

The period of this fringe pattern is a measure of smallest objective speckle size [18]. The size of the speckle is therefore given by the reciprocal of spatial frequency of the fringe pattern given in equation 1.1 and which is given by

$$\sigma = \frac{\lambda Z}{d} \quad \text{.....1.2}$$

From the above equation it is clear that the size of the speckles observed in the light scattered by a rough surface at a given distance from the surface increases, as the area illuminated decreases. This type of speckle is called objective speckle because the size of speckle depends only on size of the illuminated area and the distance at which the speckles are detected.

Subjective speckle

When the speckle pattern is imaged onto the screen using a lens then the speckle is called subjective speckle. The size of the subjective speckle calculation is similar to that of the objective speckle, except that the cross section of the illuminated area is replaced by the diameter of the imaging lens aperture to image the speckle onto the screen (Figure 1.4).

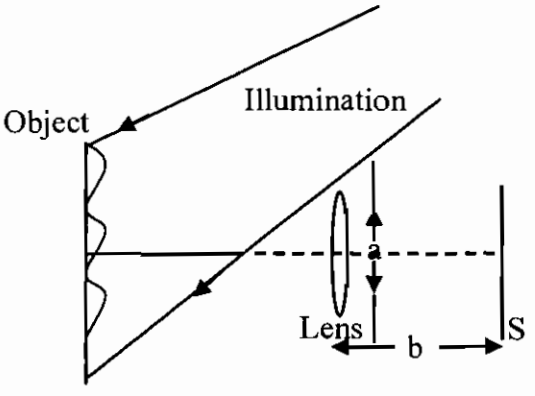

Figure 1.4 Subjective speckle

The size of the subjective speckle is given by [18]

$$\sigma_s = \frac{2.44\lambda b}{a} \quad \text{.....1.3}$$

where b = image distance, a = aperture size, λ = wavelength of light source

The phenomenon of speckle was used in an ESPI system [19]. In ESPI a CCD camera is used as the photosensitive medium. This eliminates the cumbersome photographic processing required in holographic interferometry. This method of acquiring data electronically allows the development of versatile systems useful for industrial applications. The resolution of the CCD camera need not be very high because it only has to resolve the speckles of the order of 5 to 10 μm in size. The speckle size is controlled by adjusting the aperture of the camera lens. The advantages of no chemical processing and therefore no requirement for repositioning accuracy allow ESPI to surpass holographic interferometry. ESPI is also known as TV holography, digital holography, and electronic holography. A schematic of an ESPI system sensitive to out of plane displacement is shown in Figure 1.5.

The object is illuminated with laser light at angle θ to the surface normal. The speckled scattered light from the object surface is imaged with the CCD camera. In smooth reference beam ESPI, to minimize the camera resolution requirement, the reference beam is made to diverge from the centre of the aperture stop of the camera lens. Object and reference beams are superimposed at the focal plane of the CCD camera.

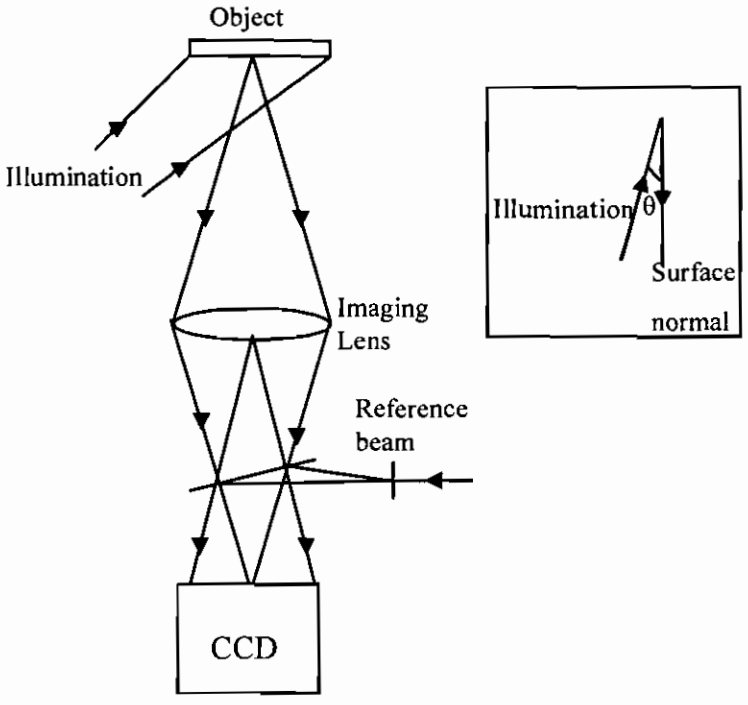

Figure 1.5 Out-of-plane sensitive ESPI system using a smooth reference beam.

Video signal subtraction or addition is used to produce the fringes in electronic speckle pattern interferometry [20]. In video signal subtraction the speckle interference between a reference beam and a beam from the object in its un-displaced position, is stored electronically. The object is displaced and the new speckle interference video signal detected by the camera is subtracted continuously from the stored interference pattern. The resulting signal is high pass filtered, full wave rectified and displayed on the computer monitor. In the addition method the speckle fields corresponding to the object in two different states are added; the resultant signal is high pass filtered and rectified as in the subtraction process. Video signal subtraction is the most widely used technique in ESPI.

Applications of ESPI technique include deformation and displacement visualization, amplitude and phase measurement of the vibration modes of objects [21, 22, 23], contouring inspection of objects [24, 25], measurement of strain distributions

[26], defect detection in materials [27, 28] and flaw detection in fibre composite materials [29].

1.3.3 Electronic speckle pattern shearing interferometry

Electronic speckle pattern shearing interferometry [20, 30] is designed to measure the spatial derivatives of surface displacements of objects due to the deformation. The principles of the technique are similar to electronic speckle pattern interferometry, except that the two interfering speckle patterns originate from the same object and are sheared with respect to each other. The shear between the interfering beams is produced by a shearing device in the imaging system. The two sheared images of the object are imaged using a CCD camera, which is connected to a computer with a frame grabber. Shearography is less susceptible to environmental and mechanical perturbations than ESPI because it is a near common-path system. The Michelson type of shear interferometer is the most common set up. Figure 1.6 shows a schematic of an electronic speckle pattern shearing interferometer.

The interferometer consists of two plane mirrors and a beam splitter in a Michelson interferometer configuration. The object is illuminated using a collimated beam of light making an angle θ with the object surface normal. Light scattered by the object surface is imaged with the CCD camera. A single image of the object is seen if the two mirrors are exactly orthogonal to each other. A tilt of one of the mirrors in the interferometer produces two sheared images of the object. The amount of shear can be varied by the tilt angle. Each pixel on the CCD sensor receives light from two points on the object surface; they combine and generate a speckle interference pattern. The shearing of the speckle pattern makes the combined speckle pattern sensitive to the phase change across it. The fringe pattern is obtained either by video signal subtraction or addition, in a way similar to electronic speckle pattern interferometry. The intensity

distribution of fringe pattern gives the derivative of the surface displacement. A shear in the interferometer can be introduced by several other methods such as a glass wedge or two inclined flat glass plates placed closed to the aperture of the imaging lens.

The shear interferometric technique is less sensitive to mechanical perturbations. It is relatively insensitive to whole body motions and only sensitive to the differential movements of the surface.

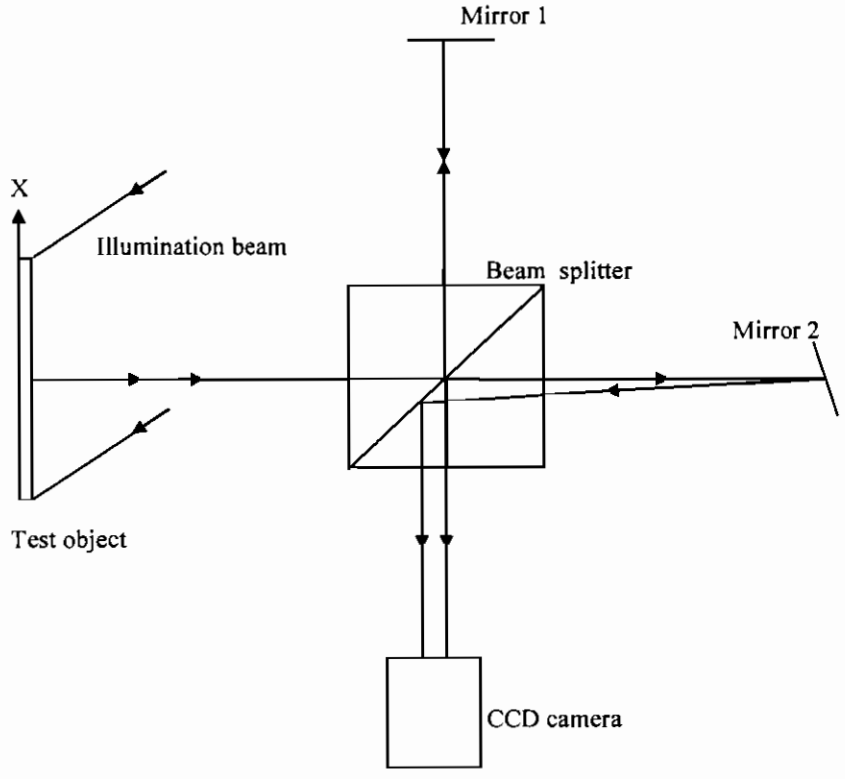

Figure 1.6 Electronic speckle pattern shearing interferometer

Applications of shearography include interfacial debonds detection in composite structures [31], thermomechanical strain of electronic devices [32], crack detection [28] and thermal deformations [33].

1.3.4 Moiré techniques

Moiré techniques are used for non destructive metrological measurements. Moiré fringes are formed when two gratings of nearly the same period are in contact with each other with a small angle between the grating lines. A fringe pattern of much

lower frequency than the individual grating frequencies is formed. A moiré fringe pattern can be formed by gratings of different types such as linear, circular, radial, and circular zone plates.

The transmittance of a sinusoidal grating of constant frequency is given by

$$t_1(x,y) = a + a\cos\left(\frac{2\pi}{p}x\right) \quad \text{.....1.4}$$

p is the grating period, 1/p = spatial frequency, a = amplitude transmittance of the grating

A grating can be phase modulated and the transmittance of the grating given by equation 1.4 can be rewritten by including the phase modulation function

$$t_2(x,y) = a + a\cos\left(\frac{2\pi x}{p(x)}\right) \quad \text{.....1.5}$$

p(x) = new spatial period

$$\phi = \text{phase} = 2\pi\left(\frac{x}{p} + \psi(x)\right)$$

$$\psi(x) = \text{modulation function} = \frac{u(x)}{p},\ u(x) = \text{object displacement}$$

If two gratings are laid in contact the resulting transmittance t(x, y) is the product of individual transmittances t_1 and t_2.

$$t(x,y) = t_1.t_2$$
$$= a^2[1 + \cos\frac{2\pi}{p}x + \cos 2\pi(\frac{x}{p} + \psi(x)) + \frac{1}{2}\cos 2\pi(2\frac{x}{p} + \psi(x)) + \frac{1}{2}\cos 2\pi\psi(x)] \quad \text{.....1.6}$$

The first three terms in equation 1.6 represent the original gratings. The fourth term is the second grating with double the frequency. The fifth term contains the modulation function only and this represents the moiré fringe pattern.

A bright fringe will result whenever $\psi(x) = n$ for n = 0, 1, 2

A dark fringe will result whenever $\psi(x) = n + \frac{1}{2}$ for n = 0, 1, 2

Shadow moiré

Shadow moiré and projection moiré are two well known techniques [34]. In shadow moiré technique a reference grating is located close to the test surface and the grating is illuminated obliquely. Fringes are formed due to the interaction of the reference grating with its shadow. A schematic of the shadow moiré is shown in Figure 1.7.

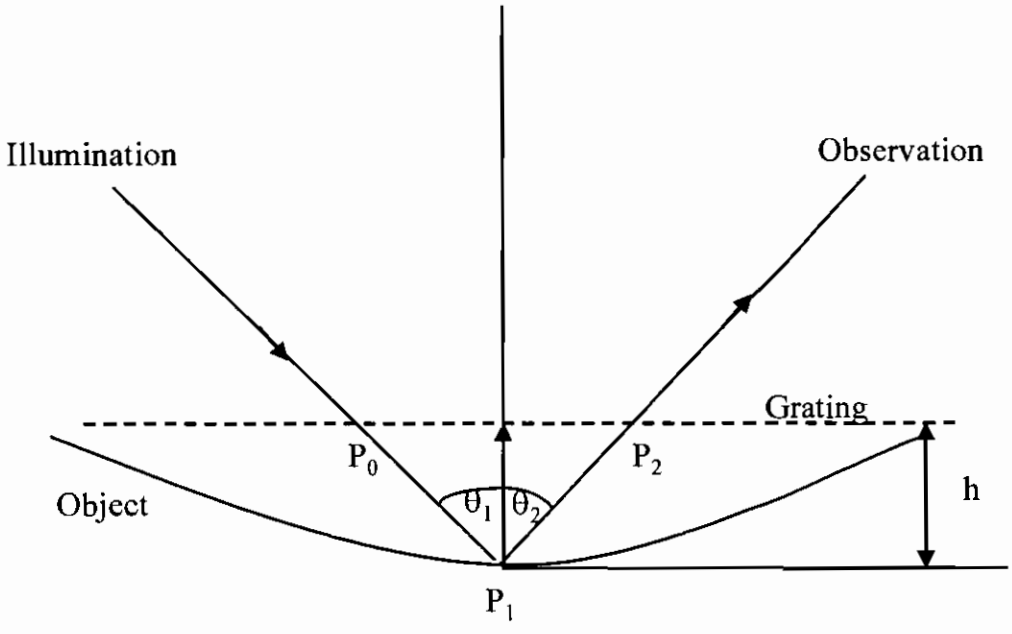

Figure 1.7 Schematic of shadow moiré

The grating is illuminated at an angle of incidence θ_1 and viewed at an angle θ_2. A point P_0 on the grating is projected to a point P_1 onto the object. While viewing, the point P_1 is projected onto P_2 on the grating. This projection is equivalent to a displacement of the grating relative to its shadow. The displacement is given by

$$u = h(x,y)(\tan\theta_1 + \tan\theta_2) \quad \text{.....1.7}$$

h(x, y) = height difference between the grating and a point P_1 on the object surface

θ_1 = angle of incidence, θ_2 = viewing angle

The phase modulation function is given by $\psi(x) = \frac{h(x,y)}{p}(\tan\theta_1 + \tan\theta_2)$ 1.8

where p is the grating period.

A bright fringe is observed whenever $\psi(x) = n$ for $n = 0,\pm1,\pm2$

and $h(x,y) = \dfrac{np}{(\tan\theta_1 + \tan\theta_2)}$

A dark fringe occurs where $h(x,y) = \dfrac{(n+\frac{1}{2})p}{(\tan\theta_1 + \tan\theta_2)}$ 1.9

This technique can be employed to determine the absolute shape or to monitor any changes in the shape of the diffusely reflecting surface. It is a relatively simple and inexpensive technique.

Projection moiré

In projection moiré, fringes are projected on a test object surface by means of interference between two plane waves. The fringe pattern can be produced using the Michelson interferometer. A schematic of projection moiré is shown in Figure 1.8

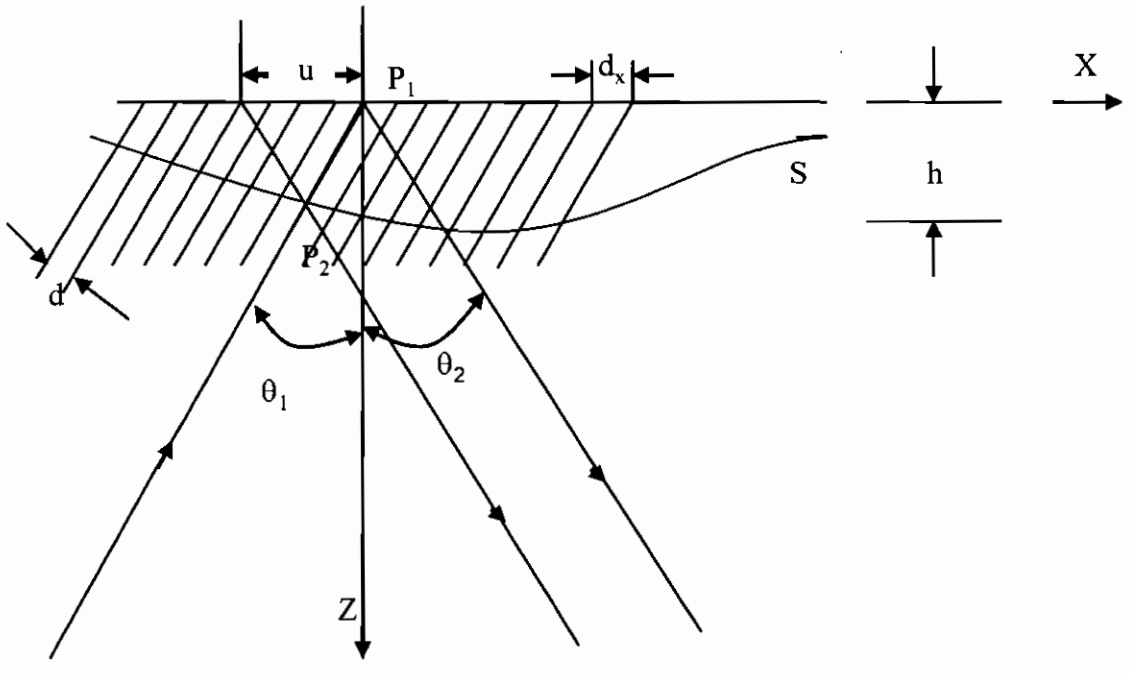

Figure 1.8 Schematic of projection moiré

Two plane waves with an interbeam angle α are projected onto the x-y plane at angle θ_1 to Z axis. Fringe spacing is given by

$$d = \frac{\lambda}{2\sin\left(\frac{\alpha}{2}\right)} \quad \text{.....1.10}$$

Fringe period along X axis is

$$p_x = \frac{d}{\cos\theta_1} \quad \text{.....1.11}$$

λ = wavelength of light source, α = interbeam angle between two plane waves. S is the surface to be contoured (Figure 1.8). A fringe originally placed at P_1 will be displaced to point P_2 onto the surface S which is to be contoured. Displacement of the fringe is given by

$$u = h(\tan\theta_1 + \tan\theta_2) \quad \text{.....1.12}$$

h = depth of the surface from the x-y plane

θ_1 = angle of incidence, θ_2 = viewing angle

The phase modulation function is given by

$$\psi(x) = \frac{u}{p_x} = \frac{h(\tan\theta_1 + \tan\theta_2)}{d/\cos\theta_1} = \frac{h}{d}(\sin\theta_1 + \cos\theta_1 \tan\theta_2) \quad \text{.....1.13}$$

A bright fringe is observed whenever $\psi(x) = n$ for $n = 0,\pm1,\pm2$

$$h(x,y) = \frac{nd}{(\sin\theta_1 + \cos\theta_1 \tan\theta_2)} \quad \text{.....1.14}$$

and a dark fringe where $h(x,y) = \dfrac{(n+\frac{1}{2})d}{(\sin\theta_1 + \cos\theta_1 \tan\theta_2)}$ 1.15

Moiré techniques have the advantages of high sensitivity, high spatial resolution, large dynamic range, a simple optical setup and no need to perform digital image subtraction.

1.3.5 Photoelasticity

Photoelasticity [35] is the oldest optical technique used in experimental stress analysis. It is widely used in industrial applications where the problems of interest could not be solved using other analytical methods. It provides the contours of stress differences and the regions of high stress concentration visually. A stress state is applied to a test object and the induced birefringence is studied to find the stress distribution within the material. If a load is applied to the object it will stretch (strain) and there will be a corresponding stress which is characterized by principal stress directions (one of maximum stress and the other of minimum stress) and corresponding to these there will be induced maximum and minimum refractive indices for light which is plane polarized in these directions. A polariscope used for stress analysis consists of a light source, a polarizer, and an analyzer. In addition to these, the device may also contain lenses, a quarter-wave plate and a camera to record the fringe pattern. Plane polariscope is one type used to analyze the stress state of the object. A schematic of the plane polariscope is shown in Figure 1.9.

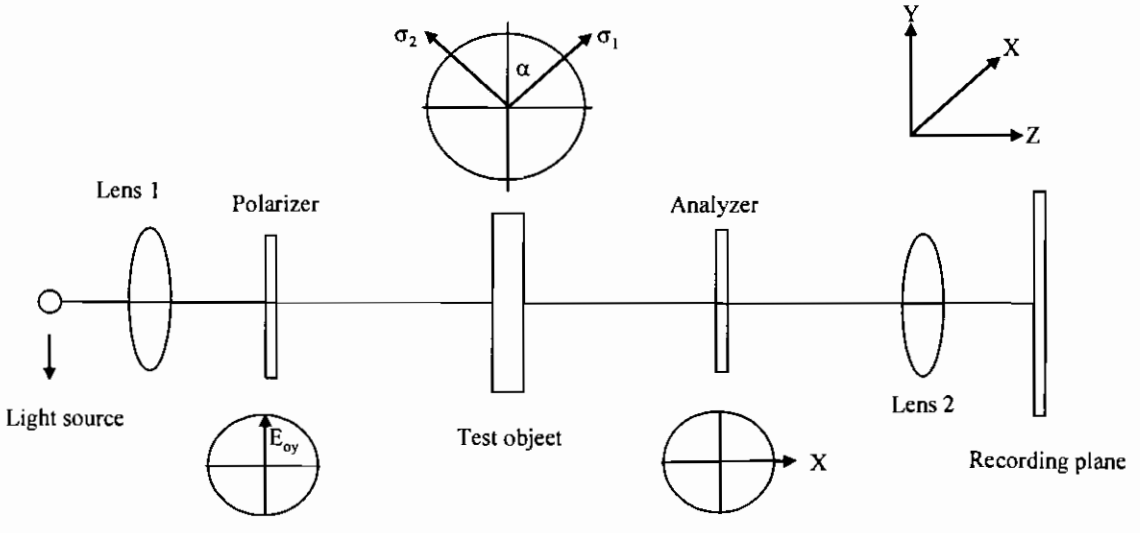

Figure 1.9 Plane polariscope

σ_1, σ_2 are the principal stress directions induced in the object. One of them (σ_1) is making an angle α with the transmission axis of the polarizer. The transmission axis of the polarizer is along the y direction. The light wave incident on the polarizer is expressed as

$$E_y(z,t) = E_{0y}\cos(\omega t - kz) \quad \text{.....1.16}$$

where k is the propagation vector.

Light incident on the test object is split into two orthogonal plane polarized components with corresponding amplitudes $E_{0y}\cos\alpha, E_{0y}\sin\alpha$. Light waves at the exit of the test object are given by

$$E_1(z,t) = E_{0y}\cos\alpha\cos[\omega t - kz - k(n_1)d] \quad \text{.....1.17}$$

$$E_2(z,t) = E_{0y}\sin\alpha\cos[\omega t - kz - k(n_2)d] \quad \text{.....1.18}$$

where

n_1 = index of refraction along thc principal stress direction σ_1

n_2 = index of refraction along the principal stress direction σ_2

Because of the different indices of refraction, two waves have a phase difference between them. The phase difference is given by

$$\phi = (\frac{2\pi}{\lambda})(n_1 - n_2)d = \frac{2\pi C}{\lambda}(\sigma_1 - \sigma_2)d \quad \text{.....1.19}$$

where d = thickness of the test object, C = a constant dependent on the material

In photoelasticity equation 1.19 is rewritten as

$$\sigma_1 - \sigma_2 = \frac{mf_\sigma}{d} \text{ where } m = fringe-order = \frac{\phi}{2\pi},\ f_\sigma = \frac{\lambda}{C} \quad \text{.....1.20}$$

This relationship is known as the stress-optics law [35].

The analyzer will resolve the stress components along and perpendicular to the direction of transmission. The components along the direction of transmission pass

through the analyzer and those whose which are perpendicular to the transmission direction are blocked by the analyzer.

The net transmitted intensity through the analyzer is [35]

$$I = E_{0y}^2 \sin^2 2\alpha \sin^2 \frac{\phi}{2} = I_0 \sin^2 2\alpha \sin^2\left[\frac{\pi(\sigma_1 - \sigma_2)d}{f_\sigma}\right] \quad \text{.....1.21}$$

The intensity of the transmitted beam is governed by α and the phase difference.

Transmitted intensity will be zero when $\alpha = 0$ or $\alpha = \frac{\pi}{2}$, and dark fringe will result. These dark fringes will give the directions of principal stresses at any point on the model and they are known as isoclinics.

When $\sin\frac{\phi}{2} = 0$ then $\phi = 2m\pi$ or $\sigma_1 - \sigma_2 = \frac{mf_\sigma}{d}$, thus the transmitted intensity is zero.

When $\sigma_1 - \sigma_2$ is an integral multiple of $\frac{f_\sigma}{d}$. The fringes represent the areas with constant $\sigma_1 - \sigma_2$ and are referred as isochromatics.

1.4 Advantages of optical techniques

In recent years the use of optical inspection techniques has significantly increased with the development of new light sources, detectors, and electronic processing techniques. Whole field and non-contact measurement ability of the optical techniques make them unique and very useful for engineering and scientific applications. The advances in electronics and computing industries provide fast and reliable imaging and data processing systems. The results obtained using optical techniques for measuring the deformation and amplitude of vibration of the objects can be checked using high performance computing techniques such as finite element analysis.

The limitation of optical interferometric techniques is that an extremely stable environment is required. This requirement limits the use of such techniques in the industrial environment.

This thesis is concerned with holographically recorded optical elements, holographic interferometry and electronic speckle pattern interferometry and shows how these can be very effectively combined. Holography is the subject of the next chapter.

References

1. R. S. Sharpe, "Research techniques in Nondestructive Testing Vol. VI," Chapter 6, pp 254, Academic Press Inc (London) Ltd, (1982).
2. TechTrends, "Non destructive testing," Innovation 128, S. A, Paris, France, (1988).
3. Ultrasonic testing, NDT course material, http://www.ndt-ed.org/EducationResources/CommunityCollege/communitycollege.htm, August, (2005).
4. A. I. Lewcock, "Neutron radiography: status report," Phys. Technol, 10, 74-76, (1979).
5. W. J. Lewis, L. G. I. Bennett, T. R. Chalovick, O. Francescone, "Neutron radiography of aircraft composite flight control surfaces," NDT.net, 8, (2003).
6. P. Vontobel, E. Lehmann, G. Frei, "Neutrons for the study of adhesive connections," Proc. 16th World conference on NDT, Montreal, Canada, (2004).
7. E. Hartouni, "Protons reveal the inside story," Science & Technol Review, 2000, Proton radiography at Las Alamos, US department of energy research news, http://www.eurekalert.org/features/doe/2003-05/danl-pra051303.php May, (2003).
8. J. Szilard, "Ultrasonic testing-non conventional testing techniques," John Wiley & Sons Ltd, (1982).

9. L. Filipczynski, Z. Pawlowski, J. Wehr, "Ultrasonic methods of testing materials," Butterworth & Co (Publishers) Ltd, England, (1966).

10. H. Vallen, "AE testing fundamentals, equipment, applications," NDT.net, Vol. 7, No. 09, (2002)

11. C. U. Grosse, "Editorial: Special issue on Acoustic emission," NDT.net, 7, No.09, (2002).

12. P. Tscheliesnig, "Detection of corrosion attack on ships, especially oil tankers with Acoustic emission," Proc, 16th World conference on NDT, Montreal, Canada, (2004).

13. R. S. Sharpe, "Research techniques in Nondestructive testing Volume-II," Chapter6, Academic Press Inc London, (1973).

14. E. Hecht, "Optics," Chapter 9, page 385, 3rd Ed, Addison Wesley Longman Inc, USA, (1998).

15. D. Gabor "A new microscopic principle," Nature, 161, 777-778, (1948).

16. R. K. Erf, "Holographic non destructive testing," Chapter 4, Academic press Inc, London, (1974).

17. D. W. Robinson, G. T. Reid, "Interferogram analysis digital fringe pattern measurement techniques," Institute of Physics publishing, Bristol, Chapter 2, 60, (1994).

18. R. Jones, C. Wykes, "Holographic and speckle interferometry," Cambridge University Press, Cambridge, (1983).

19. R. K. Erf, "Speckle Metrology," Chapter 2, Academic Press Inc, London, (1978).

20. P. K. Rastogi, "Digital speckle pattern interferometry and related techniques," John Wiley & Sons Ltd, England, (2001).

21. O. J. Lokberg, K. Hogmoen, "Vibration phase mapping using electronic speckle pattern interferometry," Appl. Opt, 15, 2701-2704, (1976).

22. K. Hogmoen, O. J. Lokberg, "Detection and measurement of small vibrations using electronic speckle pattern interferometry," Appl. Opt, 16, 1869-1875, (1977).

23. O. J. Lokberg, K. Hogmoen, "Use of modulated reference wave in electronic speckle pattern interferometry," J. Phys. E, 9, 847-851, (1976).

24. I. Yamaguchi, S. Ohta, J. Kato "Surface contouring by phase-shifting digital holography," Opt. Lasers. Engineering, 36(5), 417-428, (2001).

25. T. Santhanakrishnan, P. K. Palanisamy, N. Krishna Mohan, R. S. Sirohi, "A new optical configuration in speckle interferometry for contouring of three-dimensional objects," Opt. Comm, 152, 19-22, (1998).

26. Q. Saleem, R. D. Wildman, J. M. Huntley, M. B. Whitworth, "A novel application of speckle interferometry for the measurement of strain distributions in semi-sweet biscuits," Meas. Sci. Technol, 14, 2027-2033, (2003).

27. E. A. Zarate, Edén Custodio G, Carlos G. Treviño-Palacios, Ramón Rodríguez-Vera, Hector J. Puga-Soberanes, "Defect detection in metals using electronic speckle pattern interferometry," Solar Energy Materials and Solar Cells, 88(2), 217-225, (2005).

28. K. S. Kim, K. S. Kang, Y. J. Kang, S. K. Cheong, "Analysis of an internal crack of pressure pipe line using ESPI and Shearography," Opt. Laser. Technol, 35(8), 639-643, (2003).

29. M. Hertwig, T. Fleming, R. Usinger, "Speckle interferometry for detection of subsurface damage in fiber-reinforced composites," Meas. Sci. Technol, 5, 100-104, (1994).

30. Y. Y. Hung, H. P. Ho, "Shearography: an optical measurement technique and applications," Mat. Science. Eng, 49(3), 61-87, (2005).

31. J. F. Silva Gomes, J. M. Monteiro, M. A. P. Vaz, "NDI of interfaces in coating systems using digital interferometry," Mechanics of Materials, 32(12), 837-843, (2000).

32. S. Dilhaire, S. Jorez, A. Cornet, L. D. Patiño Lopez, W. Claeys, "Measurement of thermomechanical strain of electronic devices by Shearography," Microelectronics Reliability, 40, 1509-1514, (2000).

33. K. Habib, "Thermally induced deformations measured by Shearography," Opt. Laser. Technol, 37, 509-512, (2005).

34. D. C. Williams, "Optical methods in engineering metrology," 1st Ed, Chapter 9, Chapman-Hall, London, (1993).

35. R. S. Sirohi, F. S. Chau, "Optical methods of measurement whole field techniques," Chapter 7 183-226, Marcel Dekker Inc, New York, (1999).

2. Holography

Introduction

Holography is a powerful imaging technique, which is different from conventional photography. In photography a three dimensional scene is recorded on a photographic plate or film using a combination of optical elements such as lenses and mirrors. The light waves scattered from the object are recorded as a spatial variation of intensity. Information about relative phases of light waves from different parts of the object is not recorded in photography. This is the reason why a photograph of a three dimensional scene only appears as a two dimensional scene. Recording complete information of an object is possible with the unique optical technology known as holography. The invention of holography was a revolution in optical engineering. Recording the amplitude and the phase of the object makes the hologram different from a conventional photograph. The phase information is recorded by interfering two light waves derived from the same coherent source. The interference pattern between the light waves scattered from an object (object beam) and a reference beam is recorded on a photosensitive medium. Retrieval of the image from the hologram is known as reconstruction. During reconstruction the hologram is illuminated with a reference beam which is diffracted by the hologram. The diffracted wavefront is an exact replica of the original object wavefront so that a true three dimensional image of the object is reproduced.

2.1 Gabor Holography

The invention of holography is related to Bragg's work on x-ray crystallography. The work done by Bragg on x-ray crystallography led to the development of the x-ray microscope [1, 2]. Gabor made use of the governing principle of Bragg's x-ray

microscope and invented holography while he was trying to overcome the fundamental and practical limitations of microscopy [3]. In Gabor holography the scattered field from a transparency containing very fine opaque lines is recorded on a photosensitive medium using a monochromatic light (filtered mercury arc lamp). The Fresnel diffraction pattern of the object transparency is recorded. The complex amplitude of the diffraction pattern is the sum of two light beams, a directly transmitted beam and a scattered beam, which contains the information about the object. During the reconstruction stage, the hologram is illuminated with a reference beam. Incident light is diffracted by the hologram and produces two orders of diffraction. One order corresponding to the scattered light waves from the object forms a virtual image of the object whilst the second order corresponds to the object wavefront with the same amplitude but opposite phase (conjugate image). A schematic of Gabor hologram recording and reconstruction is shown in Figure 2.1. Superposition of the real and conjugate images on each other is a major limitation of Gabor holograms [4], because it is not possible to view them separately. In addition the holographic images are of poor quality; this is due to the limited coherence length of the light source.

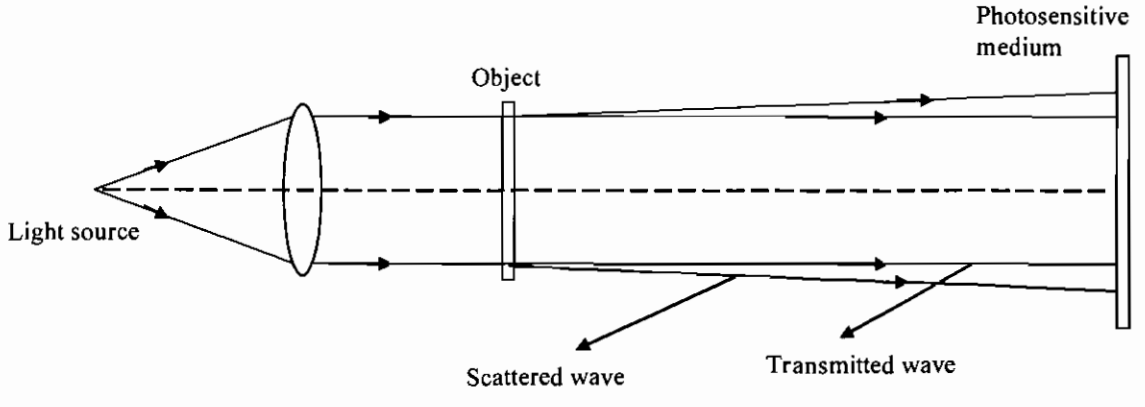

Recording

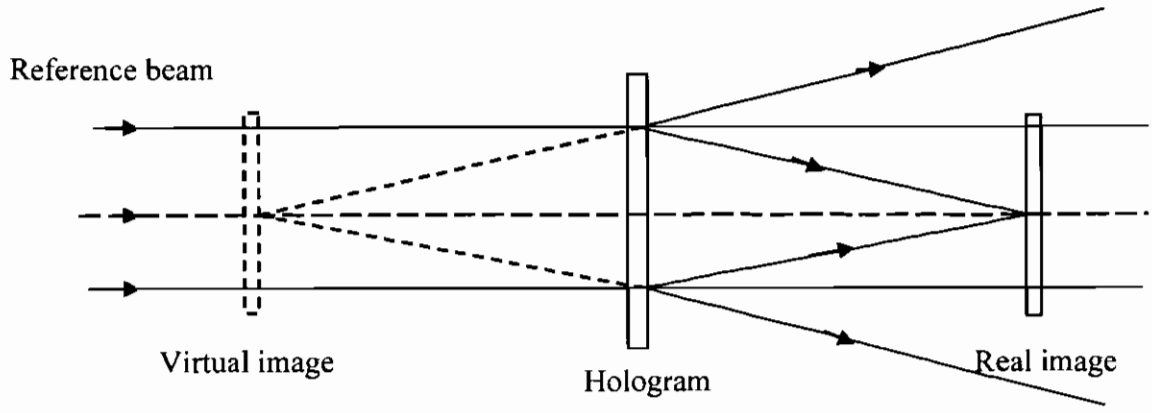

Reconstruction

Figure 2.1 Gabor (in-line) hologram recording and reconstruction

2.2 Off-axis holography

The twin image problem associated with Gabor holograms is eliminated by using an off-axis reference beam. Leith & Upatnieks made use of an off-axis reference beam soon after the invention of the laser [5, 6, 7, 8]. Instead of recording a hologram with a reference beam collinear with the object beam, a hologram is recorded with object and reference beams making an angle with each other. Figure 2.2 shows a schematic of the geometry used to record and reconstruct an off-axis hologram. Object and reference beams fall on the photosensitive medium making an angle θ with each other. During the reconstruction stage, virtual and real images (orthoscopic and pseudoscopic) are angularly separated from each other. Both the images are removed from the region of the directly transmitted un-diffracted beam.

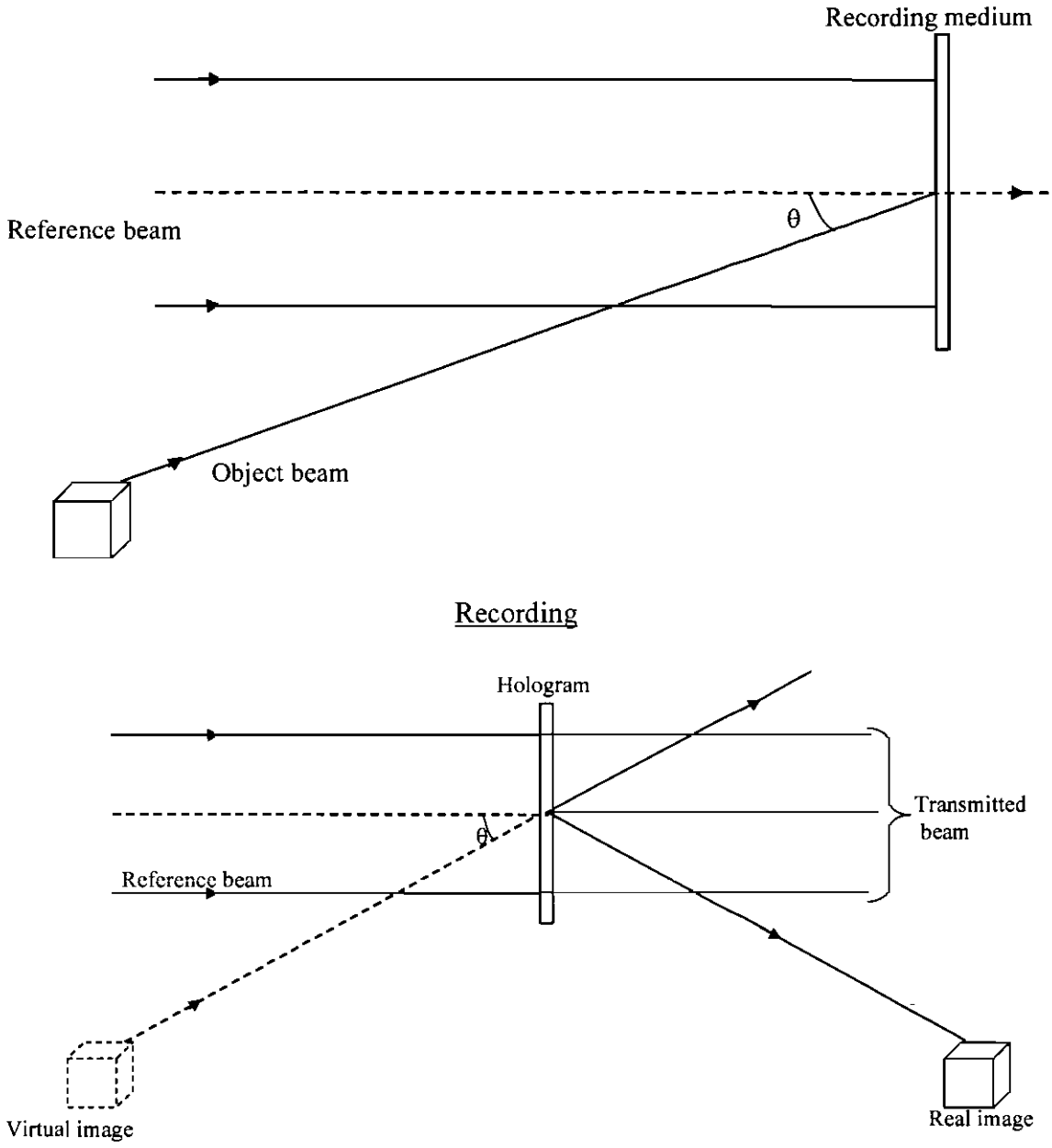

Figure 2.2 Off-axis hologram recording and reconstruction

This method of recording a hologram eliminates the problem of separating the virtual and real images which occur in Gabor holography.

2.3 Resolution of the recording medium

Unlike in photography, the recording medium used in holography must have high resolution. The recording medium has to resolve the finely spaced interference

fringes in the case of off-axis holography. When two plane waves with an inter beam angle 2θ intersect on the recording medium, the fringe spacing is given by the equation

$d = \lambda / (2\sin\theta)$ 2.1

θ = inter beam angle, λ = wavelength of light source

Suppose two beams with an inter beam angle of 60 degree are incident on the recording medium (Figure 2.3) when using a laser at 532 nm the fringe spacing is 0.532 μm. This shows that the recording medium must have a resolution of at least 2000 lines /mm.

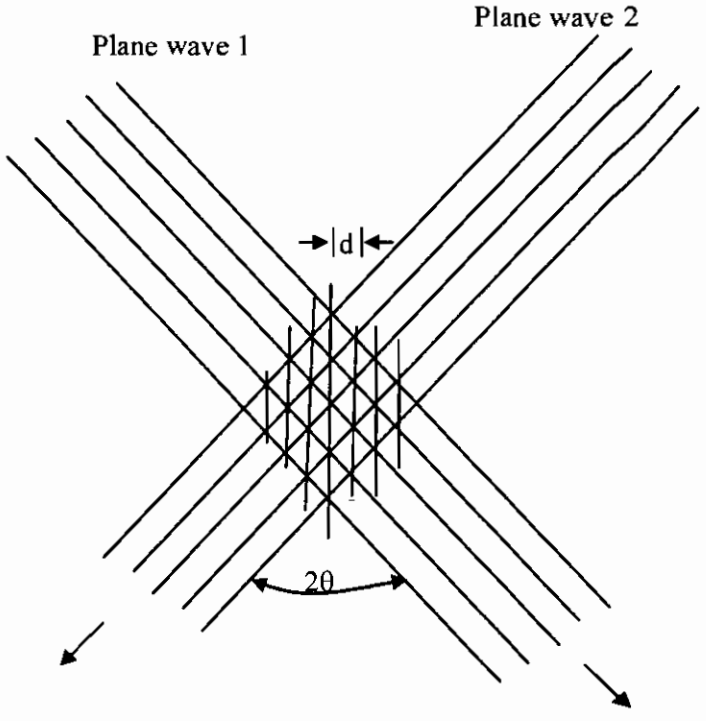

Figure 2.3 Interference fringes produced by overlap of two plane wavefronts

2.4 Factors affecting the quality of hologram

The following are important parameters, which have direct influence on the production of high quality holograms; (1) Coherence property of light (2) Polarization state of the interfering beams (3) Fringe contrast (4) Vibration isolation

2.4.1 Coherence of light

Coherent radiation is described by two properties: spatial coherence and temporal coherence [9]. Spatial coherence is defined as the degree to which a beam of light appears to have originated from a single point in space. It is inversely proportional to the apparent diameter of the light source. Temporal coherence is a measure of the time period over which the waves in a beam of light maintain the same phase relationship. Using temporal coherence, it is possible to calculate the distance over which the photons in a beam of light will be in phase with each other; this is the coherence length of the light source. For ordinary white light the coherence length is of the order of micrometers and for a filtered mercury arc lamp it is a few millimetres. The coherence length for a laser ranges from centimetres to meters depending on the type of laser.

The coherence length of the light source is an important parameter for recording and reconstructing the hologram. The spread of frequencies in a beam of light is called the bandwidth. Temporal coherence of a light source is inversely proportional to the bandwidth of the light source. A light source emitting a single frequency possesses infinite coherence length. Holography requires a light source having a long coherence length. The longer the coherence length, the more freedom one has in setting up the hologram recording geometry. In making holograms of objects with complex shapes, it is essential to have a light source with long coherence length because the light travels different distances in the object beam depending on the depths of different parts of the object. To make holograms of such objects the light source requires a coherence length of the order of centimetres or greater. A hologram can be recorded only if the path difference between the object and reference beams in the recording setup is less than the coherence length of the laser.

2.4.2 Polarization state

Hologram formation on a photosensitive medium is due to the interference fringes formed by the constructive and destructive interference between the object and reference waves. It is possible to record a high quality hologram only if the angle between the electric vectors of the two interfering beams is zero; if it is 90^0 two beams will not interfere. Although the two interfering beams are derived from the same laser, the polarization states of two beams might change due to the reflections from the metallic and dielectric surfaces on their way before they combine at the photosensitive medium.

The intensity distribution of the interference pattern formed at the hologram recording plane is given by the expression

$$I = I_1 + I_2 + 2(I_1 I_2)^{\frac{1}{2}} \cos(\phi_1 - \phi_2) \quad \text{.....2.2}$$

Where I_1 and I_2 are the intensities of the two interfering beams at the recording plane with phases ϕ_1 and ϕ_2 respectively. The above expression is true only if the angle between the two electric vectors is zero. If the two electric vectors make an angle of ψ with each other, the expression becomes

$$I = I_1 + I_2 + 2\sqrt{I_1 I_2}\cos(\phi_1 - \phi_2)\cos\psi \quad \text{.....2.3}$$

The fringe visibility decreases if the angle between the two electric vectors increases, and drops to zero if it reaches 90 degrees [10]. The holographic image quality is degraded due to polarization changes of the illuminating beam after scattering by the object. Change of polarization state of back scattered light from the object will decrease the signal to noise ratio in the reconstructed image [11].

2.4.3 Vibration Isolation

To record a hologram with high quality, the recording environment must be completely free from air turbulence and mechanical disturbances. The requirement of a vibration free environment has limited the use of holography to the laboratory environment, because the recording equipment must be stable in position to within a fraction of the wavelength of light used. Change in the phase difference between the two recording beams will result in movement of the interference fringes at the recording plane. Relative movement between the optical components in the recording setup must be avoided as well as temperature gradients in the laboratory. A pulsed laser can be used to minimize the effect of mechanical disturbances by ensuring that only movement of much less than the wavelength of light are possible during the hologram recording. The effect of object movement during recording can also be minimized by adopting an optical system in which the reference beam can be derived from a mirror mounted on the object itself. When exposure time is greater than the period of vibration of the object, a time average fringe pattern would be recorded. Mounting the optics on a stable, vibration isolation optical table reduces the mechanical disturbances. Enclosing the working area can minimize air currents and thermal drifts. By doing this the refractive index of the air surrounding the object and reference beams can be maintained constant and the phase fluctuations can be eliminated. Residual disturbances can be eliminated by a feedback system in which a photodiode picks up any motion in the interference fringes and a piezoelectric device controls the mirror in the reference beam path to restore the path difference between the two beams to its original state [14].

2.4.4 Fringe contrast

Fringe contrast is an important factor in producing the high quality holographic images. It depends on the ratio of the reference beam intensity to that of an object beam.

Maximum fringe contrast is obtained with the object and reference beams of equal intensities. Usually the intensity of the reference beam is much higher than the intensity of the object beam. Intensities of the two beams are adjusted by choosing a beam splitter with appropriate reflectance-to-transmittance ratio. The ratio of beam intensities is varied by inserting neutral density filters in one or other of the beams. Object beam intensity can also be increased by changing the reflective properties of the object surface by applying reflective coatings. The ratio of the beam intensities can also be controlled by using polarizing optics. Two half-wave plates and a polarising beam splitter are used in the experimental setup as shown in Figure 2.4.

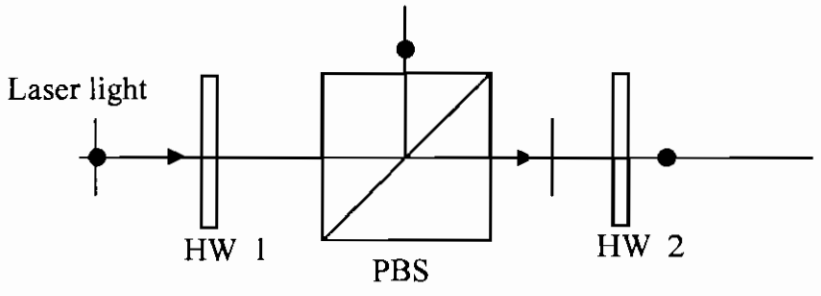

Figure 2.4 Polarizing optics for controlling beam ratio

The first half-wave plate (HW1) is used to control the relative intensities of the two beams coming through the polarizing beam splitter (PBS). Reflected light from the PBS is horizontally polarized. The vertical polarization state of the transmitted beam is changed to horizontal polarization by rotating HW2 around its optical axis. By choosing the appropriate rotation angle of HW1 it is possible to obtain a beam ratio of 1:1.

2.5 Hologram formation

Hologram formation on a photosensitive layer is due to the interference between the object beam and reference beam. The developed hologram, when illuminated with the reference beam of light, diffracts light in a way such that the object wavefront can be

reproduced. The complex amplitudes of the object and reference waves at the recording plane are given by

Object wave $U_0(x,y) = A_0(x,y)e^{-i\phi_0(x,y)}$ 2.4

Reference wave $U_R(x,y) = A_R e^{-i\phi_R(x,y)}$ 2.5

where A_0, ϕ_0 are amplitude and phase of the object wave and A_R, ϕ_R are amplitude and phase of the reference wave.

The intensity distribution of interference pattern at the film plane is given by

$$I(x,y) = [U_o(x,y) + U_R(x,y)][U_o^*(x,y) + U_R^*(x,y)]$$

$$= A_R^2 + A_o^2 + U_o^* U_R + U_o U_R^* \quad \text{.....2.6}$$

* denotes the complex conjugate.

The photosensitive medium is exposed to the irradiance pattern described by the above equation. The photosensitive medium changes its amplitude transmittance due to the irradiance pattern. Variation of the amplitude transmittance is obtained using a plot of the amplitude transmittance of the photosensitive medium vs exposure. For simplicity, it is considered that the amplitude transmittance t (x, y) of the hologram is proportional to I (x, y).

$$t(x,y) = t_0 + \beta I t \quad \text{.....2.7}$$

where t_0 is the constant background transmittance, t is the exposure time, β is a constant determined by photographic material and the processing conditions.

$$t(x,y) = t_0 + \beta t[A_R^2 + A_o^2 + U_R^* U_0 + U_R U_0^*] \quad \text{.....2.8}$$

The reconstruction from the developed transparency can be seen when it is replaced in the same position and illuminated with the reference beam whose complex amplitude is $U_R(x,y)$

The complex amplitude transmitted by the hologram can be written as

$$R(x,y) = U_R(x,y)t(x,y) = U_R(x,y)\{t_0 + \beta t[A_R^2 + A_o^2 + U_R^* U_o + U_R U_o^*]\}$$

$$= U_R(x,y)(t_0 + \beta t A_R^2) + \beta t U_R(x,y)A_o^2 + \beta t A_R^2 U_0 + \beta t A_R^2 U_0^* \quad \text{.....2.9}$$

The first term $(U_R(x,y)(t_0 + \beta t A_R^2)$ in the above equation is a uniformly attenuated wave, which is the directly transmitted beam. The second term $(\beta t U_R(x,y)A_0^2)$ is extremely small in comparison with the other terms and can be neglected because the object beam intensity is very small in comparison to the reference beam. The third term $(\beta t A_R^2 U_0)$ is similar to the original wavefront incident on the photographic plate during recording; it gives rise to the reconstructed wavefront from the hologram. The reconstructed wave appears to diverge from the hologram. It forms a virtual image of the object behind the hologram. The fourth term $(\beta t A_R^2 U_0^*)$ resembles the third term but it contains the complex conjugate of the object wavefront. It is a real image of the object with opposite wavefront curvature. It converges to form a real image and the image appears in front of the hologram. Wavefront reconstruction is shown in Figure 2.5.

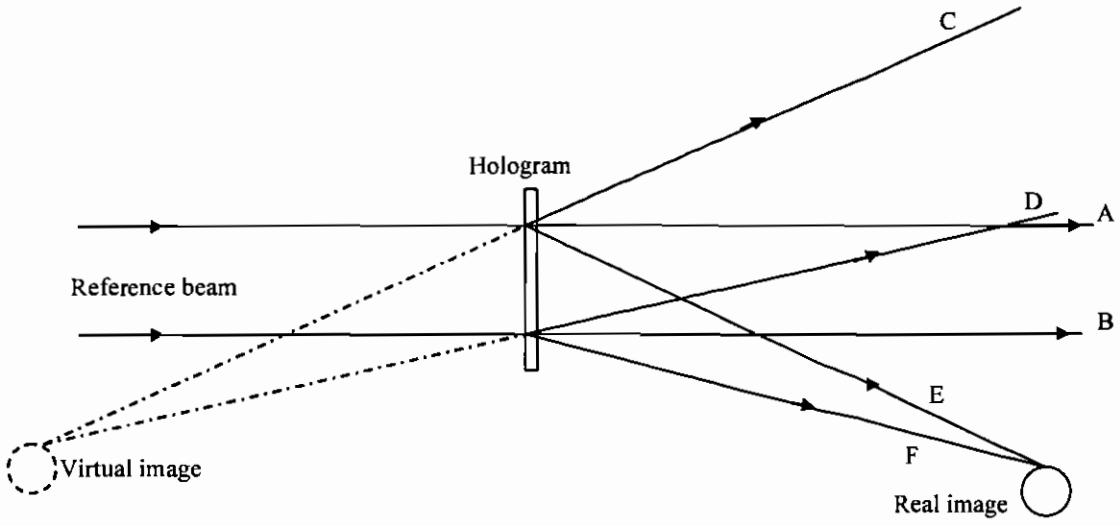

Figure 2.5 Hologram reconstruction showing virtual and real image formation

The hologram is illuminated with reference beam. The light is transmitted and diffracted by the hologram. One beam (E F) converges to form a real image. The second beam (C D) diverges and forms a virtual image. The third un-diffracted beam (A B) contains no information about the object.

2.6 Different types of holograms

Depending on the geometry used for recording, holograms are classified as transmission or reflection holograms. The principle of image formation is the same in each case. Both object and reference beams arrive onto the photosensitive medium from the same side in a transmission holography, whereas the beams arrive from opposite sides of the photosensitive medium in reflection holography.

2.6.1 Transmission hologram

A schematic of the transmission hologram recording is shown in Figure 2.6. The laser light is split into two beams using a beam splitter. One beam is directed to fall on the object using mirror 1. The scattered light from the object is incident on the photosensitive medium. The second beam is directed to incident on the photosensitive

medium using mirror 2. The path lengths of the two beams are adjusted to be equal. The two beams interfere on the photosensitive medium. After development, the hologram is illuminated with the reference beam and the object wavefront is reproduced.

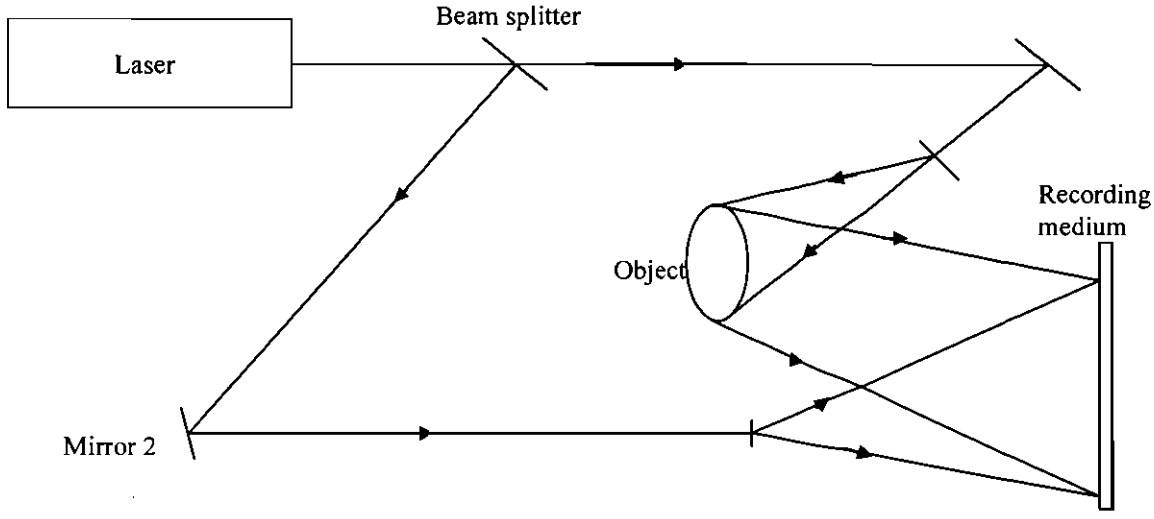

Figure 2.6 Transmission hologram recording geometry

2.6.2 Reflection hologram

Reflection holograms [15] are recorded with a laser source and reconstructed using a white light source. A schematic of reflection hologram recording geometry is shown in Figure 2.7.

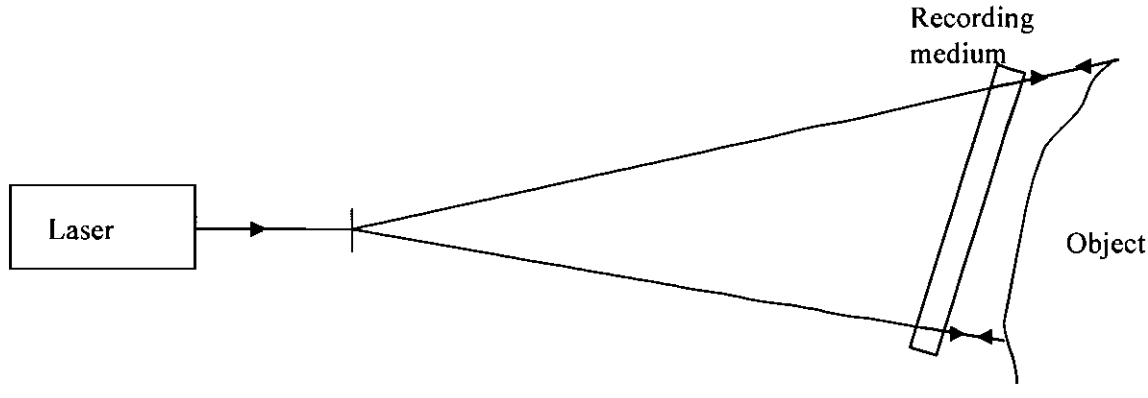

Figure 2.7 Reflection hologram recording geometry

Spatially filtered laser light falls on the photographic plate. The light is partially transmitted through the recording medium and illuminates the object. Reflected light

from the object falls on the recording medium from the opposite side. Thus, the two beams of light travelling in opposite directions meet at the recording medium and interfere and resulting in the object wavefront being recorded.

A reflection hologram reflects light only within a narrow band of wavelengths during the reconstruction. The hologram selects the appropriate wavelength from a white light source. When the hologram is illuminated with white light, it diffracts light and the object wavefront is reconstructed at the Bragg angle corresponding to the recording wavelength (Figure 2.8). The reconstruction angle is dependent on the recording wavelength.

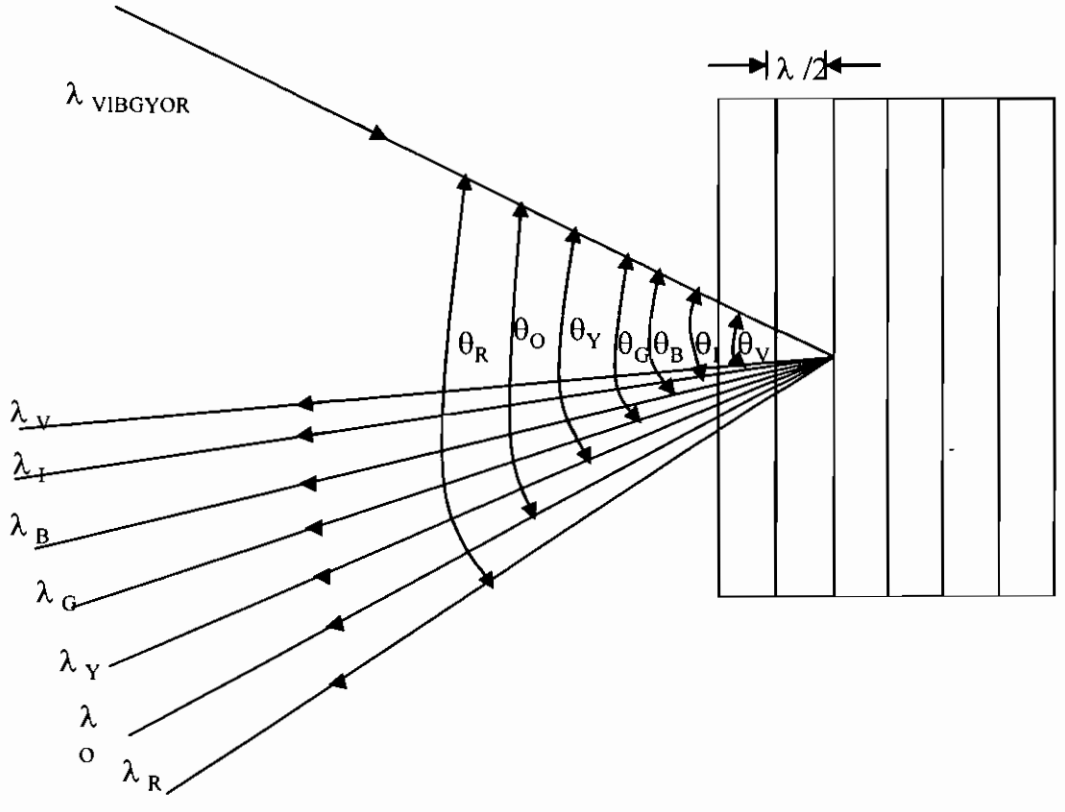

Figure 2.8 Reflection hologram reconstruction geometry

2.6.3 Amplitude and phase holograms

Holograms can be classified as amplitude and phase holograms according to how the photosensitive medium changes during the hologram recording.

In an amplitude hologram, amplitude transmittance t(x, y) depends on the recording intensity I(x, y). In a phase hologram the thickness or refractive index of the hologram depends on the recording intensity.

Use of holograms as optical elements

Since holograms reconstruct recorded wavefronts they can be used in optical systems in much the same way as conventional optical components. Indeed a single holographic element can perform several functions at the same time. Other advantages of using HOEs are their compact nature (a single flat plate) and their low cost.

In this chapter holography was discussed and the importance of high resolution recording materials for off-axis holography was explained. In the next chapter a detailed discussion about different types of holographic recording material including the photopolymer recording material is given. Application of photopolymer material in holography is of particular interest in this thesis.

References

1. W. L. Bragg, "A new type of x-ray microscope," Nature, 143, 678, (1939).
2. W. L. Bragg, "x-ray Microscope," Nature, 149, 470-471, (1942).
3. D. Gabor, "A new microscopic principle," Nature, 161, 777-778, (1948).
4. D. Gabor, "Microscopy by reconstructed wave-fronts," Proc. Roy. Soc. London, Ser. A 197, 454-487, (1949).
5. E. N. Leith, J. Upatnieks, "Wavefront reconstruction with diffused illumination and three dimensional objects," J. Opt. Soc. Am. A, 54, 1295-1301, (1964).
6. E. N. Leith, J. Upatnieks, K.A. Haines, "Microscopy by wavefront reconstruction," J. Opt. Soc. Am. A, 55, 981-986, (1965).
7. E. N. Leith, J. Upatnieks, "Wavefront reconstruction with continuous-tone objects," J. Opt. Soc. Am. A, 53, 1377-1381, (1963).

8. Arthur. L. Schawlow, W.H. Freeman, "Lasers and light," Scientific American Inc, USA, (1969).

9. E. Hecht, "Optics," Chapter 12, 2nd Edition, Addison-Wesley, (1987).

10. P. Hariharan, "Optical Holography," 2nd Edition, Cambridge University Press, Cambridge, (1996).

11. H. Ghandeharian, W. M. Boerner, "Degradation of holographic images due to depolarization of reflected light," J. Opt. Soc. Am. A, 68, 931-934, (1978).

12. J .P. Waters, "Object Motion Compensation by speckle reference beam holography," Appl. Opt, 11,630-636, (1972).

13. D. B. Neumann, R.C. Penn, "Object motion compensation using reflection holography," J. Opt. Soc. Am. A, 62, 1373, (1972).

14. D .R. Macquigg, "Hologram fringe stabilization method," Appl. Opt, 16, 291-292, (1977).

15. Y. N. Denisyuk, "Photographic reconstruction of the optical properties of an object in its own scattered radiation field," Soviet. Physics, 7(6), 543-545, (1962).

3. Recording materials

Introduction

Hologram formation in a photosensitive medium is due to the interference between the object and reference beams. A variety of recording materials are available for holographic applications [1]. It is essential that the photosensitive medium has high resolution because it has to resolve the finely spaced interference fringes. In addition to this requirement, the material should also possess the following: spectral sensitivity well matched to the wavelengths of lasers available, linear transfer characteristic (a typical transmittance versus exposure curve also known as H&D curve of a photographic plate is shown in Figure 3.1) and low noise. The H&D curve is used to characterize a photographic emulsion. Apart from the conventional recording materials, self-processing materials such as photopolymers are available for holographic applications. Photopolymer materials are easy to prepare and are less expensive than the conventional recording materials such as silver halide emulsions.

3.1 Silver halide emulsions

Silver halide emulsions [2] are the most widely used and well-known commercially available photosensitive materials. They are important materials for holography in respect to its numerous scientific and artistic applications. These materials have advantages of high sensitivity, range of spectral sensitivities matched to different wavelengths, good shelf life and good stability of holograms after processing. Exposure characteristics of the photographic emulsions are known from the Hurter and Driffield (H&D) curve (Figure 3.1), which gives the variation in the density of developed emulsion as a function of the logarithm of the exposure energy. The slope of

the linear region of the curve is denoted by the symbol γ and different emulsions have different values of γ.

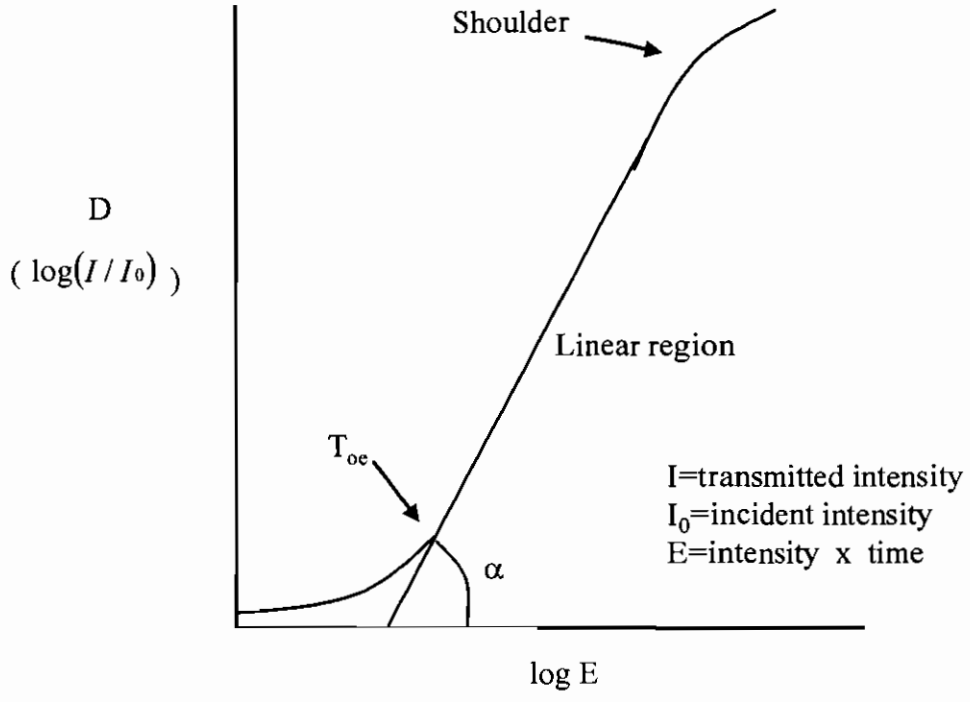

Figure 3.1 Typical H&D curve for photographic emulsion

The emulsion consists of micro crystals of silver halide (usually bromide) dispersed in gelatin. Chemical development of the holographically recorded latent image converts the silver halide grains to silver particles and results in an amplitude hologram with low diffraction efficiency. Oxidizing the latent image with an appropriate bleaching agent converts the silver particles to transparent silver salt grains, resulting in a phase hologram with high diffraction efficiency [3].

Latent image formation

When light falls on the emulsion, silver halide particles absorb light energy and release free silver atoms within the body of the sub-microscopic crystal.

$$h\upsilon + Br^- \rightarrow Br + e^-$$

$$e^- + Ag^+ \rightarrow Ag$$

A single silver atom is not stable enough but if a second electron is freed from a halide ion and trapped by a second Ag^+ ion, a two-atom centre is formed and it is more stable than a single silver atom. The process continues until a stable silver aggregate is formed. The silver aggregate is known as the latent image.

The photographic film after exposure to light is developed to convert aggregate of silver to a grain of silver metal. Unexposed silver halide is removed by fixing. The fixation process decreases the thickness of the processed film and causes emulsion shrinkage. A fixation-free process is used to reduce the emulsion shrinkage. Bleaching is an alternative to the fixation process. Bleaching is done by either of the following two techniques. In the first method the variations in optical density of hologram are converted to thickness variations of the emulsion layer. In the second method variations in optical density are converted to refractive index modulation.

The major drawback with silver halide is the requirement for wet processing. This requirement makes the material not suitable for applications such as holographic interferometry and data storage.

3.2 Dichromated Gelatin (DCG)

DCG is one of the promising materials available for recording phase holograms. It has the large refractive index modulation capability, high-resolution (>10,000 lines/mm), low scattering and absorption. The optical quality of the emulsions is superior when compared with silver halide emulsions because they do not have grains. DCG films are suitable for making holographic optical elements because of moderate exposure requirement and large refractive index modulation [4].

DCG film consists of a gelatin layer impregnated with ammonium dichromate. Absorption of light of appropriate wavelength causes the reduction of chromium ion

Cr^{+6} to lower ionization state Cr^{+3}. The trivalent chromium ion forms a cross link with gelatin. The cross-link hardens the gelatin layer and creates a hardness differential between exposed and unexposed regions.

The processing of DCG consists of soaking in distilled water followed by a series of rapid drying steps in progressively pure alcohol baths. The water soak swells the gelatin by many times its original volume. The drying process produces strains, causing voids to appear in the hardened regions, thus refractive index modulation is produced.

The sensitivity of the DCG film can be extended to the red wavelength by adding suitable dyes. Charge transfer absorption is the possible reason for the new absorption band in the red part of the spectrum in DCG films. Methylene blue sensitized DCG films are used to make holograms with red light [6, 7, 8, 9]. Methylene blue sensitized DCG films with tetramethylguanidine (TMG) [10] as the electron donors were also used to record holograms with red light. The high alkalinity of the material allows the unexposed areas on the material to have increased life time (weeks rather than days) at room temperature. Rhodamine 6G (R6G) was used as the spectral sensitizer instead of the conventional green-blue sensitizer ammonium dichromate [11]. R6G has a wide sensitivity within the blue-green region and high compatibility with red sensitizer (MB). Erythrosin B dye was used to increase the sensitivity of DCG in the green wavelength. Holograms with maximum efficiency of 80% were reported [12]. Despite the high diffraction efficiencies offered by DCG material, environmental stability of the recorded holograms limit their use in commercial applications. To protect against environmental perturbations materials such as polymethyl methacrylate, polystyrene and polycarbonate can be used as protective coatings for DCG holograms

[13]. A DCG film doped with non-hydroscopic vanilla was used as a holographic recording material. This material has high humidity resistance [14].

Fine-grained silver halide emulsions processed as silver halide sensitized gelatin (SHSG) are used as an alternative to DCG material to minimize the noise and scattering. Slavich PFG-03C emulsions were used as SHSG material. It has an added advantage of spectral sensitivity extended to red, green and in particular to blue laser wavelengths [15].

3.3 Photo resists

Photo resists are light sensitive organic films, which can form a surface relief image after exposure and development. Positive and negative photoresists are two types of photoresists. The image formation is different in each type. In negative photoresists the exposed areas are insoluble and the unexposed areas are dissolved away during development. Long exposure times are required for negative resists. The reverse happens in the case of positive photoresists. Exposed areas are washed away and unexposed areas stick to the plate during the development. The positive photo resists are most often used in holography because the bulk of the material is insoluble and only exposed areas are washed away [17].

Shipley AZ-1350 positive photoresist is widely used for recording holographic gratings [18]. It shows a non-linearity when developed with AZ-1350 developer. The diffraction efficiency is limited by the material non-linearity. Higher diffraction efficiency is achieved by developing with AZ-303 rather than AZ-1350 [19, 20]. The choice of photoresist material for recording relief holograms is based on the trade-off among sensitivity, resolution capability, ease of application and processing. Photoresist materials are ideal recording media for embossing holograms [21].

3.4 Photochromics

Hologram formation in photochromics is due to the refractive index modulation associated with photo-induced change in absorption. Light generates free carriers in the lattice; electrons are captured by the anion vacancies in the lattice or holes are captured by the cation vacancies. The resulting combinations are known as colour centers and are responsible for a characteristic colouring of the material if their absorption band lies in the visible region [17]. The photochromic materials are grainless and have a resolution of more than 2000 lines/mm. They do not require pre-processing or post-processing. The holograms can be erased and the material used again. These materials only offer low diffraction efficiencies. Photochromic glass has been investigated for possible optical data storage applications [22]. Materials such as CaF_2 La, CaF_2 Ce, $SrTiO_3$ Fe-Mo, $SrTiO_3$, Ni-Mo are commonly used photochromic materials to record holograms [23]. Fe-doped $LiNbO_3$ with incorporation of Mn is used for holographic storage. Incorporation of Mn leads to photochromic behaviour involving photo reversible conversion of Fe^{+3} to Fe^{+2} [24]. In recent years, there has been an increasing demand for materials capable of high density optical storage and photochromic materials have been successfully used for 3D optical memory applications [25, 26, 27].

3.5 Photothermoplastics

Photothermoplastic materials offer significant advantages over other materials for holographic applications because of their relatively high sensitivity, high efficiency, and record-erase capability. Photothermoplastic is made of a multilayer structure consisting of glass substrate coated successively with a transparent electrode, an organic photoconductor and a thermoplastic layer. The hologram recording sequence in a thermoplastic is the following: charge, expose, recharge, and develop.

Initially the film is sensitized in darkness by applying a spatially uniform electric charge to the top surface. As a result, a uniform negative charge is induced on the conductive coating. In the second step when the film is exposed to light, charge carriers are produced wherever the photoconductor is exposed to light. In the next step, the surface is recharged again uniformly with a constant potential. Additional charges are deposited in the areas wherever the exposure had resulted in migration of charge. The electric field in these regions increases and a spatially varying pattern is produced. In the final step, the thermoplastic is heated to a temperature near its softening point to develop the latent image. This is done by passing an electric current around the conductive layer. The thermoplastic layer undergoes local deformation as a result of varying electric field across it. The layer becomes thicker in the exposed regions and thinner in the unexposed regions. Once the film is cooled to room temperature the thickness variation is frozen and the hologram is more stable.

The film is re-used by exposing it to light and heating the layer to a temperature higher than that used for development. At this temperature the thickness variations of the film are smoothed out and the previously stored charge distribution is erased completely [17, 28]. A schematic of the steps involved for hologram formation in thermoplastic materials is shown in Figure 3.2.

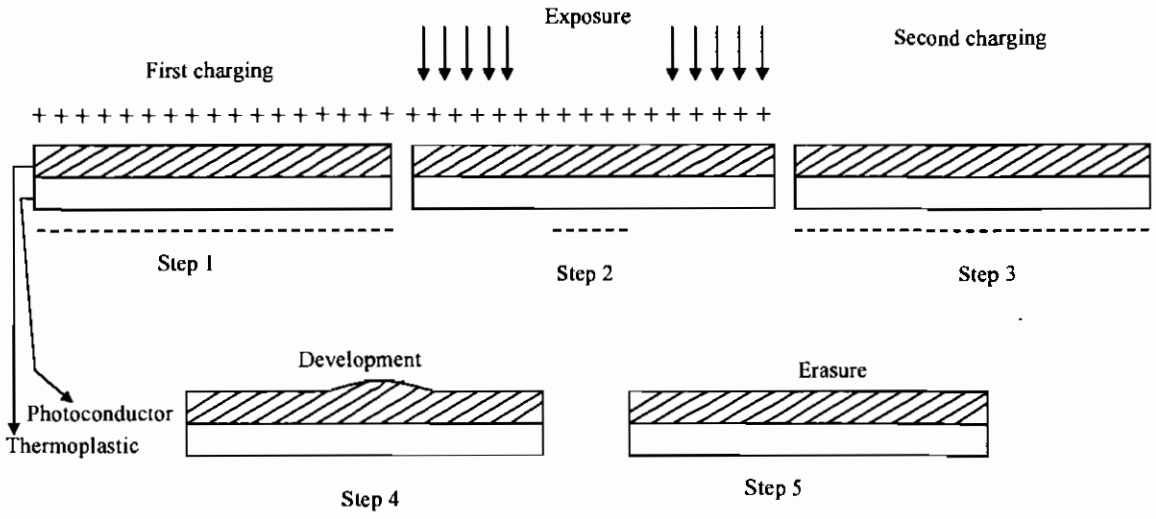

Figure 3.2 Hologram formation in thermoplastic material

Commercial thermoplastic holographic cameras are available for the industrial and laboratory applications. The holographic camera (TCC-2) from Tavex American Inc has optimum resolution of 350-1000 lines /mm and spectral sensitivity from 400-800 nm [29]. The Newport Corporation HC-300 holographic camera [30] was used for holographic applications. After 1997 they stopped producing the films.

Thermoplastic materials offer the following advantages: Low value of exposure energy is required, high diffraction efficiencies, no repositioning problem at reconstruction stage and they are re-writable.

3.6 Photorefractive crystals

Photo refractive crystals offer large holographic data storage capacity [31] close to 10^{12} bits/cm^3. The holographic image is formed in the crystals by the electro-optic effect. Upon illumination, free electrons are generated within the crystal lattice. They migrate and get trapped at defects when they pass into the area of low optical illumination [32]. Migration of the electrons usually takes place through diffusion. An electric field is generated due to the net space charge distribution. The spatially varying electric field modulates the refractive index through the electro optic effect and creates a

phase hologram. The information can be erased by exposing the crystal to a uniform beam of illumination of appropriate wavelength. The most commonly used materials for holographic applications are $LiNbO_3$, bismuth silicon oxide (BSO), bismuth germanium oxide (BGO), potassium tantalum niobate (KTN). $Ba_2\ NaNb_5O_{15}$ is another material which has electro optic coefficients comparable with that of $LiNbO_3$. $LiNbO_3$ was the first photorefractive crystal used to record holograms and it remains one of the most versatile, potentially useful and widely investigated materials. Much of the understanding of hologram formation in photorefractive crystals was developed by working with $LiNbO_3$. The sensitivity of the crystal is increased by introducing a dopant, which increases generation of free electrons. Coloration is produced by adding a second dopant such as Cu or Mn. The coloration is due to the photochromic process. Diffraction efficiency of doubly doped crystals is less compared with single dopant crystals. Diffraction efficiency of such crystals is increased by doping with Fe and Mo [1, 33]. Doping extends the absorption band for the crystal into the visible region. $LiNbO_3$ crystal doped with Rh has a new absorption peak at 480nm. Diffraction efficiency of almost 80% is reported in Rh doped $LiNbO_3$ crystal with exposure energy of $1\ W/cm^2$ [34].

The advantages of the self developing ability and indefinite reusability of photorefractive crystals makes them suitable for use in real time holographic interferometry. Photorefractive $Bi_{12}SiO_{20}$ crystal was used in real time holographic interferometry for contouring of a surface using phase shifting techniques [35]. A compact holographic camera using photorefractive crystals was reported [36]. Iron doped $LiNbO_3$ material was investigated for the holographic data storage applications [37]. In recent years Gallium and Indium doped CdF_2 crystals were used for recording

holograms. Permanent holographic memories are possible in these materials due to the metastable defects close to room temperature [38, 39].

Table 3.1 shows the important holographic characteristics of different materials.

Table 3.1 Characteristics of different of holographic recording media

	Silver halide	DCG	Photo Resist	Photo refractive crystals	Photo thermoplastic
Resolution	1000-10000 l/mm	>10000 l/mm	Up to 4000 l/mm	>1500 l/mm	300-1000 l/mm
Exposure	10^{-6} to 10^{-3} J/cm^2	3×10^{-3} to 4×10^{-1} J/cm^2	$>10^{-2}$ J/cm^2	10 to 10^4 J/cm^2	0.5×10^{-6} to 10^{-4} J/cm^2
Development	Chemical	Chemical	Chemical	Instant	Heat treatment (in situ)

3.7 Photopolymer recording material

Recording materials which don't require chemical processing became popular in recent years [40]. Photopolymerizable materials belong to this category. Despite having shortcomings such as poor photosensitivity and low refractive index modulation photopolymer holographic recording materials offer some attractive features such as freedom from chemical processing, ease of preparation, convenience, durability and low cost. Furthermore, these materials are grainless, producing an image free from scattering. Photopolymer systems consist of a monomer, a photosensitive dye, initiator and a binder.

3.7.1 Hologram recording mechanism

Volume phase hologram formation in a photopolymer recording medium is due to the refractive index modulation created by the polymerization of a monomer.

Refractive index modulation can occur for the following reasons [40]:

1. Change of the spatial arrangement of one or more components. In this case, the molecular structure of at least one component of the reaction mixture undergoes transformation upon light irradiation.
2. Change of the density of the sample at the microscopic level but not changing the composition of the reaction mixture. In this case the modulation of the refractive index is due to the migration of monomer molecules. During the initial exposure the monomer molecules in bright fringe regions polymerize highly and become less available. The concentration of monomer molecules is then higher in dark fringe regions where they are not polymerized. The resulting monomer concentration difference causes unreacted monomer molecules to migrate from dark fringe regions to bright fringe regions. The process of monomer migration creates a spatial distribution of refractive index modulation.

Formation of a volume hologram in a photopolymer material is a three step process [41]

In the first step, the material is exposed to a non-uniform interference pattern of light. The incident radiation polymerizes the monomer with the rate of polymerization depending on the exposure intensity. In the second step, variation of the amount of polymerization causes monomer diffusion from the regions of high concentration (dark) to lower concentration regions (bright). In the final step, after completion of the diffusion process, the material is exposed to light of uniform intensity until the remaining monomer is polymerized.

3.7.2 Photopolymers for holography

Photopolymer material was first used as a holographic recording material in 1969 by Close et al [42]. This system consists of a mixture of acrylamide, acrylate monomer and methylene blue as the dye. Since then, a great deal of work has been done

in developing new photopolymer systems for holographic applications. Calixto [43] used the photopolymer system with acrylamide monomer, triethanolamine as electron donor, methylene blue dye and polymer binder. Efficiencies were reported, which were quite poor at 10% using exposure energy of 90 mJ/cm^2. An acrylamide based photopolymer material was optimized for recording holograms at 514 nm green wavelength by using xanthene dye by Martin [44]. Diffraction efficiencies greater than 80% were obtained with exposure energy of 80 mJ/cm^2. Sensitivity of the photopolymer material for recording holograms at 633 nm was improved by using a different cross linker N, N-dihydroethylenebisacrylamide. Diffraction efficiencies of 70% at 1000 l/mm were achieved with exposure energy of 5 mJ/cm^2 [45]. Acrylamide based photopolymer containing cyanine dye that has a broad absorption peak at 784 nm was used for hologram recording in the near infrared region. Diffraction efficiencies above 70% were reported [46].

Most of the photopolymer materials for holographic applications are limited to the laboratory and are still in the development stage. Only a few photopolymer systems are available for commercial applications. Photopolymers from DuPont, Polaroid and InPhase technologies are available for commercial use. DuPont has been developing commercial photopolymer systems for holographic applications since 1970. The first DuPont photopolymer material was based on acrylic monomer and a cellulose binder with a photoinitiator system [47]. Diffraction efficiency of 40% with exposure energy of 50 mJ/cm^2 was achieved. Post-exposure treatment was used to achieve high diffraction efficiency [48].

Commercial Polaroid photopolymer systems are available for holographic applications. DMP-128 Polaroid photopolymer was developed by Ingwall [49]. This material requires pre-processing such as exposure to white light and immersion in special developer/fixer bath and rinsing followed by drying. Photopolymer recording

material is used in holographic data storage systems at InPhase technologies [50]. Using InPhase's Tapestry™ holographic recording medium, storage density of 15.50 Gbit/cm^2 on a sample of 1.5 mm thickness was demonstrated by multiplexing 3200 holograms [51].

3.7.3 Acrylamide based photopolymer

An acrylamide based photopolymer material has been formulated and developed at the Centre for Industrial & Engineering Optics [52]. It has been used in holographic interferometry, for fabricating holographic optical elements and for holographic data storage. The advantage of self processing ability makes it useful for holographic interferometry. The material has been characterized for holographic applications [44, 52, 53].

3.7.3.1 Physical Properties

The physical properties of the photopolymer material are important factors to be considered. For applications such as the fabrication of holographic optical elements, despite the high diffraction efficiency offered by the material it has to be environmentally stable so that the recorded hologram persists for a long time. The optical quality of the layers is also an important physical property of the material. Good quality layers can be obtained by different coating methods, spin coating, dip coating and gravity settling. Dip coating produces layers with low thickness, which is not ideal for most of the applications unless lower values of diffraction efficiencies are required. Gravity settling is reported [52] as an ideal method to produce thicker layers. This method was used to prepare the photopolymer layers.

3.7.3.2 Environmental Stability

The acrylamide based photopolymer layer composition contains a water soluble binder. Humidity has an effect on the rate at which the recorded hologram disappears from the layer. The diffraction efficiency of the recorded gratings decreases with an increased humidity. This is due to the decrease of refractive index modulation due to the diffusion of the polymer chains through the more permeable binder. The addition of cross linker to the monomer reduces the degradation of the diffraction efficiency [52]. It forms cross linked polymer chains which can not easily diffuse into dark fringe regions. A detailed study of the environmental effects is given in reference 52.

3.7.3.3 Recording Mechanism

The photopolymer recording material [53] consists of a monomer, binder, initiator, and sensitizing dye. A hologram is formed in a photopolymer material due to the refractive index modulation arising from several photochemical and photophysical processes taking place in the photopolymer material.

When a dye molecule is exposed to light of suitable wavelength it is excited to a higher energy singlet state.

$$Dye + h\nu \rightarrow {}^{1}Dye^{*}$$

The excited singlet state dye molecule can return to ground state by radiationless transfer. This process is known as fluorescence quenching. The singlet state dye molecule may undergo inter system crossing; this will lead to more stable and long lived triplet excited state.

$${}^{1}Dye^{*} \rightarrow Dye + h\nu \text{ (Fluorescence)}$$

$${}^{1}Dye^{*} \rightarrow {}^{3}Dye^{*} \text{ (Intersystem crossing)}$$

The excited triplet state dye molecule reacts with an electron donor to form free radicals.

Triethanolamine donates an electron to the triplet state dye leaving the dye molecule with an unpaired electron having a negative charge.

$$^3Dye^* + (HOCH_2CH_2)_3N :\rightarrow Dye^{\bullet -} + (HOCH_2CH_2)_3N^{\bullet +}$$

The triethanolamine becomes an uncharged free radical by losing a proton.

$$(HOCH_2CH_2)_3N^{\bullet +} \rightarrow (HOCH_2CH_2)NCH^{\bullet}CH_2OH + H^+$$

The triethanolamine radical produced in the above reaction is the initiating species for the polymerization process. Hydrogen is extracted from the triethanolamine radical to form dihydro dye and an unstable triethanolamine intermediate containing a carbon-carbon double bond.

$$(HOCH_2CH_2)NCH^{\bullet}CH_2OH + H^+(Dye)^{\bullet -} \rightarrow (HOCH_2CH_2)NCH = CHOH + H_2(Dye)$$

The unstable product is rearranged

$$(HOCH_2CH_2)_2NCH = CHOH \rightarrow (HOCH_2CH_2)_2NCH_2CHO$$

In brief, the excited triplet state of the dye abstracts two hydrogen atoms from the triethanolamine molecule (TEA).

$$^3Dye^* + TEA \rightarrow H_2(Dye) + TEA_{oxd}$$

The free radical triethanolamine reacts with acrylamide monomer (ACR) and thus free radical polymerization will be initiated.

$$TEA^{\bullet} + ACR \rightarrow TEA - ACR^{\bullet}(initiation)$$

The rate of growth of diffraction efficiency depends on several physical and chemical factors. The main factor is the rate of polymerization, which in turn, depends on the rates of initiation, propagation and termination. The three steps (initiation, propagation and termination) depend on the concentration of the monomer and the exposure intensity. The local concentration of the monomer also depends on the diffusion of monomer from unpolymerized dark fringe regions to polymerized bright fringe regions.

3.7.3.4 Holographic characteristics of the photopolymer material

Holographic characteristics of the material are sensitivity, resolution and maximum achievable diffraction efficiency. These parameters have been studied in detail [53].

Holographic sensitivity of a material is defined as the exposure energy required to record a hologram with specific diffraction efficiency under fixed illumination conditions. The material is said to be more sensitive than other materials if it requires less exposure energy under fixed illumination conditions to produce the same diffraction efficiency. In the current photopolymer material exposure density of 65 mJ/cm^2 is required to achieve a diffraction efficiency of 50% at 3000 l/mm spatial frequency.

The reciprocity law states that the same exposure always leads to the same diffraction efficiency regardless of incident intensity. For an ideal recording material the reciprocity law holds good. There is a linear relationship between the grating growth rate and incident intensity up to an incident intensity of $30mW/cm^2$ for photopolymer material and greater intensities produce non-linear holographic recording [53]. A possible reason for this is the rate of polymerization and diffusion rates will not increase indefinitely with an increasing supply of photons.

The modulation transfer function of the material can be found by plotting the diffraction efficiency against spatial frequency of the recorded interference pattern. For an ideal material the diffraction efficiency has to be flat over a range of spatial frequencies. For most materials this graph is flat up to certain cut off spatial frequency, which is characteristic of the material. This photopolymer material has an optimum spatial frequency response at 1500 l/mm.

Photopolymer recording materials are low cost, yield high diffraction efficiencies and are easy to prepare but it is their self developing property that makes them very suitable for use in holographic interferometry and the preparation of holographic optical elements.

Holographic and electronic speckle pattern interferometry both depend on the phenomenon of interference. A discussion about interference, fringe formation and different types of classical interferometers is given in the next chapter.

References

1. L. Solymar, D. J. Cooke "Volume holography and volume gratings," Chapter 10, Academic Press Inc, London, (1981).
2. H. I. Bjelkhagen, "Silver halide recording materials for holography and their processing," Springer-Verlag, Berlin, (1993).
3. V. Weiss, A. A. Friesem, "Storage mechanism of volume phase holograms recorded in silver halide emulsions," J. Opt. Soc. Am. A, 11, 2004-2010, (1994).
4. B. J. Chang, C. D. Leonard "Dichromated gelatin for the fabrication of holographic optical elements," Appl. Opt, 18, 2407, (1979).
5. T. A. Shankoff, "Phase holograms in dichromated gelatin," Appl. Opt, 7, 2101, (1968).

6. C. Solano, R. A. Lessard, P. C. Roberge, "Red sensitivity of dichromated gelatin films," Appl. Opt, 24, 1189-1192, (1985).

7. T. Kubota, T. Ose, M. Sasaki, K. Honda, "Hologram formation with red light in methylene blue sensitized dichromated gelatin," Appl. Opt, 15, 556-558, (1976).

8. C. Solano, R. A. Lessard, P. C. Roberge, "Methylene blue sensitized gelatin as a photosensitive medium for conventional and polarizing holography," Appl. Opt, 26, 1989-1997, (1987).

9. J. Zhu, G. Dong, X. Guo, Li. Chen, J. Li, "Methylene-blue sensitized dichromated gelatin: wide-range colour adjustment of reflection hologram," J. Opt. A: Pure. Appl. Opt, 6, 132-136, (2004).

10. J. Blyth, "Methylene blue sensitized dichromated gelatin holograms: a new electron donor for their improved sensitivity," Appl. Opt, 30, 1598-1602, (1991).

11. J. Zhu, Y. Zhang, G. Dong, Y. Guo, L. Guo, "Single-layer panchromatic dichromated gelatin material for lipmann color holography," Opt. Comm, 241, 17-21, (2004).

12. D. Pantelic, B. Muric, "Improving the holographic sensitivity of dichromated gelatin in the blue-green part of the spectrum by sensitizing with xanthene dyes," Appl. Opt, 40, 2871-2875, (2001).

13. G. M. Naik, A. Mathur, S. V. Pappu, "Dichromated gelatin holograms: an investigation of their environmental stability," Appl. Opt, 29, 5292-5297, (1990).

14. B. Pinto-Iguanero, A. Olivares-perez, A. W. Mendez-Alvarado, I. Fuentes-Tapia, C. G. Trevino-Palacios, "Non-hydroscopic vanilla doped dichromated gelatin holographic material," Opt. Materials, 22, 397-404, (2003).

15. J. M. Kim, B. S. Choi, Y. S. Choi, J. M. Kim, H. I. Bjelkhagen, N. J. Phillips, "Holographic optical elements recorded in silver halide sensitized gelatin

emulsions. Part2 reflection holographic optical elements," Appl. Opt, 41, 1522-1533, (2002).

16. M. V. Collados, I. Arias, A. Garcia, J. Atencia, M. Quintanilla, "Silver halide sensitized gelatin process effects in holographic lenses recorded on Slavich PFG-01 plates," Appl. Opt, 42, 805-810, (2003).
17. P. Hariharan, "Optical Holography principles, Techniques, and Applications," Cambridge University Press, London, (1996).
18. L. Mashev, S. Tocchev, "Formation of holographic diffraction gratings in photoresist," Appl. Phys. A: Solids and surfaces, 26, 143-149, (1981).
19. R. A. Bartolini, "Improved development for holograms recorded in photoresists," Appl. Opt, 11, 5, (1972).
20. R. A. Bartolini, "Characteristics of relief phase holograms recorded in photoresists," Appl. Opt, 13, 129-139, (1974).
21. F. Iwata, J. Tsujiuchi, "Characteristics of a photoresist hologram and its replica," Appl. Opt, 13, 1327-1336, (1974).
22. G. K. Megla, "Optical properties and applications of photochromic glass," Appl. Opt, 5, 945-960, (1966).
23. D. R. Bosomworth, H. J. Gerritsen, "Thick holograms in photochromic materials," Appl. Opt, 7, 95-98, (1968).
24. D. L. Staebler, W. Phillips, "Hologram storage in photochromic $LiNbO_3$," Appl. Phy. Lett, 24, 268-270, (1974).
25. A. Toriumi, J. M. Herrmann, S. Kawata, "Non destructive readout of a three-dimensional photochromic optical memory with a near-infrared differential phase-contrast microscope," Opt. Lett, 22, 555-557, (1997).

26. A. Toriumi, S. Kawata, "Reflection confocal microscope readout system for three-dimensional photochromic optical data storage," Opt. Lett, 23, 1924-1926, (1998).

27. S. Kawata, Y. Kawata, "Three-dimensional optical data storage using photochromic materials," Chem. Rev, 10, 1777-1788, (2000).

28. W. S. Colburn, E. N. Tompkins, "Improved thermoplastic-photoconductor devices for holographic recording," Appl. Opt, 13, 2934-2941, (1974).

29. TCC-2 Electronic holographic camera, "http://www.tavexamerica.com/film_specifications.htm," 10-08-2005.

30. Operators Manual HC-300 Holographic recording device, Newport Corporation, Irvine, USA.

31. D. Psaltis, F. Mok, "Holographic memories," Scientific American, 52, November (1995).

32. K. Buse, "Light induced charge transport process in photorefractive crystals I: Models and experimental methods," Appl. Phy. B, 64, 273-291, (1997).

33. J. J. Amodei, D. L. Stebler, A. W. Stephens, "Holographic storage in doped barium sodium niobate ($Ba_2NaNb_3O_{15}$)," App. Phy. Lett, 18, 507-509, (1971).

34. A. Ishida, O. Mikami, S. Miyazawa, M. Sume, "Rh-Doped LiNbO3 as an improved new material for reversible holographic storage," Appl. Phys. Lett, 21, 192-193, (1972).

35. M. R. R Gesualdi, D. Soga, M. Muramatsu, "Surface contouring by phase shifting real-time holography using photorefractive sillenite crystals," Opt. Laser. Tech, 5th July, (2005).

36. M. P. Georges, V. S. Scauflaire, Ph. C. Lemaire, "Compact holographic camera based on photorefractive crystals and applications in interferometry," Opt. Materials, 18, 49-52, (2001).

37. M. H. Yukselici, R. Ince, A. T. Ince, "Data storage characteristics of iron doped $LiNbO_3$ under a 90^0 geometry two-beam coupling configuration," Opt. Laser. Engg, 42, 277-287, (2004).

38. B. Koziarska-Glinka, J. M. Langer, A. Suchocki, L. Arizmendi, "Image holography in CdF_2 crystals," Opt. Materials, 10, 313-318, (1998).

39. A. Suchocki, J. Rauluszkiewicz, "Photoinduced metastable lattice dilation of CdF2: ln crystals," Appl. Phy. Lett 71, 1552-1554, (1997).

40. C. Carre, D. J. Lougnot, "Photopolymers for holographic recording: from standard to self-processing materials," J. de Physique, 3, 1445-1460, (1993).

41. W. S. Colburn, K. A. Haines, "Volume hologram formation in photopolymer media," Appl. Opt, 10, 1636-1641, (1971).

42. D. H. Close, A. D. Jacobson, J. D. Margerum, R. G. Brault, F. J. McClung, "Hologram recording on photopolymer materials," Appl. Phy. Lett, 14, 177-184, (1968).

43. S. Calixto, "Dry polymer for holographic recording," Appl. Opt, 26, 3904-3909, (1987).

44. S. Martin, P. Leclere, Y. Renotte, V. Toal, Y. Lion, "Characterization of an acrylamide-based dry photopolymer recording material," Opt. Eng, 33, 3942-3946, (1994).

45. S. Blaya, R. Mallavia, L. Carretero, A. Fimia, and R. F. Madrigal, "Highly sensitive photopolymerizable dry film for use in real time holography," Appl. Phys. Lett. 73, 1628–1630, (1998).

46. 1. Banyasz, "Hologram build-up in a near infrared sensitive photopolymer," Opt. Comm, 181, 215-221, (2000).

47. W. S. Colburn, K. A. Haines, "Volume hologram formation in photopolymer materials," Appl. Opt, 10, 1636-1641, (1971).

48. B. L. Booth, "Photopolymer materials for holography," Appl. Opt, 14, 593-601, (1975).

49. R. T. Ingwall, H. L. Fielding, "Hologram recording with a new photopolymer system," Opt. Engg, 24, 808-811, (1985).

50. L. Dhar, A. Hale, H. E. Katz, M. L. Schilling, M. G. Schnoes, F. C. Schilling, "Recording media that exhibit high dynamic range for digital holographic data storage," Opt. Lett, 24, 487-489, (1999).

51. K. Anderson, E. Fotheringham, A. Hill, B. Sissom, K. Curtis, "High speed holographic data storage at 100 Gbit/in^2," http://www.inphase-technologies.com/technology/whitepapers/pdfs/high_speed_data_storage.pdf 10-08-2005.

52. S. Martin, "A new photopolymer recording material for holographic applications: photochemical and holographic studies towards an optimized system," PhD Thesis, Trinity College, Dublin, August, (1995).

53. S. Martin, C. A. Feely, V. Toal, "Holographic Characteristics of an Acrylamide Based Recording Material," Appl, Opt, Vol. 36, 5757-5769, (1997).

4. Interferometry

Introduction

Precise measurement with high accuracy is an essential and prime requirement in metrology applications. Optical interferometers provide the measurements with high accuracy. Measurement accuracy of the optical techniques is of the order of the wavelength of light source. Since the wavelengths of laser sources used in interferometry are precisely known and highly stable, the measurements obtained are extremely precise and accurate. An interferometer can be considered as a measuring ruler with the wavelength of light as the measuring scale.

4.1 Interference of light

Consider two beams of light described by

$$A_1 = a_1 e^{i\phi_1} \quad \text{.....4.1}$$

where a_1, ϕ_1 are amplitude and phase of the first wave and

$$A_2 = a_2 e^{i\phi_2} \quad \text{.....4.2}$$

where a_2, ϕ_2 are the amplitude and phase of the second wave.

The resultant field created at the overlapping region is given by the summation of the two individual wave fields [2].

The intensity distribution at the plane of summation is given by

$$I = |A|^2 = |A_1 + A_2|^2 = a_1^2 + a_2^2 + 2a_1 a_2 \cos(\phi_1 - \phi_2)$$

$$I = I_1 + I_2 + 2\sqrt{I_1 I_2}\cos\Delta\phi \quad \text{.....4.3}$$

where $\Delta\phi = \phi_1 - \phi_2$ and I_1, I_2 are the intensities of the two waves.

The third term in equation 4.3 is an interference term $2\sqrt{I_1 I_2}\cos\Delta\phi$, interference fringes are produced in accordance with the variation of the phase difference $\Delta\phi$ between the two waves.

The intensity is maximum when the two waves are in phase with each other: $\Delta\phi = 2n\pi$ for $n = 0,1,2..$

The intensity is minimum when the two waves are out of phase with each other: $\Delta\phi = (2n+1)\pi$ for $n = 0,1,2..$

In a special case if the two waves are of equal intensity $I_1 = I_2 = I_0$, the intensity distribution at the plane of interference is given by

$$I = 2I_0[1+\cos\Delta\phi] = 4I_0\cos^2\left(\frac{\Delta\phi}{2}\right) \quad \text{.....4.4}$$

The intensity varies between the maximum and minimum values of 0 and $4I_0$. The variation of intensity is observed as bright and dark fringes.

4.2 Types of interferometer

An interferometer is an optical instrument which uses the interference of light and fringe patterns that result from optical path differences in a variety of ways to measure length, surface irregularities and index of refraction.

Interferometers are classified by the number of interfering beams, either two beam or multiple beam and the method used to split the beams.

Separate beam interferometers

In a separate beam interferometer incident light beam is divided into separate beams. If the radiation from the source is passed through one of several apertures then the interferometer is said to be a "division of wavefront" type. If the division of the beam is effected by a beam splitter the interferometer is said to be of the "division of

amplitude" type. The Michelson interferometer is the oldest and best known division of amplitude type of interferometer.

4.2.1 Michelson interferometer

Michelson interferometry [3] is a well known technique used for precise distance measurement. A beam splitter divides and recombines the two light beams. A schematic of the interferometer is shown in Figure 4.1.

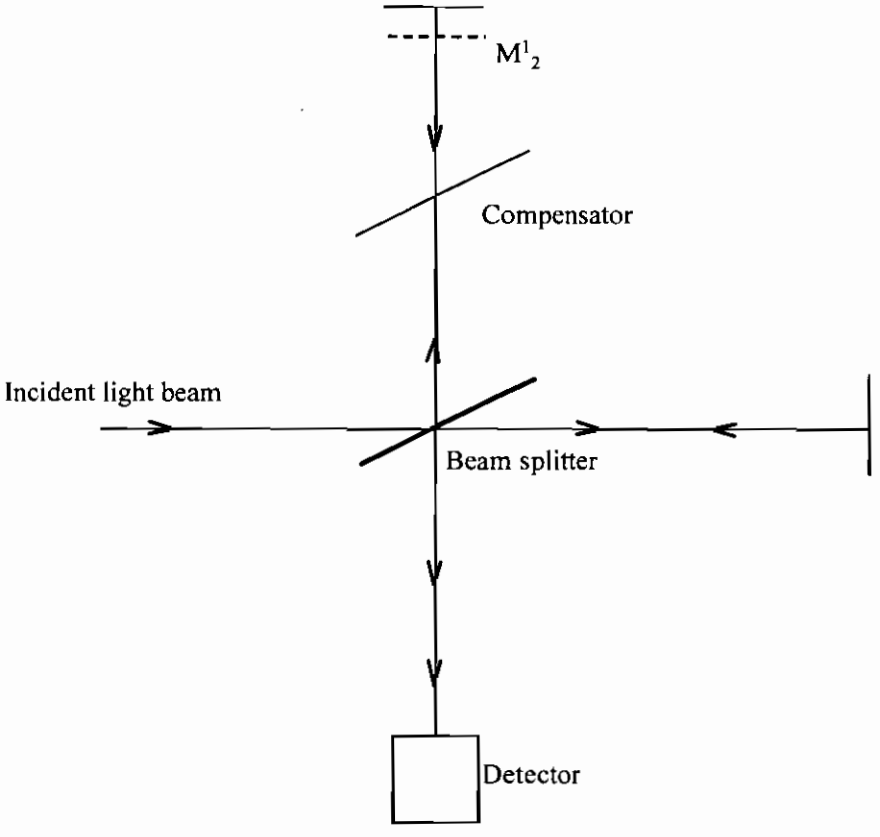

Figure 4.1 The Michelson interferometer

Light from an extended source is split by a partially reflecting beam splitter. The two separated beams in the interferometer are reflected by the mirrors M_1 and M_2 and they are recombined at the beam splitter to interfere with each other. A detector placed in the path of the recombined beams detects the interference signal. The path length difference in the interferometer is changed by moving one of the mirrors (M2). A compensator plate is inserted in order to make the optical paths in glass traveled by two

beams to be the same. The intensity of the interference fringe pattern at the detector plane is given by

$$I(X) = 2I[1 + \cos(\frac{4\pi x}{\lambda})] \quad \text{.....4.5}$$

where x is the distance moved by the mirror M2. λ is the wavelength of light.

When the two mirrors are not making any angle with each other, the fringes observed at the detector plane are concentric and of equal inclination. The fringes represent contours of equal path length difference.

The Michelson interferometer is used to measure the wavelength difference between two closely spaced spectral lines. The wavelength difference between two lines such as the components of the sodium D line is determined from their average wavelength and the visibility of the fringes [4, 5]. Two sets of fringes are formed at the plane of observation corresponding to two slightly different wavelengths (λ, λ^{1}) of the sodium line. At certain positions of the mirror M2 fringes are sharp and at intermediate positions the fringes are not sharp. These two states of the fringe pattern correspond to fringe visibility maximum and minimum. The separation of the positions of the maximum (or minimum) visibility determines the wavelength difference. The wavelength difference is calculated using the formula

$$\frac{\lambda\lambda^{1}}{2(d_a - d_b)} \quad \text{.....4.5}$$

where d_a represents a point where two sets of fringes form a maximum visibility and mirror M1 is translated from maximum visibility to next maximum visibility and this position is d_b.

4.2.2 Mach-Zehnder interferometer

The Mach-Zehnder interferometer [6] is a variation of Michelson interferometer. It is used for comparing optical paths in two separated beams. The separation of the beams is large compared to that in a Michelson interferometer. A schematic of the Mach-Zehnder interferometer is shown Figure 4.2. An incident beam of parallel light is divided into two beams (B, C) at BS. Each of the beams is totally reflected at M1, M2. The two beams (D, E) are again made coincident by the beam combiner (BC). Superposition of the two beams produces the interference fringes.

Because of its relatively large and freely accessible working space and the flexibility of location of the fringes, the Mach-Zehnder interferometer is most suitable for study of the density variations in gas-flow patterns, heat transfer, and the temperature distribution in plasmas. It is useful in aerodynamic research to study the geometry of air flow around an object in a wind tunnel. A windowed test chamber is placed in one arm of the interferometer, into which a steam line flow of air is introduced. An identical empty chamber is placed in the other arm of the interferometer to maintain the equal optical paths. The air-flow pattern is revealed by the fringe pattern.

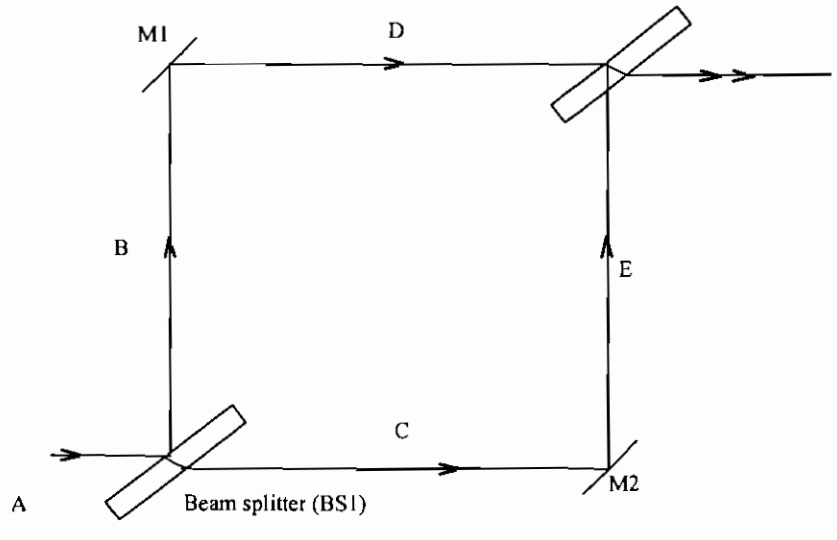

Figure 4.2 Mach-Zehnder interferometer

4.2.3 Fizeau interferometer

The Fizeau interferometer is used for testing optical components. Interference fringes of equal thickness are formed between two flat surfaces separated by an air gap when illuminated with a collimated beam of light. Optical components are tested using one flat reference surface in the interferometer. The irregularities on the test sample create the path length difference and interference fringes formed are the contours of the errors on the test surface. A schematic of the interferometer is shown in Figure 4.3.

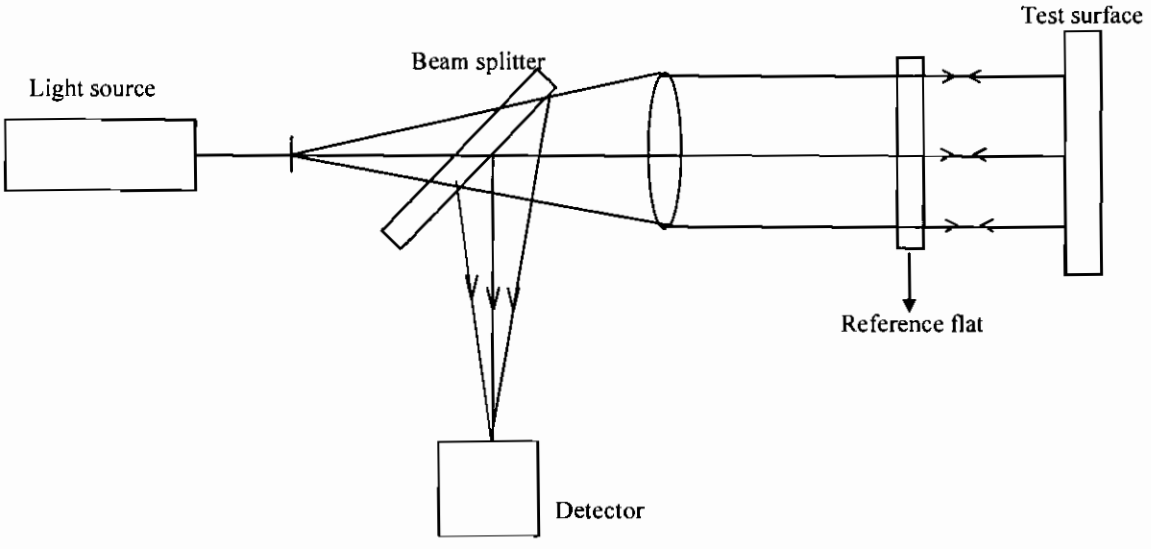

Figure 4.3 Fizeau interferometer

4.2.4 Fabry-Perot interferometer

The Fabry-Perot interferometer is used for precision wavelength measurement, analysis of hyperfine spectral line structure and to determine the refractive index of gases. The interferometer uses the multiple reflections between two reflecting surfaces aligned precisely parallel. If the distance between the mirrors is fixed it is called a Fabry-Perot etalon. The Fabry-perot etalon is also the basis of a laser resonant cavity. The inner surfaces of the mirrors are coated to give high reflectance. An incident light beam is partly transmitted by the first mirror and partly reflected at the second reflecting surface. This process continues and a large number of rays are generated due to the

multiple reflections within the cavity. A schematic of the interferometer is shown in Figure 4.4. Interference is created between the multiple beams due to the multiple reflections from the semi-silvered mirrors. The fringes formed in a Fabry-Perot interferometer are sharp with high contrast compared with fringe patterns obtained with Michelson interferometer [7, 8].

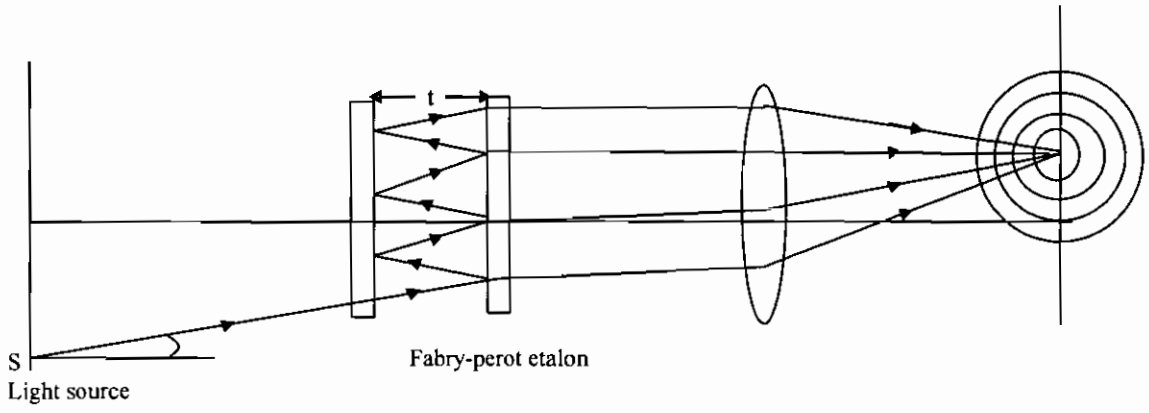

Figure 4.4 Fabry Perot interferometer

4.3 Advantages of optical interferometers

Optical interferometers are used for precision measurements such as the length, wavelength of light sources and profiles of a surface with precision of the order of wavelength of light used, but they are only applicable to highly polished surfaces of optical quality. There is a need for whole field techniques such as holographic interferometry and electronic speckle pattern interferometry able to work with rough surfaces with high precision and accuracy.

The interferometers described in this chapter are useful instruments for high precision measurements using the wavelength of light as the scale of measurement, however only high optical quality surfaces with simple shapes can only be tested. In the next chapter the practical use of holographic interferometry is described. It is seen that wavelength scale measurements can be made even on an optically rough surface using

holographic interferometry. The self-processing ability of the photopolymer material allows the use of live fringe technique in holographic interferometry.

References

1. W. H. Steel, "Interferometry," Cambridge University Press, London, (1967).
2. K. J. Gasvik, "Optical Metrology," John Wiley & Sons Ltd, England, (1995).
3. F.G. Smith, T.A. King, "Optics and Photonics," John Wiley & Sons Ltd, England, (2000).
4. http://helios.augustana.edu/~cv/351/EXPERIMENTS2003/MICHELS0N2003.doc, July, (2005).
5. http://repairfaq.ece.drexel.edu/sam/CORD/leot/course10_mod04/mod10-04.html, July, (2005).
6. F. L. Pedrotti. S. J, L. S. Pedrotti, "Introduction to optics," 2nd edition, Prentice-Hall Inc, New Jersey, (1993).
7. G. W. Chantry, "The use of Fabry-Perot interferometers, etalons, and resonators at infrared and longer wavelengths- an overview," J. Phys. E: Sci, Instrum, 15, 1-6, (1982).
8. J. R. Meyer-Arendt, "Introduction to classical and modern optics," Chapter 12, 4th ed., Prentice-Hall Inc, New Jersey, (1995).

5. Holographic interferometry using photopolymer recording material

Introduction

Holographic interferometry is a non-contact, whole field non-destructive evaluation technique [1]. It is a valuable tool for measuring displacements of optically rough materials and components under static and dynamic loading conditions with sensitivity of the order of the wavelength of the light used. Unlike in the conventional interferometers described in the previous chapter, in holographic interferometry one of the wavefronts is generated from a hologram. Live fringe and double exposure techniques are used in holographic interferometry. These techniques are described in section 5.2. The main theme of this chapter is the use of photopolymer recording material in holographic interferometry. The self processing ability of the photopolymer recording material eliminates the chemical processing involved in using conventional recording materials such as silver halide emulsions and dichromated gelatin.

5.1 Fringe formation

Holographic interference fringes are formed as a result of the interference between the light wavefronts scattered from identical surfaces placed at slightly different positions in space [2]. The wavefronts interfere on a common plane; the fringes can be seen by an observer or they can be photographed.

Let ψ be the phase of light scattered from a given point on the undisplaced object. ψ^1 is the phase of light scattered from the object in its displaced position. Both wavefronts can be observed from the same point of observation in the viewing plane. The phases of the two wavefronts are related by the equation

$$\psi' = \psi + \left(\frac{2\pi}{\lambda}\right)[n_o - n_s] \bullet d \quad \text{.....5.1}$$

d = displacement of object point.

n_0, n_s are unit vectors in the directions of illumination and viewing the object point.

The amplitude of light arriving at a point in the viewing plane before displacement can be written as

$$U_1 = u_0 \sum_{p=1}^{n} e^{i\psi_p} \quad \text{.....5.2}$$

where u_0 = amplitude of light scattered by an individual scattering point in a resolution element (assuming all points scatter the same amplitude).

ψ_p = phase of light scattered by p^{th} point. The resolution element has n points.

Amplitude of light at the same point after the object displacement is given by

$$U_2 = u_0 \sum_{p=1}^{n} e^{i(\psi_p + \phi_p)} \quad \text{.....5.3}$$

where $\phi_p = (\frac{2\pi}{\lambda})[n_0 - n_s] \bullet d_p$

The resultant intensity at the plane of interference is given by [2]

$$I = (U_1 + U_2)(U_1^* + U_2^*)$$
$$= u_0^2 \sum_p \sum_q e^{i(\psi_p - \psi_q)} + e^{i(\psi_p^1 - \psi_q^1)} + 2\cos(\psi_p + \phi_p - \psi_q) \quad \text{.....5.4}$$

The value of I varies across the viewing plane. The mean value can be found by separating the summation of equation (5.4) into terms with p = q, and terms with $p \neq q$. The mean value of the intensity is given by

$$\langle I \rangle = 2u_0^2 n(1 + \cos\phi_p) + cross\ terms \quad \text{.....5.5}$$

Equation 5.5 is averaged over many speckles, the cross terms cancel out during the average process. The final intensity value is

$$\langle I \rangle = 2u_0^2 n(1+\cos\phi_p) \quad \text{.....5.6}$$

Intensity is maximum when $\phi_p = 2n\pi$ with n=0, 1, 2,

Intensity is minimum when $\phi_p = (2n+1)\pi$ with n=0, 1, 2,

The variation of intensity distribution between the maximum and minimum values results in a bright and dark interference fringe pattern.

5.2 Different techniques of holographic interferometry

Double exposure, live fringe are two techniques used in holographic interferometry. Time average holographic interferometry is a technique used to study the vibration modes of object.

5.2.1 Double exposure technique

In this technique a hologram of test object is recorded twice on a photosensitive medium [3]. The first hologram is recorded when the object is in an un-displaced position. A second hologram is recorded on the same recording medium with the object displaced from the initial position. Thus the hologram effectively contains the wavefronts of the object in two different states. Upon reconstruction, the hologram reproduces two wavefronts, one corresponding to an un-deformed position of the object and the second corresponding to a deformed position of the object. The two wavefronts superimpose and produce the interference fringes. The image of the test object is covered with dark and bright fringes due to the object displacement. A schematic of the technique is shown in Figure 5.1.

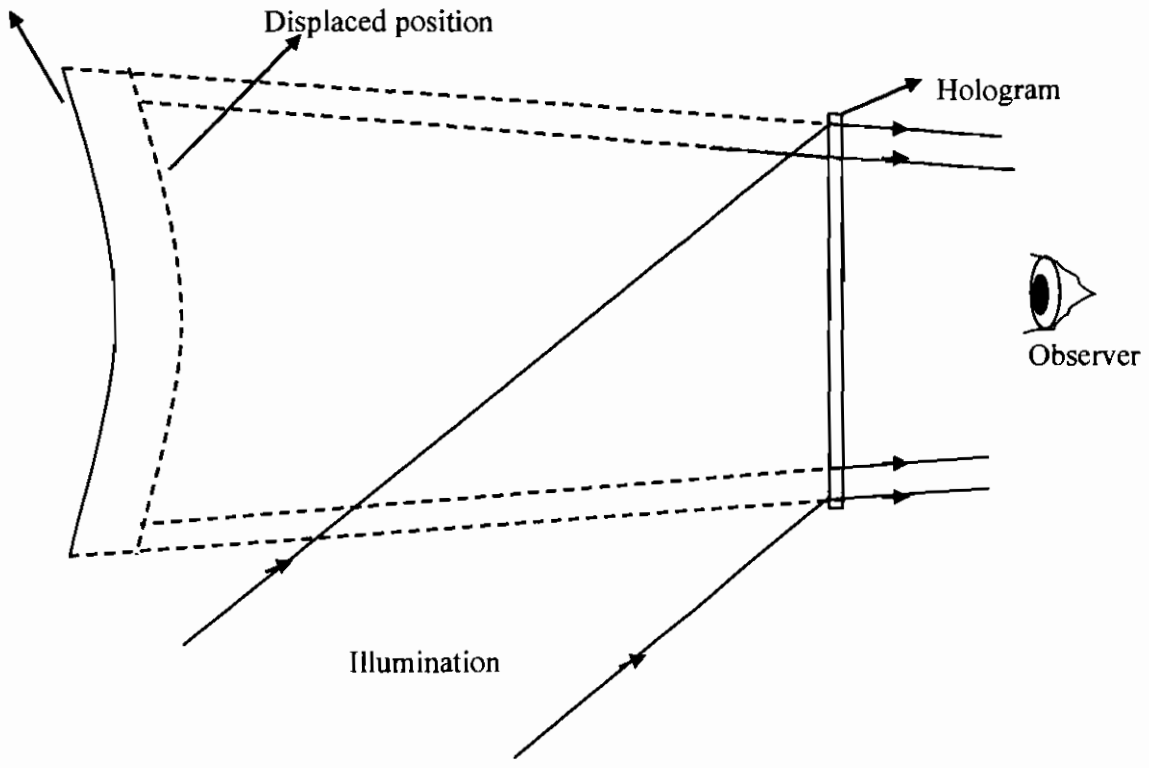

Figure 5.1 Double exposure holographic interferometry

The object wavefront in two different states is given as U_{01}, U_{02}. The reference wave U_R and the two object wavefronts interfere on the photosensitive medium.

The intensity distribution recorded in the hologram is given by the equation similar to the equation (2.6), except with two complex amplitude distributions of the object wavefront.

$$I = |U_{01}|^2 + |U_{02}|^2 + |U_R|^2 + U_R^*(U_{01} + U_{02}) + U_R(U_{01}^* + U_{02}^*) \quad \text{.....5.7}$$

* denotes the complex conjugate of the function. When the hologram is illuminated with the reference wave, the reconstructed wave contains the term $(U_{o1} + U_{o2})$

$$U_i \propto (U_{01} + U_{02}) \quad \text{.....5.8}$$

The complex amplitudes of the object wavefront in two states are expressed by

$$U_{01} = A_0 e^{i\phi_{01}(x,y)}$$

and

$$U_{02} = A_0 e^{i\phi_{02}(x,y)} \quad \text{.....5.9}$$

A small displacement causes the phase of the object wavefront to alter. ϕ_{o1} and ϕ_{02} are the phases due to the object in its un-displaced and displaced positions.

The intensity distribution of the reconstructed image is given by

$$I_d = |U_0|^2 \propto 2|A_0|^2 \{1 + \cos(\phi_{02} - \phi_{01})\} \quad \text{.....5.10}$$

$(\phi_{o2} - \phi_{o1})$ is the direct measure of the additional path length introduced due to the object displacement.

A bright fringe is produced whenever the phase difference is $2n\pi$, with n=0, 1, 2

A dark fringe is produced whenever the phase difference is $(2n+1)\pi$, with n=0, 1, 2

Double exposure holographic technique has been used in many areas as a non-destructive evaluation tool. Some of the application areas include the behaviour of the human chest during free and forced inhalation [4], vibration study of engineering structures and flaw detection [5] and detection of detached regions in ancient paintings [6].

5.2.2 Live fringe or real time technique

In the live fringe technique [3] a hologram of an object is recorded, after development the hologram is placed exactly in the same position where it was before. The hologram has to be replaced in its original position with accuracy of the order of the wavelength of light used in order to ensure that no fringes are produced due to phase differences between the object wave and the reconstructed wave. Any fringes seen must be due only to the displacement of the object. Usually the laser wavelength is around 0.5 μm so the replacement accuracy required is difficult to achieve. The hologram is illuminated with the reference beam; at the same time the object is also illuminated with

the same beam as when the hologram was recorded. The reconstruction from the hologram is thus superimposed on the object. The object is subjected to change and the interference fringes are generated between the wavefront reconstruction from the hologram and the new state of the object wavefront. The fringe pattern is seen by the observer or recorded with a CCD camera, in real time. A schematic of the technique is shown in Figure 5.2.

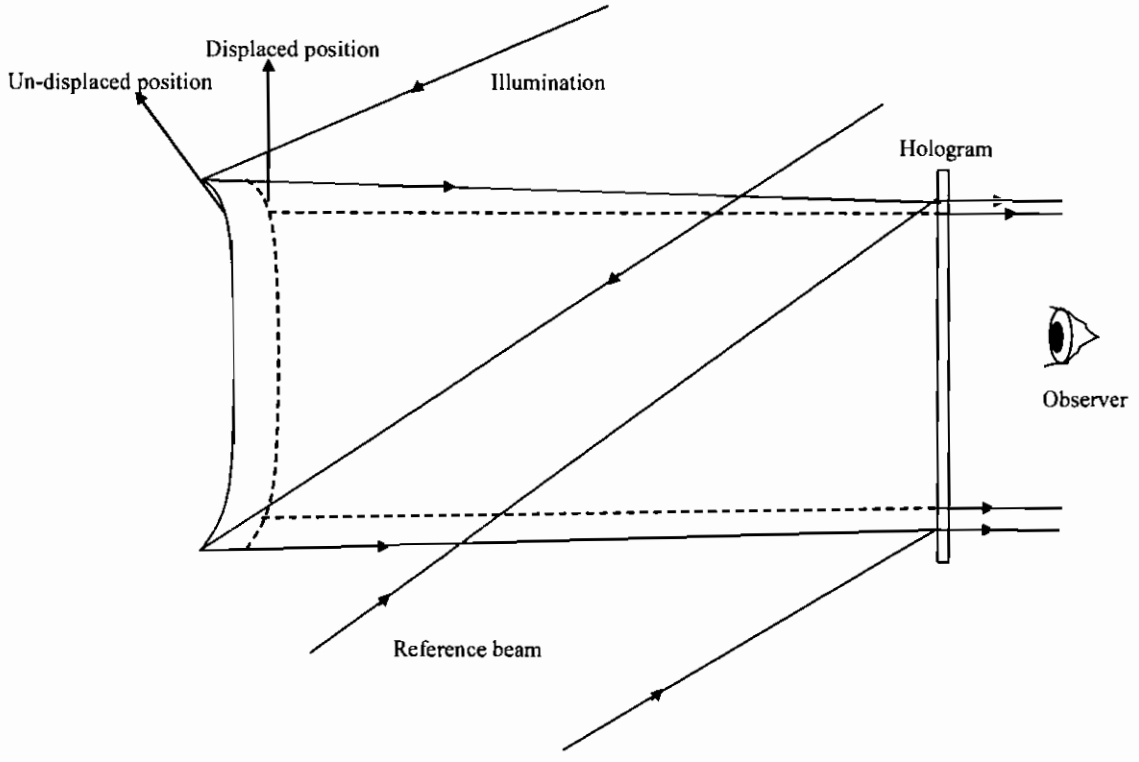

Figure 5.2 Live fringe holographic interferometry

This technique is advantageous compared with the double exposure technique because there is no need to make a hologram of the object when it is subjected to a change. The change in object is observed in real time. Dynamic and static motions are measured using this technique.

The complex amplitude distribution of the reconstructed image is given by equation 5.8

Here U_{01} is the complex amplitude of the object wavefront reconstructed from the hologram when the object is at rest. U_{02} is the complex amplitude of the wavefront scattered from the object when it has undergone a change.

The intensity distribution of the reconstructed image is given by

$$I_r \propto 2|A|^2\{1+\cos(\phi_2-\phi_1)\} \quad \text{.....5.11}$$

The equation is similar to equation (5.10) and bright and dark fringes appear as stated for double exposure technique. The only difference between the two techniques is the way the two object wavefronts are obtained.

5.2.3 Time average technique

In this technique the hologram of an object is recorded while it is subjected to vibratory motion. The hologram recording time is long compared to one period of vibration. An assembly of images corresponding to all positions of the object during its vibration is recorded. Upon illuminating the hologram with the reconstruction beam, interference takes place among the assembly of wavefronts. A fringe pattern corresponding to the vibration of the object is formed [7].

The complex amplitude of an object vibrating with a frequency ω and amplitude "a" is given by

$$U = A_0 e^{i(ka\cos\omega t)} \quad \text{.....5.12}$$

where k is the wave number.

The hologram is recorded for every position of the object when it is vibrating. After taking time averaging and applying the Bessel integral the intensity distribution of the reconstructed image is given by [8]

$$I_t \propto |A_0|^2 J_0^2\left(\frac{4\pi}{\lambda}a\right) \quad \text{.....5.13}$$

The intensity distribution of the reconstructed image is a zero order Bessel function with an argument containing amplitude of vibration "a". The areas with maximum brightness in the fringe pattern vibrate with zero amplitude and are also known as nodes of vibratory motion. The areas vibrating with maximum amplitude are known as anti nodes. With increased fringe number the intensity of the fringes decreases as the square of the zero order Bessel function. Stetson and Powell used this technique for vibration analysis of diffuse objects for the first time soon after the invention of off-axis holography [9].

In vibration analysis the real time technique is very useful because it is essential to record a series of holograms successively in order to achieve the right excitation, frequency and the amplitude of the vibration modes. Real time technique reduces the time and labour to record the hologram for each excitation frequency to find the vibration mode of interest [7, 10].

5.3 Sensitivities

Holographic interference fringes are generated due to the phase shift caused by the change of path length as a result of object displacement. The displacement of the object is measured by analyzing the fringe pattern. The displacement can be resolved in two directions; along the direction normal to the surface of the test object (out-of-plane) and in the direction parallel to the object surface (in-plane).

5.3.1 Out-of-plane sensitivity

In an out-of-plane sensitive system the object surface is illuminated along the surface normal and it is viewed along the surface normal through the hologram during reconstruction. The fringe equation with this type of optical geometry is given by [11]

$$N\lambda = 2d \quad \text{.....5.14}$$

d = out-of-plane displacement, N = number of fringes counted (appearing or disappearing) in the field of view, λ = wavelength of laser light.

In reality it is impractical to meet the above condition because it is not possible to illuminate and view the object along its surface normal. The object is viewed at an angle θ to the object surface normal (Figure 5.3). In this case the equation is modified to read

$$N\lambda = d(1 + \cos\theta) \quad \text{.....5.15}$$

θ is angle between the illumination and observation directions.

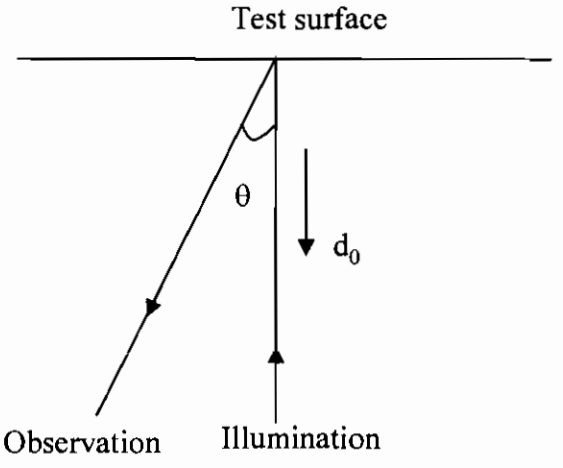

Figure 5.3 Geometry of out-of-plane sensitivity

5.3.2 In-plane sensitivity

Holography is more sensitive to out-of-plane motion, because the object surface is displaced more or less normal to the directions of observation and illumination. In in-plane motion the component of the displacement is parallel to the object surface, or the component of the displacement and surface normal are perpendicular to each other. A schematic of the in-plane sensitivity is shown in Figure 5.4. In-plane motion of the object can be measured by illumination and/or observation at an angle to the surface normal [12].

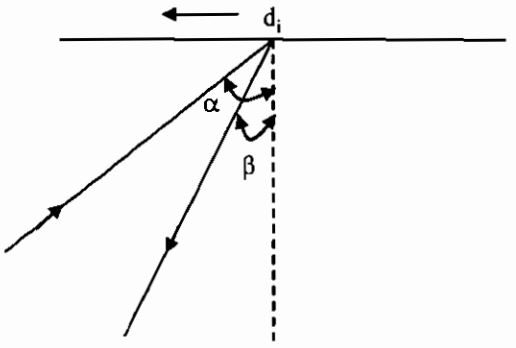

Figure 5.4 Geometry of in-plane sensitivity

The in-plane displacement, d_i is calculated using the equation [11].

$$d_i = \frac{N\lambda}{\sin\alpha + \sin\beta} \quad \text{.....5.16}$$

where α, β are the angles of illumination and observation with respect to the surface normal.

N is the number of fringes counted in the field of view due to the object displacement. It is assumed here that there is only in-plane displacement. In general the configuration described is most suitable when the test object is flat. If the test specimen is not flat, some parts of the object will be in shadow. To overcome this problem when measuring in-plane displacement on non-flat objects the geometry of an in-plane sensitive interferometer (Figure 5.4) has to be modified. The test surface is illuminated at an angle from two sides to the surface normal (Figure 5.5). The fringes can be viewed along the direction of the surface normal. The in-plane displacement is calculated by modifying the equation 5.16 with $\alpha = \beta$

$$d_i = \frac{N\lambda}{2\sin\alpha} \quad \text{.....5.17}$$

2α is the angle of separation between the two beams. The direction of maximal sensitivity will be in the plane of the two illuminating beams and normal to the bisector.

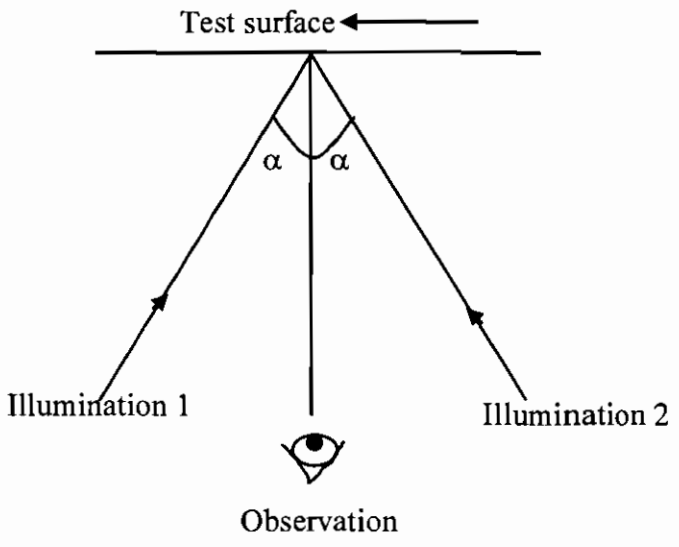

Figure 5.5 Modified geometry for measurement of in-plane sensitivity

5.4 Live fringe technique using photopolymer recording material

The repositioning problems which usually occur when using conventional recording materials such as silver halide emulsions and dichromated gelatin are completely eliminated by using this self-developing photopolymer. The fringes are seen while a change is applied to the object. The advantages with live fringe technique using self developing photopolymer over double exposure technique include: no delay between recording and viewing the hologram, ability to measure under dynamic and static loading conditions and no need to record a number of holograms.

An acrylamide based photopolymer formulated and developed at the Centre for Industrial and Engineering Optics [13] was used as a recording material in holographic interferometry. The holographic characteristics of the material are explained in chapter 3 (section 3.7.3.4).

5.4.1 Photopolymer material preparation

Photopolymer layers were prepared in the laboratory the day before conducting the experiment. The layers have to be dried at least for 24 hours. The laboratory was

equipped with facilities such as an accurate humidity controller, completely dark environment and electronic balance. The humidity in the laboratory was maintained at 60 to 70% using a humidity controller. The layers were coated on clean glass plates 5 cm×5 cm. It is highly recommended to level the surface on which the glass plates were placed because the layers were dried by gravity settling and any degree of tilt produces layers with variable thickness. The polymer coated glass plates were placed on a finely polished granite slab, which was accurately leveled to one millimeter over its dimensions (120 cm × 50 cm).

Polyvinyl alcohol (PVA) was used as the binder. 17.5 ml of 10% PVA solution was prepared and 2 ml of triethanolamine (electron donor) was added to the binder. The dye solution was prepared by dissolving 0.11 grams of erythrosin B in 100 ml of water. 4 ml of dye solution, 0.6 gm of acrylamide and 0.2 gm of bisacrylamide were added to the mixture of PVA and triethanolamine. The mixture was stirred well. 4 ml of the solution was used to produce layers of approximately 180 μm.

5.4.2 Experimental measurement of radial strain measurement in a thick polyvinyl chloride pipe using live fringe HI

The live fringe technique was used to characterize a thick walled polyvinyl chloride pipe of inner and outer diameters, 31.2 cm and 37.2 cm respectively and 28.3 cm length. It was closed at both ends with steel rods bolted through flat steel plates and vertically supported (Figure 5.6). A pump was attached to the top to pressurize the pipe. The pressure gauge attached to the pump could read the pressure value up to 2×10^5 N/m^2. The experiment was carried out at a room temperature of 20° C.

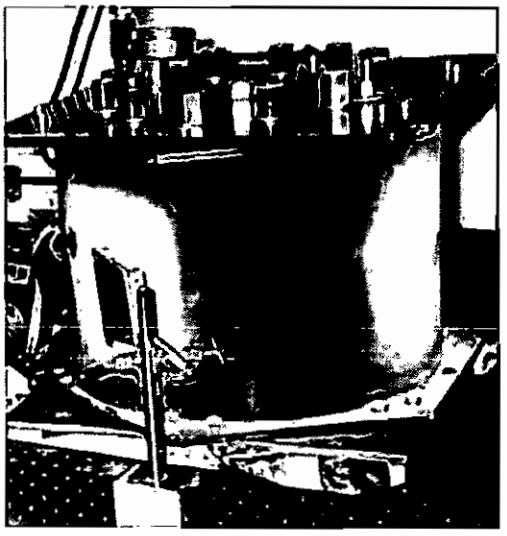

Figure 5.6 PVC pipe test object

As a result of applied pressure the pipe experiences strain. Using holographic interferometry the strain was measured and its Young's modulus of elasticity was calculated.

Theory:

When a thick cylinder is subject to internal pressure (P), the tangential stress (σ) at the outer surface is given by [14]

$$\sigma_t = \frac{2PR_1^2}{(R_2^2 - R_1^2)} \quad \text{.....5.18}$$

R_1 and R_2 are internal and external radii of the pipe respectively. P is the internal pressure. A schematic of the top view of the pipe is shown in Figure 5.7.

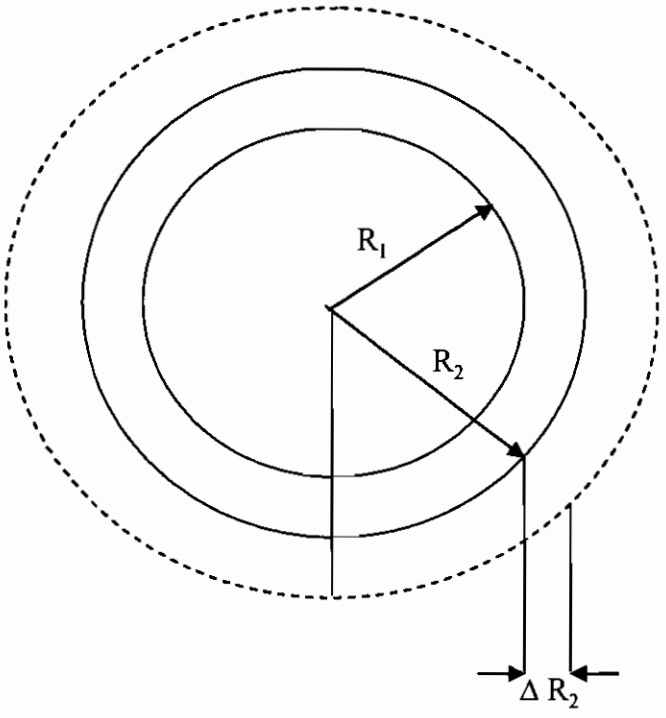

Figure 5.7 Top view of the pipe

The Young's modulus of elasticity of the material is calculated using the formula whose derivation is given in references 14, 15.

$$E = \left(\frac{PR_1^2(2-\nu)}{(R_2^2 - R_1^2)\varepsilon_t} \right) \quad \text{.....5.19}$$

ν = Poisson's ratio = 1/3, P= Pressure, ε_t = radial strain

When the pipe is pressurized internally it expands radially. It will have maximum radial displacement normal to the surface, i.e. out-of-plane displacement.

The radial strain is the change in length per unit length in a direction radially outward due to the applied change and it was calculated in the present situation using the formula [15]

$$\varepsilon_t = (\frac{\Delta R_2}{R_2}) \quad \text{.....5.20}$$

ΔR_2 is the change in outer radius of the cylinder due to the applied pressure. It was calculated using equation (5.15).

Experimental description

The experiment was conducted on a 3 m × 1.3 m Newport research tabletop with pneumatic isolation on all four support legs, in order to minimize the transmission of vibrations from the floor to the table. Newport magnetic stands were used to hold the optical components in position. The laser (Coherent) with power output of 5 Watt CW operating at 532 nm, operated with a water-cooling unit (Thermostat). The polarization state of the laser light was vertical. The laser light was spatially filtered with a 20X microscopic objective with a pinhole diameter of 20 μm. The PVC pipe was placed in the path of laser light and some of the light was made to fall on a mirror beside the pipe. An area of 10 cm × 10 cm on the surface of the object was illuminated with the laser light. The scattered light from the pipe and the light reflected from the mirror were made to interfere at the recording plane where a polymer coated glass plate was placed as shown in Figure 5.8.

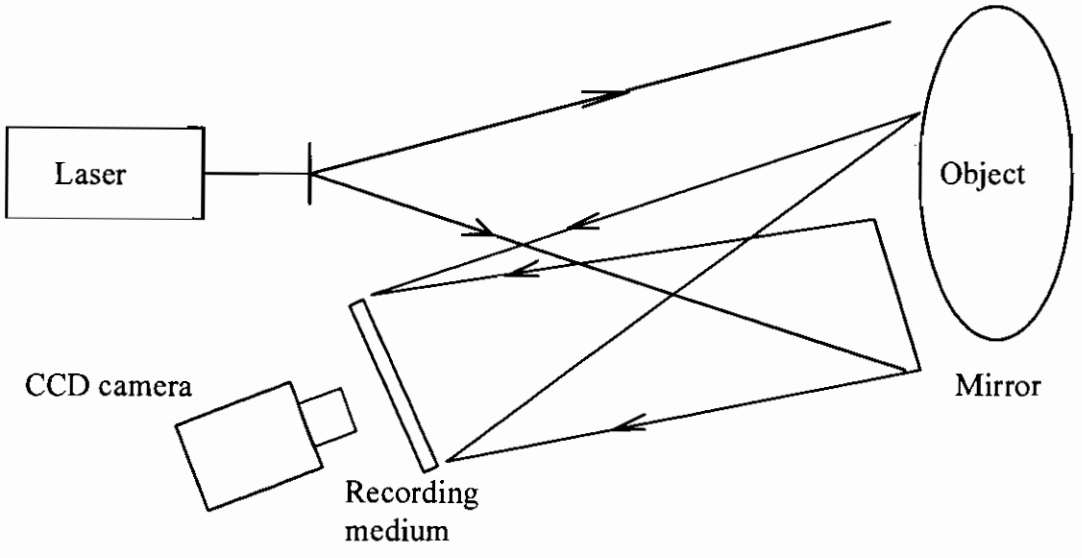

Figure 5.8 Experimental setup

The exposure time was controlled by an electronic shutter system (Uniblitz T132 timer and VS 25 shutter). Repeated recordings showed that the optimum exposure to obtain interference fringes with good contrast was 20 mW/cm^2 with 45 seconds

exposure time. The experiment was carried out when the laboratory environment was free from outside disturbances such as mechanical disturbances. The holographically reconstructed image of the pipe was seen with the naked eye by blocking the object with black cloth. This exercise was required to make sure that a good quality hologram was recorded. The pipe was then pressurized and fringes were generated by the interference between the reconstructed wavefront of the object and wavefront from the object itself, in real time. Circular fringes were seen at the centre of the hologram, expanding outwards from the centre. A letter H was marked on the object surface with a permanent marker pen. Holographic reconstruction of the object wavefront was easily observed by finding the image of the letter H with the object covered with block cloth. Also the position of the letter was used as reference point to count the number of holographic interference fringes crossing through the point. The number of fringes passing through the letter H (Figure 5.9) appearing in the field of view were counted. The fringes were also captured with a CCD camera. An example of the live holographic out-of-plane displacement fringe pattern for a pressure of 0.5×10^5 N/m^2 is shown in Figure 5.9. The fringes are contours of constant optical path difference in the interferometer, created due to the pressure change. The fringes grew outward from the centre of the field of view as the cylinder expanded radially.

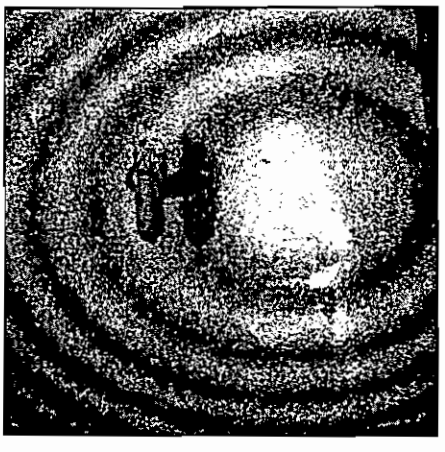

Figure 5.9 Out-of-plane displacement holographic interference fringes

In an out-of-plane sensitive interferometer the observation direction should be along the direction of illumination in an ideal situation but this is often not possible can be seen from Figure 5.8. In the present interferometer the angle between the observation and illumination directions was made as small as possible. The angle between the directions of illumination and observation (measured by using the geometry shown in Figures 5.3 & 5.9) was found to be 19°.

The pipe was inflated to different pressures in the range from 0 to 2 $\times$ 10^5 N/m^2. The number of fringes appearing was counted for each increment of pressure. Experimental results are shown in table 5.1. The radial strain value was calculated using equation 5.20 for four different pressure increments. It was observed that the fringe count was the same for equal increments of pressure. From this it can be concluded that the radial strain is proportional to applied pressure and it was assumed that the expansion of the pipe is linear over the range of pressure used.

Table 5.1 Results radial strain measurement

Pressure ($\times$ 10^5 N/m^2)	d(μm)	Fringe Number(N)	Radial strain (micro strain)
0.5	13.39	49	72.03
1.0	26.79	98	144.07
1.5	40.19	147	216.11
2.0	53.59	196	288.14

The Young's modulus of elasticity of the material was calculated using equation 5.19. The value was found to be 2.74 GN/m^2. This value is close to the value quoted by the manufacturer which is 2.80-3.2 GN/m^2 [15].

5.4.3 Error sources

The value of Young's modulus of elasticity calculated using holographic interferometry does not fall within the range of values quoted by manufacturer. The reason for this could be due to error in the angle between illumination and observation (θ) and error in counting the number of fringes (N).

Error due to angle between illumination and observation (θ):

Out-of-plane displacement was calculated using the expression

$$d = \frac{N\lambda}{(1+\cos\theta)} \quad \text{.....5.21}$$

Error in out-of-plane displacement due to the angle θ in the above expression is calculated by taking the partial derivative with respect to θ.

$$\frac{\partial d}{\partial \theta} = -N\lambda(1+\cos\theta)^{-2}(-\sin\theta) = \frac{N\lambda\sin\theta}{(1+\cos\theta)^2}\Delta\theta \quad \text{.....5.22}$$

Usually an error of ± 0.5° would occur in measuring the angle.

Using the values θ = 19°, $\lambda = 0.532\times 10^{-6}$, N = 49, $\Delta\theta$ = ± 1/2 degree in equation 5.22 the error in out-of-plane displacement is found to be ± 0.02μm. The error due to angle produces an uncertainty of ± 0.1% error in the Young's modulus of elasticity.

Error due to fringe counting (N):

The error due to the fringe count is calculated by taking the partial derivative of equation 5.21 with respect to N

$$\frac{\partial d}{\partial N} = \left(\frac{\lambda}{1+\cos\theta}\right)\Delta N \quad \text{.....5.23}$$

Usually an error of ± 0.5 would occur in the fringe number (N)

Using θ = 19°, $\lambda = 0.532\times 10^{-6}$, ΔN = 0.5 in equation 5.23, error in out-of-plane displacement is found to be ± 0.14 μm. The error due to fringe number produces an uncertainty of ±1% in the Young's modulus of elasticity.

The root mean square error is found to be 0.14 μm. So the uncertainty in fringe number is the greater source of error.

5.5 Conclusions

The acrylamide based photopolymer formulated and produced in the Centre for Industrial & Engineering Optics was successfully used in holographic interferometry. The self processing capability of the recording material reduces the time required for testing. Tedious chemical development procedures are completely eliminated. The interference fringes were seen in real time while the change was applied to the object. These advantages make the material useful in industrial applications. Although HI is a useful non contact and whole field measurement technique, the measurement capability of the technique is limited by the ability to resolve the interference fringes. In the present experiment it was possible to count the fringes up to a pressure of 2×10^5 N/m^2 and after that the fringes were too close together and it was not possible to count them. This drawback can be overcome by using the alternative technique known as ESPI. In the next chapter optical testing using ESPI is described. This technique has been in use since for more than three decades. The advance presented in this thesis is the use of a photopolymer HOEs to make the ESPI system simple and compact. The HOE is used as the key element in an ESPI system. This is discussed in detail in the following chapters. It will also be seen that in this type of optical system, both holographic interferometry and ESPI techniques can be implemented at the same time.

References

1. R. K. Erf, "Holographic nondestructive testing," Academic Press Inc, London, (1974).
2. R. Jones, C. Wykes, "Holographic and speckle interferometry," Cambridge University Press, Cambridge, (1983).

3. P. K. Rastogi, "Optical measurement techniques and applications," Artech House Inc, Norwood, USA, (1997).

4. P. Greguss, "Holographic interferometry in biomedical sciences," Opt. Laser. Tech, 8, 153-159, (1976).

5. R. C. Sampson, "Holographic interferometry applications in experimental mechanics," Exp. Mech, 10, 313-320, (1970).

6. S. Amadesi, F. Gori, R. Grella, G. Guattari, "Holographic methods for painting diagnostics," Appl. Opt, 13, 2009-2013, (1974).

7. K. A. Stetson, R. L. Powell, "Interferometric hologram evaluation and real-time vibration analysis of diffuse objects," J. Opt. Soc. Am, 55, 1694-1695, (1965).

8. C. M. Vest, "Holographic interferometry," John Wiley & Sons Ltd, USA, (1979).

9. H. Bjelkhagen, "Holographic time average vibration study of a structure dynamic model of an airplane fin," Opt. Laser. Tech, 6, 117-123, (1974).

10. K. Biedermann, N. E. Molin, "Combining hyper sensitization and rapid in situ processing for time average observation in real time holographic interferometry," J. Phys. E: Sci. Instrum, 3, 669-680, (1970).

11. N. Abramson, "The making and evaluation of holograms," Academic Press Inc, London, (1981).

12. A. E. Ennos, "Measurement of in-plane surface strain by hologram interferometry," J. Phys. E: Sci. Instrum, 1, 731-734, (1968).

13. S. Martin, "A new photopolymer recording material for holographic applications: photochemical and holographic studies towards an optimized system," PhD Thesis, Trinity College, Dublin, August, (1995).

14. A. H. Burr, J. B. Cheatham, "Mechanical analysis and design," London, Prentice-Hall, (1995).

15. E. Mihaylova, B. Potelon, S. Reddy, V.Toal and C. Smith "Mechanical characterization of unplasticised polyvinyl chloride thick pipes by optical methods," Opt. Laser. Eng, 41, 889-900, (2004).

6. A simple ESPI system using holographic optical elements

Introduction

Holographic interferometry [1] is a useful tool developed for measurements on optically rough surfaces. The advantages of holographic interferometry include: ability to measure displacements with sensitivity of the order of the wavelength of light, whole field measurement, and non-contact. Despite its advantages, the primary requirement for vibration isolation confines its use to research laboratories only. Also the extensive, tedious chemical processing and the requirement for high spatial frequency of the recording medium to resolve the finely spaced fringes formed between object and reference beams limits the application potential of holographic interferometry. ESPI [2] is the chief competitor to holographic interferometry. In this chapter the modification of ESPI systems using HOES is described.

6.1 Electronic speckle pattern interferometry

Speckle interferometry is an alternative technique to overcome the disadvantages associated with holographic interferometry [3, 4]. Displacements parallel and perpendicular to the test surface are measured by utilizing the speckle effect. Speckle was regarded as a noise in holography and later it was realized that it is sensitive to movement; this effect is used to measure the surface displacement [5]. Speckle photography and speckle interferometry utilize the properties of speckle to measure displacements. Speckle photography utilizes the positional changes of speckle, whereas speckle interferometry is based on the irradiance change of the speckle [6]. The image processing is done electronically and a CCD camera is used instead of a photographic recording medium in electronic speckle pattern interferometry (ESPI) [7]. In the past 15 years, the application potential of ESPI has increased enormously due to

the availability of high performance image processing and computing technologies. The ESPI system consists of a CCD camera, computer with frame grabber, a laser and optical elements such lenses, mirrors and beam splitters. Use of the camera instead of a conventional photographic recording medium, makes it superior to holographic interferometry. ESPI is also called TV holography or electronic holography.

The sensitivity of the camera is much higher when compared with holographic recording media and shorter exposure times are enough to record the images. The operational costs are low for electronic speckle pattern interferometry because it does not require holographic recording plates and chemicals for development. It is easy to operate the system because of lower positioning accuracies. The results are displayed on the computer instantaneously with the availability of high performance computing techniques [8]. At the same time, ESPI has some drawbacks: the spatial resolution of the camera is much less than that of a holographic recording medium; the quality of the images is poor compared with that of holographic interferometry. The initial setup cost for ESPI is expensive because it requires a computer with a frame grabber and a CCD camera, whereas in holographic interferometry initial system setup cost is cheap because it does not require expensive computer hardware.

The advantages of speckle techniques over conventional film based techniques include: ability to measure large deformations with in-plane and out-of-plane sensitivity, ability to measure displacement derivatives. Displacements ranging from 0.25 to 100 μm for in-plane and 0.25 to 30 μm for out-of-plane sensitivity can be measured using speckle techniques [9]. ESPI is widely used to measure displacements, strain, thermal and mechanical stress [10, 11, 12].

6.1.1 Principle

When a test object is illuminated with a coherent light source, light is scattered by the object surface (object beam). A reference beam is combined with object beam; they produce a speckle interference pattern or specklegram upon superposition. The specklegram is imaged with a CCD camera and transferred to a frame grabber on a computer where it is saved in memory and displayed on a monitor [13]. When the object under investigation is deformed, the phase of the specklegram changes as a result of a change applied to the test object and a second specklegram is transferred to the computer and subtracted from, or added to, the one previously stored. The resulting interferogram on the monitor is a pattern of dark and bright fringes. The intensity distribution of the interference pattern depends on the phase difference between the two individual specklegrams. It is possible to grab the frames with the object in different positions while undergoing deformation. In this way real time formation and the progressive changes of the fringe pattern related to the deformation of the investigated surface are observed.

6.1.2 Fringe formation

Formation of the fringes is explained by considering the intensity distribution in the image plane, of the interfering object and reference wavefronts before and after displacement.

The intensity distribution of the specklegram at the image plane with the object in its un-displaced position is given by

$$I_{undisplaced} = I_1 + I_2 + 2\sqrt{I_1 I_2}\cos(\psi) \quad \text{.....6.1}$$

where ψ (x, y) is the phase difference between the object wavefront in its undisplaced position and the reference wave, I_1 and I_2 are the intensities of the two waves. The intensity distribution with the object in its displaced position is given by

$$I_{displaced} = I_1 + I_2 + 2\sqrt{I_1 I_2}\cos(\psi + \Delta\phi) \quad \text{.....6.2}$$

$\Delta\phi$ is the phase change introduced due to the object displacement.

The subtracted signal is given by

$$V_s = 4\sqrt{I_1 I_2}\sin\left(\psi + \frac{\Delta\phi}{2}\right)\sin\left(\frac{\Delta\phi}{2}\right) \quad \text{.....6.3}$$

This signal contains both positive and negative values. The negative signal is displayed on the monitor as an area of blackness. To avoid loss of signal, the subtracted signal is rectified before displaying on the monitor. Brightness on the monitor is given by

$$B = 4K\left[I_1 I_2 \sin^2\left(\psi + \frac{\Delta\phi}{2}\right)\sin^2\left(\frac{\Delta\phi}{2}\right)\right]^{\frac{1}{2}} \quad \text{.....6.4}$$

If the brightness is averaged along a line of constant $\Delta\phi$, it varies between B_{max} and B_{min}

The brightness will be maximum whenever the phase $\Delta\phi = (2n+1)\pi$. n= 0, 1, 2

$B_{max} = 2K\sqrt{I_1 I_2}$; this condition corresponds to a bright fringe.

The brightness is minimum whenever $\Delta\phi = 2n\pi$ n= 0, 1, 2

$B_{min} = 0\ when\ \Delta\phi = 2n\pi$, this condition corresponds to a dark fringe.

6.2 Configurations

6.2.1 Out-of-plane sensitivity

ESPI can be used to measure the component of the displacement vector in both in-plane and out-of-plane directions. Uniform reference wave and speckle reference beam configurations are commonly used to measure the out-of-plane displacement. In a uniform reference wave system the test object is illuminated at an oblique angle. The reference beam is brought to the image plane of the CCD camera lens. The reference

beam must appear to originate at the centre of the aperture stop in order to minimise the spatial frequency of the specklegram. The geometry of the uniform reference wave is already described in chapter 1 (refer Figure 1.5). The geometry of a speckle reference wave system is shown in Figure 6.1.

It is similar to the Michelson type of interferometer [14]. In this setup two mirrors in the Michelson interferometer are replaced by scattering surfaces. One of the surfaces is the test object. The two surfaces are illuminated along their surface normal. Scattered light from the two surfaces is made to superimpose at the image plane of the camera lens using a beam splitter [6].

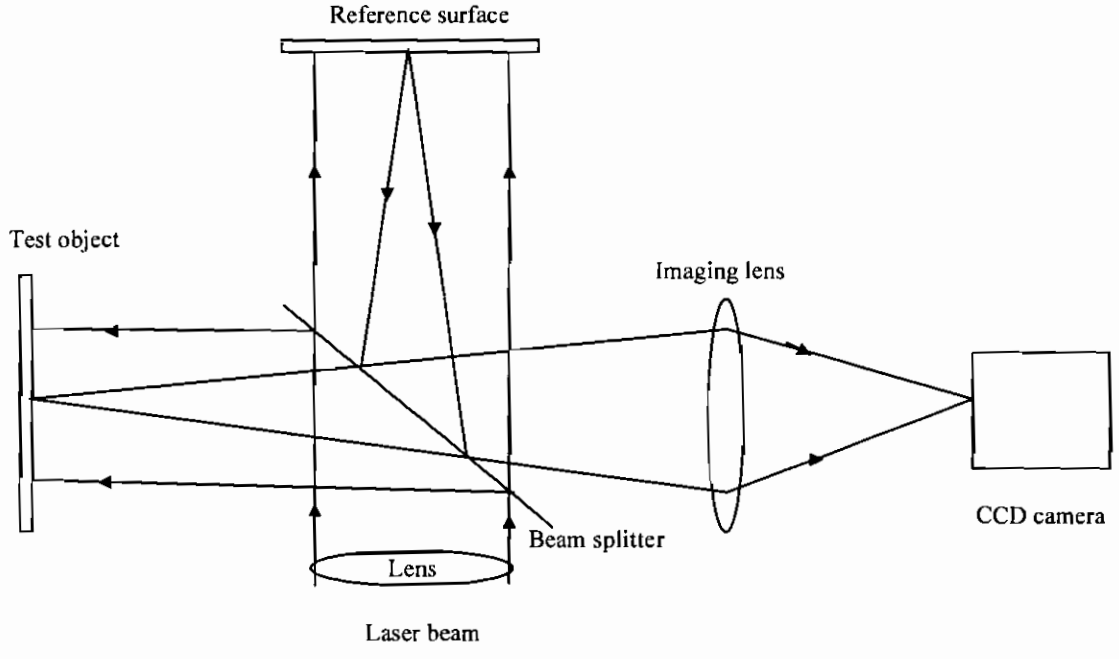

Figure 6.1 Out-of-plane ESPI system using a speckle reference wave

The phase change due to the object deformation in an out-of-plane sensitive system is calculated using the geometry shown in Figure 6.2. The object wavefront after deformation is shown by dotted lines. θ is the angle between surface normal and the observation direction. The path length in the interferometer is (abc). The path length after object deformation is (def).

The change of the optical path length due to the object deformation is given by

$$\Delta l = Z(1+\cos\theta) + Y \quad \text{.....6.5}$$

$Y = d_x \sin\theta$,

d_x = in-plane displacement, d_z =out-of-plane displacement.

Phase change is given by

$$\Delta\phi = \left(\frac{2\pi}{\lambda}\right)\left[d_Z(1+\cos\theta) + d_X \sin\theta\right] \quad \text{.....6.6}$$

λ = wavelength of the laser.

If the angle of illumination is chosen to be very small, the above expression is approximated to $\left(\frac{4\pi}{\lambda}\right)d_z$ 6.7

In practical situations it is not possible to attain this condition because the illumination and observation directions cannot be collinear except in the Michelson interferometer set-up with a speckled reference beam.

It is possible to choose the illumination direction close to the surface normal and the system is sensitive mainly to out-of-plane motion. The object deformation is calculated from the phase change given by [15]

$$\Delta\phi = \left(\frac{2\pi}{\lambda}\right)d_Z(1+\cos\theta) \quad \text{.....6.8}$$

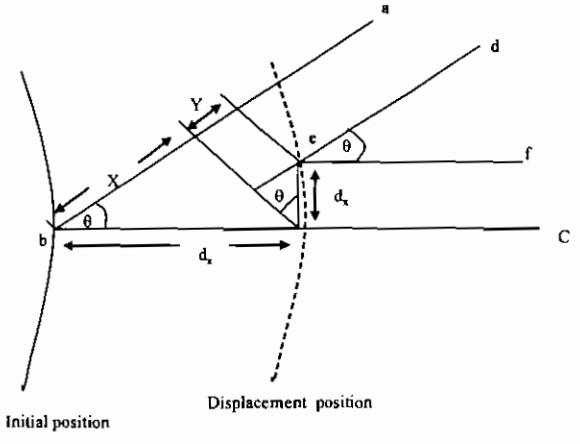

Figure 6.2 Phase calculation in an out-of-plane sensitive ESPI system

6.2.2 In-plane sensitivity

The optical configuration for in-plane sensitive ESPI requires two illumination beams [16, 17, 18]. A schematic of the in-plane sensitive system is shown in Figure 6.3. The two illuminating beams subtend equal and opposite angles with respect to the object surface normal. A CCD camera positioned along the surface normal collects the scattered light from the object. The optical path length of each beam changes due to the object displacement.

$\Delta l_1 = d_z(1+\cos\theta)+d_x\sin\theta$,

$\Delta l_2 = d_z(1+\cos\theta)-d_x\sin\theta$

The effective path length is the sum of path length change due to each beam [18].

Phase change is given by

$$\Delta\phi = \left(\frac{2\pi}{\lambda}\right)\left[\Delta l_1 - \Delta l_2\right] = \left(\frac{4\pi}{\lambda}\right)d_x\sin\theta \quad \text{.....6.9}$$

where d_x = in-plane displacement along the x axis.

λ = wavelength of laser, Δl_1 = path length change in beam 1, Δl_2 = path length change in beam 2, 2θ = angle between the two beams

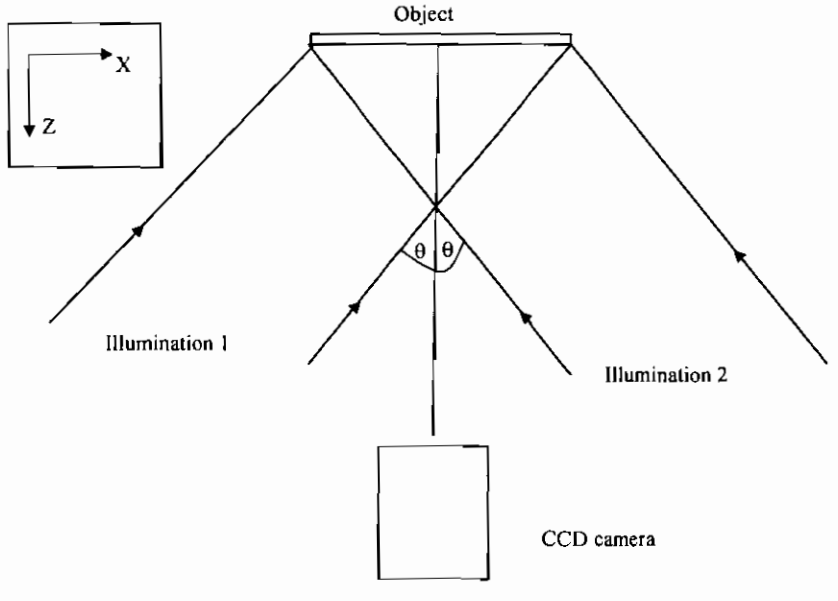

Figure 6.3 In-plane sensitive ESPI system

6.3 A new approach – ESPI system using a holographic optical element

6.3.1 Conventional ESPI system

New directions for making compact electronic speckle pattern interferometers using holographic optical elements were investigated. This allows us to greatly reduce the number of components without affecting the system performance. A single HOE can replace a beam splitter/combiner and mirrors as well as producing a speckle reference wavefront. A conventional ESPI system is described before describing the new technique to show the number of optical components used in the system and the complexity to align the optics.

A conventional practical out-of-plane sensitive ESPI system using a uniform reference wave is shown in Figure 6.4. The laser beam is split into two beams using the beam splitter (BS1). One beam illuminates the object under test and the second serves as the reference beam. The two beams meet at the image plane of the CCD camera by using the beam-combining device BS2 in front of the camera. Alignment of a smooth reference beam with the object beam can be difficult [ref 10, p182]. A speckle reference wave is used to minimize the alignment difficulties and also to match the intensities of the object and reference beams to obtain a good quality interferogram. So a speckle reference wave obtained by inserting a ground glass plate between M2 and BS2 (Figure 6.4) is used to make alignment easier. A much simple system using a speckle reference wave (Figure 6.1) is used instead of the system shown in Figure 6.4. This system contains two lenses and a beam splitter.

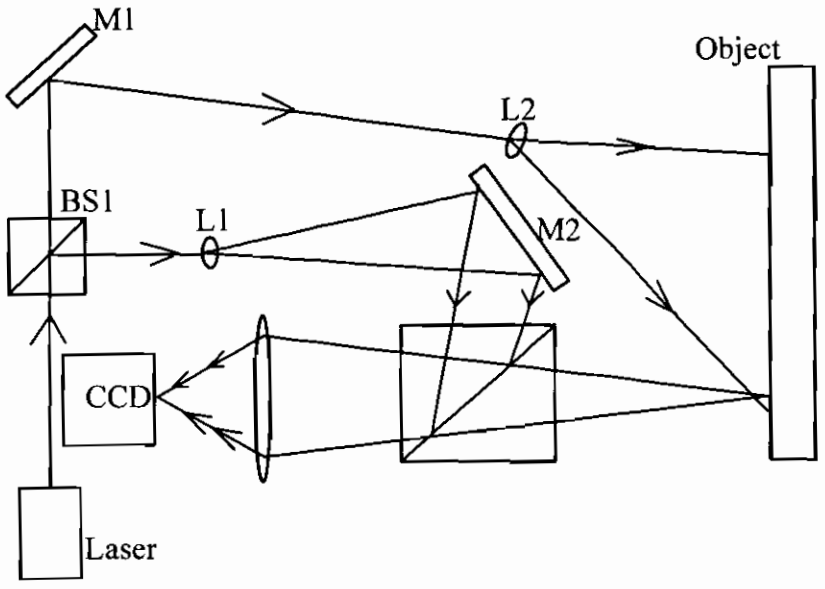

Figure 6.4 Conventional out-of-plane sensitive ESPI system

The geometry of the above ESPI system is made simple using a hologram in the system. A holographic element is incorporated in the above system to replace BS1, BS2, M1, M2, L1, and L2 in the system (Figure 6.4), to replace two lenses, the beam splitter in the system shown in Figure 6.1. This hologram generates the speckle reference wave when it is illuminated in an ESPI system.

HOEs have not been used much in ESPI systems. Holographic lens elements have been used in speckle photography for measuring in-plane displacement and rotation [6]. An ESPI system using holograms recorded on thermoplastic and silver halide media to study in-plane displacements has been reported [19]. This system is more complex than the system reported in this thesis. A holographically reconstructed master object wave recorded on thermoplastic material has been used to compare object surfaces using comparative ESPI [20].

For the first time holograms recorded in the acrylamide based photopolymer material are used as HOEs in an ESPI system. The self processing ability makes the material superior when compared to the holographic optical elements recorded in

thermoplastic and silver halide materials which were used in the work reported in the previous references.

Recording the hologram is not a complicated procedure; geometry similar to the one described in chapter 2 is used (section 2.6) to record the holograms. Either a transmission or reflection hologram is used in the ESPI system. It is important to note that the hologram need not be of the test object. Its purpose is to produce a speckle reference wavefront. Any object which gives a diffuse reflection can be used to record the hologram. This is an important advantage because the hologram recording can be made in the laboratory and the HOE later taken to the test location.

For this work a transmission hologram was used because the photopolymer recording medium had only enough spatial frequency response to record transmission holograms but not reflection holograms.

6.3.2 Experimental

Acrylamide photopolymer transmission HOE recording

The main reason for incorporating HOEs in the ESPI system is to make the system simple and compact. A transmission HOE was used in the in the first ESPI system. Transmission HOEs were fabricated using an acrylamide based photopolymer material. Layer preparation is presented in section 5.4.1. A schematic diagram of transmission HOE recording is shown in Figure 6.5

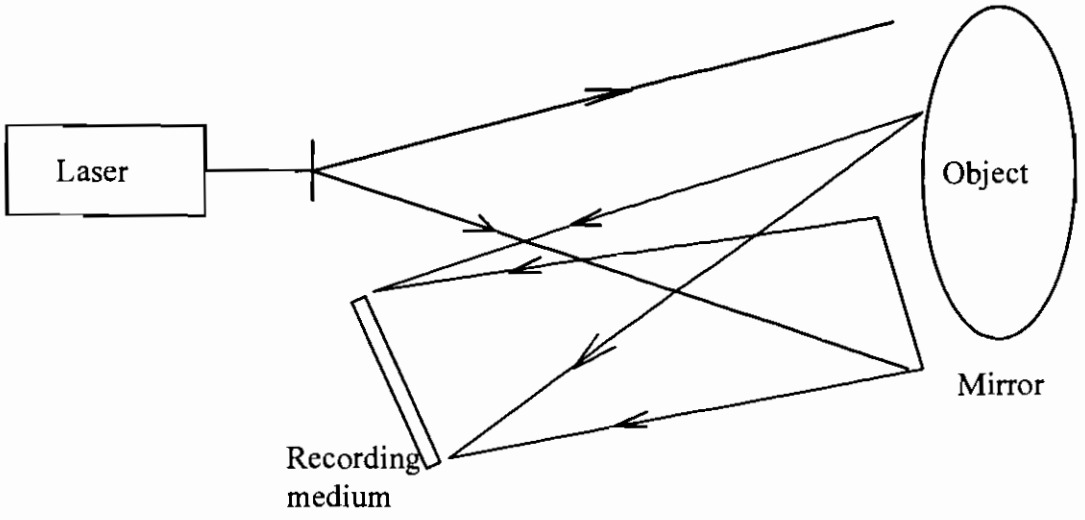

Figure 6.5 Setup for recording a transmission HOE

The object was illuminated using a diverging beam of laser light. A plane mirror was placed beside the test object. Scattered light from the object and reflected light from the mirror reach the photographic recording medium and interfere with each other. A transmission hologram of an object was recorded. The object or the hologram is deliberately moved from its existing position so that the holographic fringes completely disappear. The object is ready for testing using HOE based electronic speckle pattern interferometry.

6.3.3 Radial strain measurement using HOE based ESPI system

A thick polyvinyl chloride pipe manufactured by Wavin Ireland Ltd was tested for radial strain measurement using the transmission HOE based ESPI system. A schematic of the pipe is presented in the previous chapter (Figure 5.6).

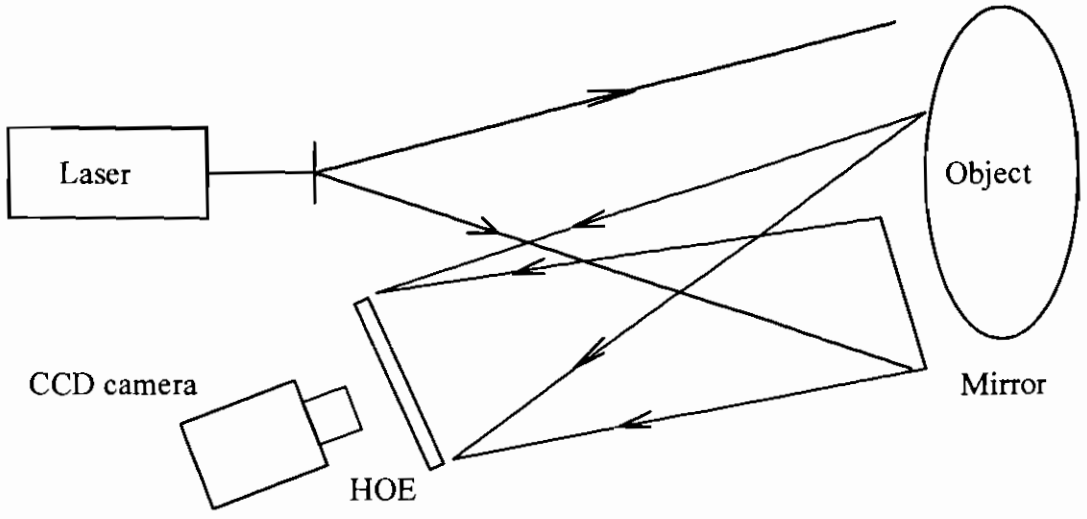

Figure 6.6 Transmission HOE based ESPI system

Figure 6.6 show the schematic of the HOE based ESPI system. The experiment was carried out on a Newport vibration isolation table. The HOE was recorded using a 5 Watt CW Nd-YVO_4 laser operating at 532 nm from Coherent Inc. The photopolymer layer was exposed for 40 seconds with exposure intensity of 20 mW/cm^2. The HOE was illuminated with the reference beam without altering its position. The object wavefront was reconstructed and it was used as the reference speckle wavefront in an electronic speckle pattern interferometer. The efficiency of the transmission HOE is high, thus the brightness of object reconstruction is more than that of the object beam. The effect of emulsion shrinkage was not taken into account. A photograph of the reconstruction is shown in Figure 6.7. A letter H was marked on the test object. Two images of H, one corresponds to holographic reconstruction and the second original letter marked on the object surface was imaged using the CCD camera. It was easy to align the object wavefront with the reference wavefront by placing the two H's one exactly on top of the other while looking at the two images carefully on the computer monitor in real time. ESPI frame subtraction was carried out while inflating the pipe.

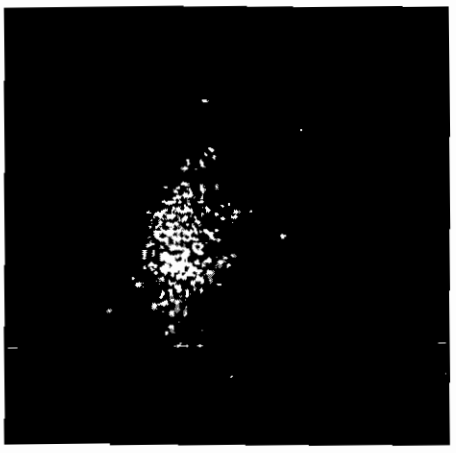

Figure 6.7 Photograph of the reconstruction from the hologram and of the illuminated object

A LabVIEW program was used (LabVIEW version 6.0) to generate ESPI fringe patterns using a National Instruments IMAQ-1407 frame grabber card. No image processing filters were used in the fringe generation. Fringe patterns are shown in Figure 6.8. The fringe pattern obtained with a pressure of 0.5×10^5 N/m^2 is shown in Figure 6.8 (a) and the fringe pattern for a pressure of 1×10^5 N/m^2 is shown in Figure 6.8(b). The fringes are contours of constant optical path difference in the interferometer, created due to the pressure change. The fringes grew outward from the centre of the field of view as the cylinder expanded radially.

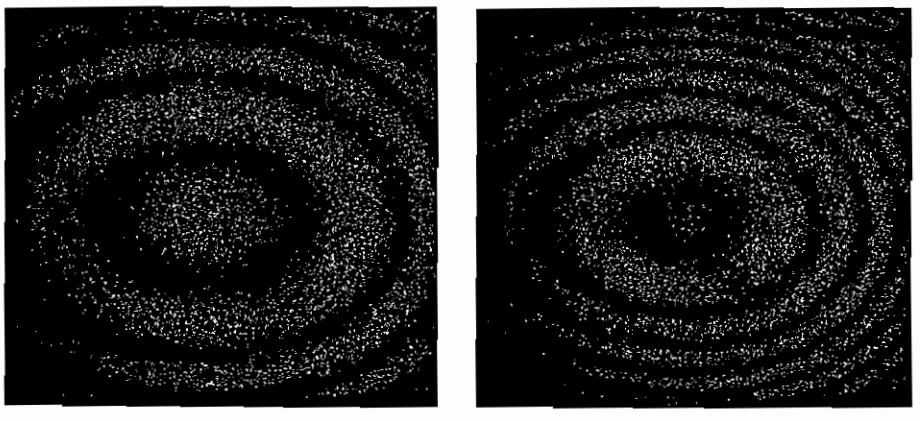

(a) Pressure $=0.5 \times 10^5$ N/m^2 (b) Pressure $=1 \times 10^5$ N/m^2

Figure 6.8 ESPI Fringe patterns obtained using the HOE based ESPI system

The pipe was inflated to different pressures. Radial strain was measured for pressure values of 0.5, 1, 1.5 and 2 × 10^5 N/m^2. The pipe expanded radially outwards with maximum displacement in the direction perpendicular to the surface. The angle between the illumination direction and the CCD camera optical axis was 14°. This gave greater sensitivity than the 19° angle used in the last chapter. This could be achieved in the current set up because of the increased flexibility of the optical arrangement in ESPI. The experimental setup is shown in Figure 6.9.

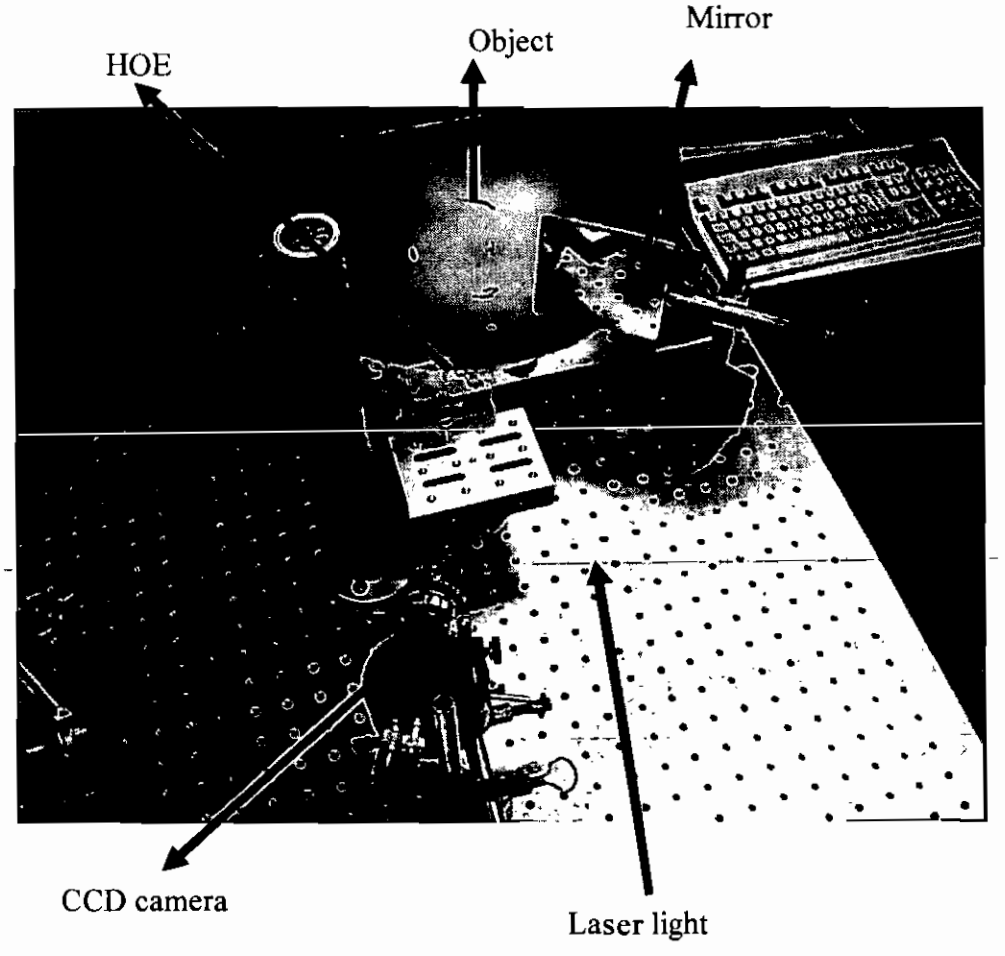

Figure 6.9 Laboratory experimental setup using a transmission HOE in ESPI system

The transmission HOE based ESPI system consisted of the following components: a plane mirror, test object, CCD camera, HOE and a laser. The only optical component used in the HOE based ESPI system was the plane mirror, which was used

to provide the reference beam for recording and reconstructing the hologram. The results are shown in table 6.1. The out-of-plane displacement d was calculated using equation 5.15. Young's modulus of elasticity and radial strain were found using equations 5.19 and 5.20.

Table 6.1 Results Radial strain measurement

Pressure ($\times 10^5 N/m^2$)	d(μm)	Fringe Number(N)	Radial strain (micro strain)
0.5	13.49	50	72.57
1.0	26.99	100	145.15
1.5	40.49	150	217.73
2.0	54.05	200	290.31

The radial strain values obtained are in good agreement with those obtained using holographic interferometry and the Young's modulus of elasticity of the material was calculated using equation 5.19 to be 2.72 GN/m^2. This value is close to the manufacturer's value which is in the range of 2.80-3.2 GN/m^2. This demonstrates that despite the simplicity of the ESPI system, the results obtained are as accurate as those obtained by Holographic Interferometry.

The errors discussed in section 5.4.3 are considered to calculate uncertainty in out-of-plane displacement. The errors can occur due to the error in the angle between illumination and observation (θ) and error in counting the number of fringes (N).

Error due to angle between illumination and observation (θ):

An error of ± 0.5° would occur in measuring the angle. Error due to the fringe count is calculated by using equation 5.22. Using $\theta = 14°$, $\lambda = 0.532 \times 10^{-6}$, N = 50, $\Delta\theta = \pm$ 0.5 degree, error in out-of-plane displacement is found to be ± 0.014 μm. The

error due to the angle produces an uncertainty of ±0.1% in the value of Young's modulus of elasticity.

Error due to fringe counting (N):

Error due to the fringe count is calculated by using equation 5.23. An error of ± 0.5 can occur in the fringe number (N). Using the values $\theta = 14°$, $\lambda = 0.532 \times 10^{-6}$, $\Delta N = 0.5$ error in out-of-plane displacement is found to be ± 0.14 μm. The Root Mean Square error is found to be 0.136 μm. The error due to the fringe number produces an uncertainty of ±1% in the value of Young's modulus of elasticity.

In the calculation of radial strain, the in-plane displacement component is not taken into account in this instance. This would introduce an error in the value of Young's modulus of elasticity of the pipe. In section 6.5 preliminary results obtained using phase shifting techniques include consideration of the in-plane component of displacement.

6.4 Phase shifting techniques

Optical measurement techniques such as electronic speckle pattern interferometry provide the mesurand data in the form of bright and dark fringe patterns [21]. Fringe counting measurements do not produce complete phase information associated with the object deformation. Phase shifting methods are used to measure the phase of the object wavefront in an interferometer relative to that of the reference beam at every pixel. Usually a camera is used to record the interference fringes in an interferometer. The phase of the wavefront is calculated by measuring the changes in the recorded intensity at each pixel with the introduction of a known phase difference between the object and reference beams. A number of frames are grabbed while the phase difference between the object and reference beams is changed in a known manner. Using phase shifting techniques the displacement at each pixel in the image of

the object is measured so that a complete displacement profile of the object can be obtained.

Phase measurement techniques are of two types, temporal phase modulation and spatial phase modulation. In temporal phase evaluation methods phase information is separated into a time sequence of interferograms. In spatial phase measurement methods, the phase information can be obtained from a single frame. They are also known as Fourier methods. Spatial phase modulation techniques are a useful alternative to the temporal phase modulation when dynamic events are investigated. The advantage of spatial modulation techniques is that the phase measurement is possible in adverse conditions such as vibration because only one frame of data is needed. Due to the high immunity to environmental disturbances spatial phase modulation techniques are more suitable for industrial applications [22]. Temporal phase modulation techniques offer accurate results when compared with spatial modulation techniques when a stable environment is available.

6.4.1 Phase modulation methods

Phase shift in an interferometer can be introduced by methods such as moving a mirror, tilting a glass plate, moving a grating [23], rotating a half-wave plate or analyzer [24, 25, 26], or using an acoustic or electro-optic modulator. A common technique to introduce phase shift is to move the mirror in the reference beam path by means of a piezoelectric transducer [21]. Phase shifting devices produce either continuous or discrete phase shifts between the object and reference beams in the interferometer. The intensity of the interference pattern is measured at different relative phase shifts. The intensity of the each frame is given by [22]

$$I = I_0[1 + V\cos(\phi + \alpha)] \quad \text{.....6.10}$$

I_0 = background intensity, V = visibility of the interference fringe pattern or fringe contrast, ϕ = wavefront phase, α = known relative phase shift between the object and reference beams of the interferometer.

There are three unknowns (V,ϕ,I_0) in equation 6.10. At least three measurements are required to determine the phase (ϕ).

In a general case, N measurements of intensity are recorded as the phase is shifted. The phase shift is assumed to change during the detector integration period, but the change is assumed to be the same from data frame to data frame.

The intensity of one frame of recorded intensity is written as [22]

$$I_i(x,y)=\left(\frac{1}{\Delta}\right)\int_{\alpha_i-\frac{\Delta}{2}}^{\alpha_i+\frac{\Delta}{2}} I_0(x,y)\{1+V(x,y)\cos[\phi(x,y)+\alpha(t)]\}d\alpha(t) \quad \text{.....6.11}$$

Δ = change in relative phase, $\alpha(t)$ = relative phase between the test and reference beams, α_i = average value of the phase shift for the i^{th} exposure

Integration for a single frame of data over a phase shift Δ makes equation 6.11 applicable for any phase shifting technique. Integrating equation 6.11 gives the following expression

$$I_i(x,y)=I_0(x,y)\left\{1+V(x,y)\sin c\left(\frac{\Delta}{2}\right)\cos[\phi(x,y)+\alpha_i]\right\} \quad \text{.....6.12}$$

Simplifying equation 6.12 further results in the following equation

$$I_i(x,y)=I_0(x,y)\{1+V_0(x,y)\cos[\phi(x,y)+\alpha_i]\} \quad \text{.....6.13}$$

Where V_0 = detected fringe visibility, $\sin c\left(\frac{\Delta}{2}\right)=\frac{\sin\left(\frac{\Delta}{2}\right)}{\left(\frac{\Delta}{2}\right)}$

Equation 6.13 is used as the basic equation to find the phase of the interferogram using different algorithms.

6.4.2 Phase shifting algorithms

Three-frame technique

A minimum of three frames are required to solve the three unknowns in equation 6.13. Using the three frame technique the phase is calculated with $\alpha_i = \pi/4,\ 3\pi/4,\ 5\pi/4$ with a phase shift of 90^0 per frame [22].

The phase of the interferogram is calculated by substituting these values in equation 6.13; the phase value at each detector point is given by

$$\phi = \tan^{-1}\left(\frac{I_3 - I_2}{I_1 - I_2}\right) \quad \text{.....6.14}$$

I_1 = Intensity of the interferogram with phase step $\alpha = \pi/4$

I_2 = Intensity of the interferogram with phase step $\alpha = 3\pi/4$

I_3 = Intensity of the interferogram with phase step $\alpha = 5\pi/4$

Four-frame technique

The four frame technique is a common technique used to calculate the phase. Phase step values of $\alpha_i = 0, \frac{\pi}{2}, \pi, \frac{3\pi}{2}$ are used [22].

The phase is calculated using equation 6.13 by substituting the phase values mentioned above. The phase at each detector point is given by

$$\phi = \tan^{-1}\left(\frac{I_4 - I_2}{I_1 - I_3}\right) \quad \text{.....6.15}$$

where

I_1 = Intensity of the interferogram with phase step $\alpha = 0$

I_2 = Intensity of the interferogram with phase step $\alpha = \frac{\pi}{2}$

I_3 = Intensity of the interferogram with phase step $\alpha = \pi$

I_4 = Intensity of the interferogram with phase step $\alpha = \frac{3\pi}{2}$

4-frame algorithm is widely used and simplest algorithm. The major problem with this algorithm is that it is more susceptible to errors due to the miscalibration of the phase shifting device.

Five-frame technique:

This technique was developed to minimize the phase calibration errors [27, 28]. It also uses phase shifts of 90 degrees. This algorithm also avoids the possibility of the numerator and denominator in equation 6.15 being both zero. Using phase shifts $\alpha_i = -\pi, -\frac{\pi}{2}, 0, \frac{\pi}{2}, \pi$ in equation 6.13 the phase at each point on the detector is calculated.

The phase is given by

$$\phi = \tan^{-1}\left(\frac{2(I_2 - I_4)}{2I_3 - I_5 - I_1}\right) \quad \text{.....6.16}$$

where

I_1 = Intensity of the interferogram with phase step $\alpha = -\pi$

I_2 = Intensity of the interferogram with phase step $\alpha = -\frac{\pi}{2}$

I_3 = Intensity of the interferogram with phase step $\alpha = 0$

I_4 = Intensity of the interferogram with phase step $\alpha = \frac{\pi}{2}$

I_5 = Intensity of the interferogram with phase step $\alpha = \pi$

Phase extraction algorithm insensitive to laser power change-6 frame technique:

When a laser diode is used as a light source in phase shift interferometry, measurement accuracy is degraded by intensity modulation of the interferogram due to the laser power change associated with variations in current. A phase extraction algorithm, which is insensitive to laser diode power changes, was developed by Onodera and Ishii [29]. The phase of the interferogram is extracted using six frames. An un-balanced Twyman green interferometer was used to measure the phase of the interferogram.

The phase of the interferogram is given by [29]

$$\phi = \tan^{-1}\left(\frac{3I_1 - 5I_2 + 5I_5 - 3I_6}{-I_1 - 3I_2 + 4I_3 + 4I_4 - 3I_5 - I_6}\right) \quad \text{.....6.17}$$

The phase value calculated using the above phase shifting techniques lies between $-\pi, +\pi$ and the signs of both numerator and denominator in the above expressions have to be examined in order to make the phase lie in the range 0-2π.

6.4.3 Phase unwrapping - removal of phase ambiguities

Due to the nature of the arctangent used to calculate the phase of the interferogram, 2π phase steps occur in the phase map. It is essential to remove the phase steps to obtain a smooth phase map of the object deformation. Removal of 2π phase steps is known as phase unwrapping or integrating the phase [30]. The most common method of removing the 2π phase ambiguities is by adding or subtracting an offset of 2π at each pixel if a phase jump greater than π is detected between that pixel and the previous one examined. Starting from the top of any column in a phase map, the offset is set to zero. By scanning downwards, the phase jumps are checked by examining the phase difference between the adjacent pixels. When a phase jump greater

than π is detected the offset is incremented either + or - 2π depending on the sign of the jump.

6.5 Transmission HOE based ESPI system using a near infrared diode laser

A transmission HOE fabricated at 532 nm was used in the ESPI system. To make the ESPI system still more compact a diode laser was used, as these are cheaper, compact and reliable for use in interferometry [29]. The laser is a Hitachi 50 mW diode laser operating at 784 nm. It can be operated in constant current and power modes by using a diode laser controller LDC-202 (Optische Systeme GmbH). The experimental setup is similar to the one shown in Figure 6.9. The HOE was reconstructed using the diode laser. The angular orientation of the HOE was changed to obtain a bright reconstruction because the reconstruction wavelength has a different Bragg angle. The contrast of the holographic reconstruction is less when compared with the reconstruction at 532 nm. A photograph of the reconstruction is shown in Figure 6.10.

Figure 6.10 Photograph of the reconstruction from the hologram using a diode laser

The experimental arrangement using a diode laser in the HOE based ESPI system is shown in Figure 6.11. A fringe pattern is shown in Figure 6.12. The fringes

are contours of constant optical path length difference in the interferometer created due to the pressure change, appearing from the centre of the field of view as the object is pressurized.

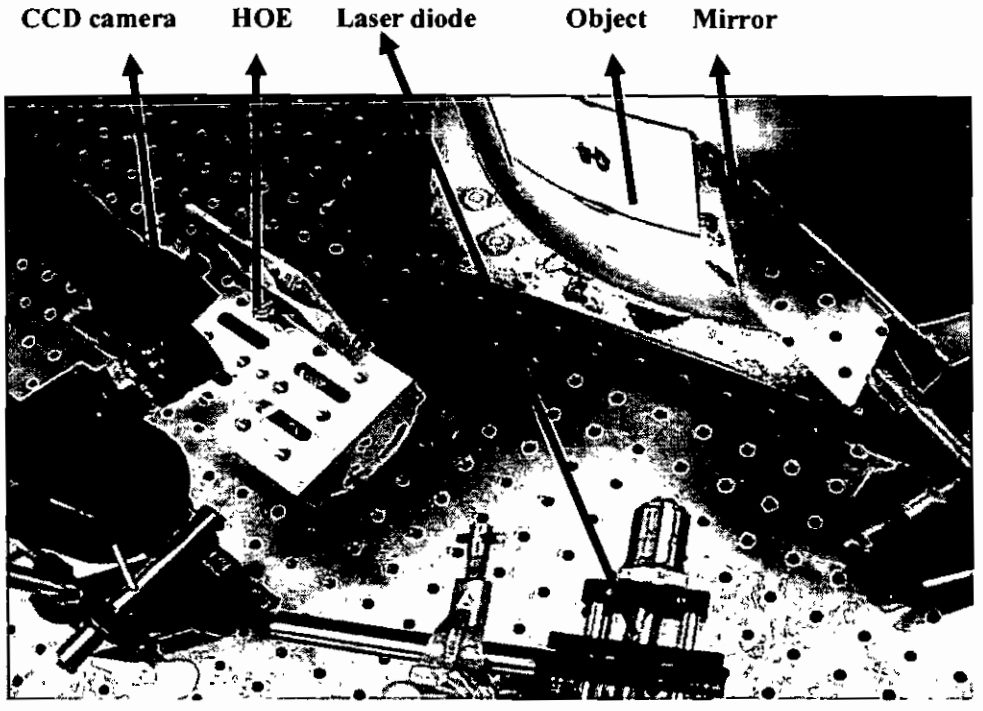

Figure 6.11 HOE based ESPI system using a laser diode

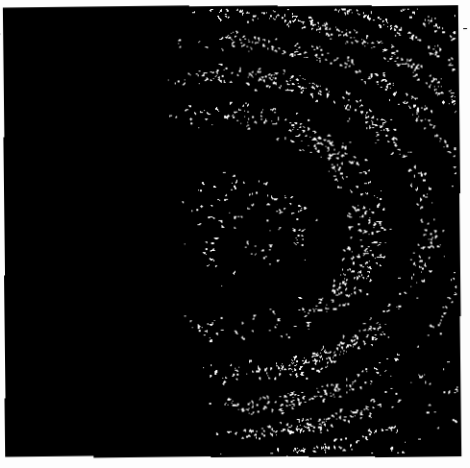

Figure 6.12 Fringe pattern obtained with the HOE based ESPI system using the diode laser

The important advantage of using diode lasers is that they can be modulated for implementing phase shifting in an ESPI system.

6.5.1 Phase shifting with laser diode

Phase shifting techniques are used to obtain the complete 3D displacement map of the object deformation. In an ESPI system the phase shift is introduced by changing the optical path difference between the reference and the object beams. Phase shifting in this compact ESPI system was introduced by modulating the wavelength of the laser diode by changing the drive current. The modulating voltage was supplied from a National Instruments D/A PCI-1200 board. During the modulation of the diode laser drive current the power of the laser is kept constant. Power changes due to current modulation are neglected. The source modulation of the diode laser is used for the first time. In chapter 7 source current modulation is explained in detail to study the vibration mode patterns of test object. The wrapped phase map was obtained using the ESPITest software developed by the Joint Research Centre (JRC), Ispra, Italy [30].

6.5.2 ESPITest Software

ESPITest software uses a Windows based program "Framegrabber" for acquisition and post processing of images [30]. A 5-frame algorithm was incorporated in the software. This software is hardware independent and supports various frame grabber boards and D/A conversion boards. Three different modules are provided, for standard static ESPI, phase shifting ESPI and vibration ESPI. A phase shifting device has to be controlled for phase shifting ESPI and the software is equipped with a phase shifter calibration module. In the standard static ESPI a first specklegram is saved as reference and all subsequently acquired images are subtracted from the reference specklegram. The phase shifting device is controlled using the output voltage from the D/A board. Changing the out put voltage modulates the phase difference between the reference and object beams, resulting in a sinusoidal intensity change of each of several pixels on the CCD camera which is displayed in the calibration window. The voltage

change corresponding to a complete cycle is taken by clicking the cursor on two crests of the selected curve. The values are stored in the .INI file. The wrapped phase map is generated in a separate phase shifting window. The unwrapped phase map is generated by removing the 2π ambiguities.

6.5.3 Phase calculation - experimental

The phase value from the wrapped phase map was calculated using Scion Imaging software version 6.0. A rectangular selection tool was used to select an area in the wrapped phase map. The coordinates of the two extreme ends within the selection were noted (P&Q) (Figure 6.13). The software generates the phase jumps within the selection. The number of phase jumps was counted within the selection and used to calculate the phase.

In this experiment both the out-of-plane and in-plane components of displacement were taken into account because the illumination direction was not along the test surface normal. The phase change between the points P and Q (Figure 6.13) was measured.

Total phase change due to (out-of-plane + in-plane) displacement components is given by

$$\Phi = \left[\Delta R(1-\cos\phi)(1+\cos\theta)\left(\frac{2\pi}{\lambda}\right) + \Delta R \sin\phi \sin\theta \left(\frac{2\pi}{\lambda}\right) \right] \quad \text{.....6.18}$$

Φ is measured from the wrapped phase map by counting the number of phase jumps taking account of their signs.

Change in radius ΔR was found by rearranging the equation 6.18 and it is given by

$$\Delta R = \frac{\lambda \Phi}{2\pi[(1-\cos\phi)(1+\cos\theta)+\sin\phi\sin\theta]} \quad \text{.....6.19}$$

The radial strain was calculated by dividing the above expressing with radius R.

$$\frac{\Delta R}{R} = \frac{\lambda\Phi}{2\pi R[(1-\cos\phi)(1+\cos\theta)+\sin\phi\sin\theta]} \quad \text{.....6.20}$$

ϕ = angle between the surface normal and the in-plane displacement component

$= \frac{R_2}{\overline{PQ}}$ (Figure 6.13).

The distance between the two points P and Q ($\overline{PQ}$) was calculated using the coordinates obtained from Scion Image software. The distance was converted into the corresponding distance on the imaging window on the computer screen by multiplying by a factor of (15/512). (The imaging window has a length of 15 cm and it has 512 × 512 pixels)

θ = angle between the CCD camera position and the laser axis (calculated using trigonometry to be 17.2°.)

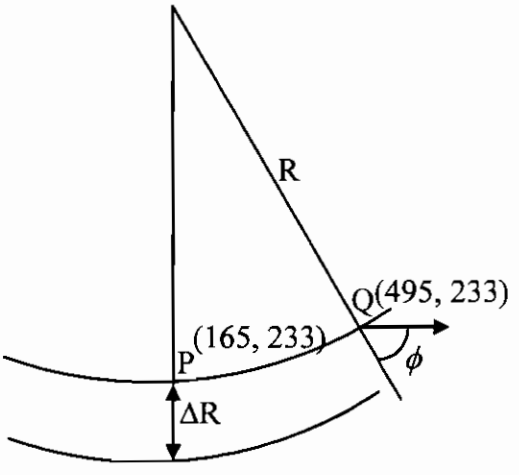

Figure 6.13 Phase calculation from the phase map

The wrapped and un-wrapped phase maps of the cylinder are shown in Figure 6.14. The wrapped fringes have considerably less noise than the ESPI fringe pattern. The fringes are no longer sinusoidal in nature but they resemble ramp waves. The gray

level value at any point in the wrapped fringe pattern represents the surface displacement. A grey level of 255 in the wrapped fringe pattern represents a phase shift of 2π and in the unwrapped image the phase shift represented by a grey level of 255 depends on the number of 2π phase shifts in the wrapped phase pattern. This number can be easily be obtained from the visual observation of wrapped fringe pattern.

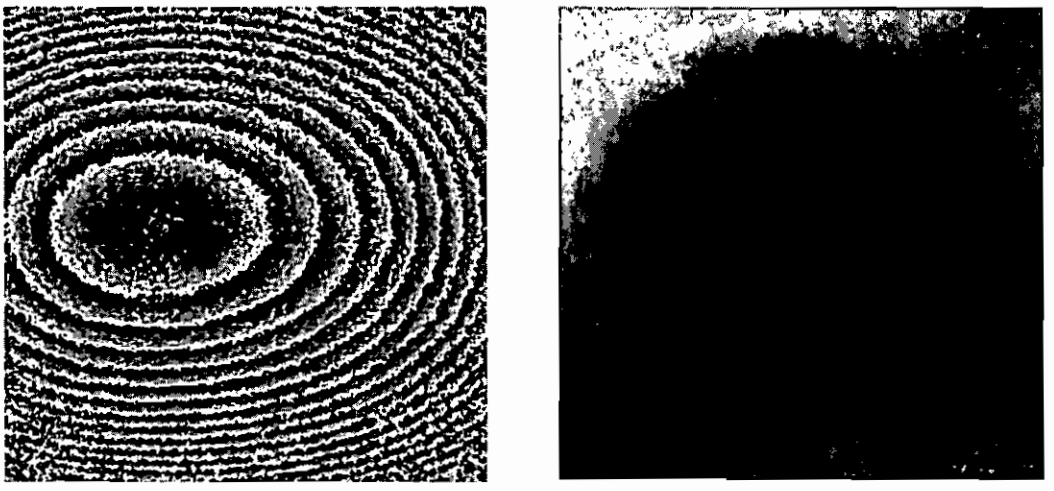

(a) - Wrapped phase map (b) - Unwrapped phase map

Figure 6.14 Wrapped and un-wrapped phase maps obtained using ESPITest software.

The radial expansion of the cylinder was found to be 13.17 μm for an applied pressure of 0.5 N/m^2. The Young's modulus of the elasticity of the pipe was found to be 2.8 $G.N/m^2$. This value is in good agreement with the manufacturer's value (2.80-3.2 $G.N/m^2$) [33], and closer than that in section 6.3.3 because the in-plane displacement was also taken into account.

6.6 Conclusions

The acrylamide based photopolymer material was used to record transmission HOEs. Compared to the ESPI system of Figure 6.4, the transmission HOE based ESPI system is simple and compact. Incorporating a HOE in an ESPI system makes the system simple. The only additional optical component in the HOE based system (Figure 6.6) is a plane mirror.

Using a HOE in an ESPI system has the following important advantages when compared to a conventional ESPI system. The system is simple, compact and low cost. The alignment difficulties are minimized because it is easy to superimpose the holographically reconstructed image and the test object. In addition, to obtain good quality ESPI fringes it is important to match the intensities of the two beams precisely, in a simple ESPI system this can be done easily by rotating the HOE so that it is no longer illuminated at the Bragg angle. The use of holography can also allow the two techniques (holographic interferometry and ESPI) to be used in the same optical arrangement.

Preliminary results show that phase shifting can implemented by modulating the laser source. In this way a full field displacement map is obtained using a simple and compact ESPI system [34, 35].

Results obtained using transmission holograms are encouraging, but a carefully designed reflection hologram could allow the simplest possible system to be constructed, i.e. that including only a laser, HOE and camera.

In the next chapter an ESPI system using a reflection HOE is discussed and experimental results are presented.

References

1. R. K. Erf, "Holographic non-destructive testing," Academic Press Inc, London, (1974).
2. O. J. Lokberg, "Electronic speckle pattern interferometry," Phys. Tech, 11, 16-22, (1980).
3. J. A. Leendertz, "Interferometric displacement measurement on scattering surfaces utilizing speckle effect," J. Phys. E: Sci. Inst, 3, 214-218, (1970).

4. J. N. Butters, J. A. Leendertz, "A double exposure technique for speckle interferometry," J. Phys. E: Sci. Inst, 4, 277-279, (1971).

5. R. K. Erf, "Speckle Metrology," Chapter 2, Academic Press Inc, London, (1978).

6. R. S. Sirohi, "Speckle Metrology," Marcel Dekker Inc, New York, (1993).

7. J. N. Butters, J. A. Leendertz, "Holographic and video techniques applied to engineering measurements," J. Meas. Control, 4, 349-354, (1974).

8. F. Doval, "A systematic approach to TV holography," Meas. Sci. Technol, 11, R1-R36, (2000).

9. P. K. Rastogi, "Optical measurement techniques and applications," Artech House Inc, Norwood, USA, (1997).

10. R. Jones, C. Wykes, "Holographic and speckle interferometry," Cambridge University Press, Cambridge, (1983).

11. K. M. Abedin, M. Kawazoe, K. Tenjimbayashi, T. Eiju, "Electronic speckle pattern interferometry using compressed images from a digital still camera," Opt. Engg, 37, 1599-1601, (1998).

12. M. V. Rao, R. Samuel, A. Ananthan, "Applications of electronic speckle interferometry (ESI) techniques for spacecraft structural components," Opt. Lasers in Engg, 40, 563-571, (2003).

13. P. K. Rastogi, "Digital speckle pattern interferometry and related techniques," John Wiley Sons Ltd, New York, (2001).

14. G. A. Slettemoen, "Electronic speckle pattern interferometry system based on speckle reference beam," Appl. Opt, 19, 616-623, (1980).

15. C. Joenathan, R. Torroba, "Modified electronic speckle pattern interferometer employing an off-axis reference beam," Appl. Opt, 30, 1169-1171, (1991).

16. J. N. Butters, J. A. Leendertz, "Holographic and video techniques applied to engineering measurements," J. Meas. Control, 4, 349-354, (1974).

17. B. Bowe, S. Martin, V. Toal, A. Langhoff, M. Whelan, "Dual in-plane electronic speckle pattern interferometry system with electro-optical switching and phase shifting," Appl. Opt, 38, 666-673, (1999).

18. R. S. Sirohi, N. K. Mohan, "In-plane displacement measurement configuration with twofold sensitivity," Appl. Opt, 32, 6387-6390, (1993).

19. V. Petrov, B. Lau, "Electronic speckle pattern interferometry with a holographically generated reference wave," Opt. Engg. 35, 2363-2370, (1996).

20. L. Laszlo, Z. Fuzessy, J.Kornis, F.Gyimesi, "Comparative measurement by speckle pattern interferometry using holographically reconstructed object," Opt. Eng. 36, 3323-3326, (1997).

21. P. K. Rastogi, "Holographic Interferometry Principles and Methods," Chapter 5, Springer series in optical sciences, Vol 68, Springer-Verlag, Berlin, (1994).

22. D. W. Robinson, G. T. Reid, "Interferogram analysis," Institute of Physics, Bristol, (1993).

23. W. H. Stevenson, "Optical frequency shifting by means of rotating a diffraction grating," Appl. Opt, 9, 649-652, (1970).

24. R. N. Shagam, J. C. Wyant, "Optical frequency shifter for heterodyne interferometers using multiple rotating polarization retarders," Appl. Opt, 17, 3034-3035, (1978).

25. G. E. Sommargren, "Up/down frequency shifter for optical heterodyne interferometry," J. Opt. Soc. Am, 65, 960-961, (1975).

26. H. Z. Hu, "Polarization heterodyne interferometry using a simple rotating analyzer. 1: theory and error analysis," Appl. Opt, 22, 2052-2056, (1983).

27. P. Hariharan, B. F. Oreb, T. Eiju, "Digital phase-shifting interferometry: a simple error-compensating phase calculation algorithm," Appl. Opt, 26, 2504-2506, (1987).

28. C. C. Kao, G. B. Yeh, S. S. Lee, C. K. Lee, C. S. Yang, K. C. Wu, "Phase-shifting algorithms for electronic speckle pattern interferometry," Appl. Opt, 41, 46-54, (2002).

29. R. Onodera, Y. Ishii, "Phase-extraction analysis of laser diode phase-shifting interferometry that is insensitive to changes in laser power," J. Opt. Soc of Am. A, 13, 139-146, (1996).

30. D. C. Williams, "Optical methods in engineering metrology," 1st edition, University Press, Cambridge, (1993).

31. C. Wykes, M. Flanagan, "The use of a diode laser in an ESPI system," Opt. Laser. Tech, 19, 3739, (1987).

32. ESPITest software, Copyright © 1999-2000 Andreas Langhoff, Milan, Portions Copyright © European Commission, Joint Research Centre, Ispra, Italy, (1998).

33. Wavin Main pressure system, Wavin Ireland Ltd, Balbriggan, Co Dublin, Ireland.

34. S. R. Guntaka, V. Toal, S. Martin "Holographically recorded diffractive optical elements for holographic and electronic speckle pattern interferometry," Appl. Opt, 41, 7475-7479, (2002).

35. S. R. Guntaka, B. Bowe, V.Toal and S. Martin "Holographic optical elements for combined holographic and digital speckle pattern interferometry," Speckle Metrology, Trondheim, Norway, Proc. SPIE vol. 4933, eds. K. Gastinger, O.J.Lokberg & S. Winther, 239-245, (2003).

7. Reflection HOEs in ESPI systems

Introduction

A conventional ESPI system (Figure 6.4) was made compact by using an acrylamide based photopolymer transmission holographic optical element. The ESPI system contains one plane mirror (Figure 6.6). The transmission HOE based ESPI system contains the following components: plane mirror, transmission HOE, CCD camera, the laser and a test object. The presence of the mirror is essential to record and reconstruct the HOE. The system can be made more compact by eliminating the plane mirror.

7.1 New directions in designing the ESPI system

If a reflection HOE is used instead of a transmission HOE (Figure 6.6), the plane mirror can be eliminated. Incorporating a reflection HOE in the ESPI system makes the interferometer more compact. Unfortunately, this photopolymer material was not able to record reflection holograms with high diffraction efficiency due to its poor spatial frequency response. (During the period of this work, research was in progress to improve the spatial frequency response of the photopolymer material by other researchers in the Centre for Industrial and Engineering Optics). It is essential to balance the intensities of the scattered light from the test object and the speckle reference wave generated from the HOE to obtain a good quality interferogram. This is possible if the reflection hologram has reasonably high diffraction efficiency. This implies that the recording medium must have high spatial frequency response to record a reflection hologram with high efficiency. Alternative materials which can record reflection holograms are silver halide emulsions. Even though they require chemical processing to make a simple and compact ESPI system these materials were chosen to

record reflection HOEs as they are capable of recording reflection holograms with high diffraction efficiency.

7.2 HP series silver halide emulsions

Silver halide holographic recording plates [1, 2] produced in the Central Laboratory for Optical Storage and Processing of Information (CLOSPI), Bulgarian Academy of Sciences, Sofia, Bulgaria were used to fabricate the reflection HOEs. They have high resolution (greater than 6000 lines/mm), which is due to their fine grain structure. The optimum diameter of the developed silver grains is about 30 nm. In the experiments original size of the grains in the silver halide emulsions is 10 nm and after development the size of the grains grew to 30 nm. The analytical and experimental results confirm the possibility of obtaining high diffraction efficiencies in volume reflection holograms without bleaching [2]. The high resolution of the material makes it very attractive for art holography and for scientific applications such as holographic interferometry and for making holographic optical elements. The plates can be made sensitive to record holograms at 490 nm or 784 nm by adding an appropriate sensitizer [3, 4]. The spectral sensitivity at near infrared wavelength (784 nm) is less than its sensitivity at 633 nm. Quantitative description of the spectral sensitivity is presented in section 7.9.1.

7.3 Necessity for reconstruction of holograms at 784nm

The HP-650 plates are very promising materials for formulation of holograms with very high diffraction efficiency. These materials have a sensitivity of 500μJ/cm^2 [2]. One of the main aims of this research was to incorporate phase shifting techniques in a simple ESPI system so that the complete displacement map of the object under test can be generated. Results from chapter 6 showed that phase shifting in the compact transmission HOE based ESPI system can be done by modulating the drive current of

the laser diode. In the present system silver halide HOEs were used, to implement phase shifting by source modulation in the system either of the following conditions has to be satisfied. The hologram has to be recorded using the near infrared diode laser or hologram recorded at different wavelength has to be reconstructed using the diode laser. CLOSPI emulsions are particularly sensitive at 635 nm so the reflection HOE is recorded at 635 nm and the hologram emulsion was swollen so that the image could be reconstructed at 784 nm, the wavelength of the laser diode which is current modulated for phase shifting. The only practical way to implement phase shifting in this system is by current modulation of the laser. The swelling and reconstruction procedure at 784 nm is discussed section 7.7. The swelling technology was developed at CLOSPI.

7.4 HP-650 Plates at CLOSPI

The emulsion fabrication and development procedures are well established at CLOSPI. HP-650 emulsions are produced in a manner similar to Lippmann's technology [2]. The advantages of using the HP series emulsions are:

High diffraction efficiencies are readily achieved and the technique of swelling holograms recorded in these emulsions at 635 nm is well established and enables them to be used at near infrared wavelengths. The emulsions have already been used successfully in the fabrication of HOEs for infrared communications systems [6].

7.4.1 Procedures before developing

Before recording the holograms the following steps were taken;

- A plate was removed from the box/envelope and immersed, emulsion side up, in water at 20^0 C for approximately 2 minutes. This has to be done in low intensity scattered safelight, whose wavelength should be in the range of 570-590 nm.

- The plate was removed from water and excess water removed using a wet soft towel.
- The plate was dried in horizontal position (with the emulsion side up) at a temperature of not more than 25^0 C
- The glass surface on the side opposite to the emulsion layer was cleaned with a dry towel.
- The plates were ready for recording and they had to be used within 2 hours after the above process was started.

7.4.2 Developing procedures

Modified GP-9 was used to develop the holograms recorded on HP-650 plates [1].

The composition of the developer solution is;

Na_2SO_3-100 g,

Phenidone-0.2 g,

Hydroquinone-5.0 g,

KOH-3.8 g,

NH_4CNS-24.0 g,

H_2O- up to 1 litre.

The developer was diluted 1 in 10 parts of 15% aqueous solution of Na_2SO_4 before using. The development time was 4-4.5 min at 20^0C. 1 litre of developer was usually sufficient to develop the plates with an area of 1 square metre.

After developing the hologram, the normal white light could be turned on and the hologram had to be washed in running water at 20^0C for 5 to 10 minutes in the horizontal position. The excess water from the hologram surface could be removed by a wet soft towel. The hologram was dried with emulsion side up at 20-25^0C.

7.5 Recording HOEs

Reflection HOEs were recorded on HP-650 silver emulsions with a 30 mW He-Ne laser operating at 633 nm. The geometry of the hologram recording is shown in Figure 7.1. The laser was on a stable rectangular granite slab, which in turn was placed on four vertical legs positioned at the four corners of the slab. It was allowed to run continuously for at least 4 hours before recording the holograms, to ensure thermal stability.

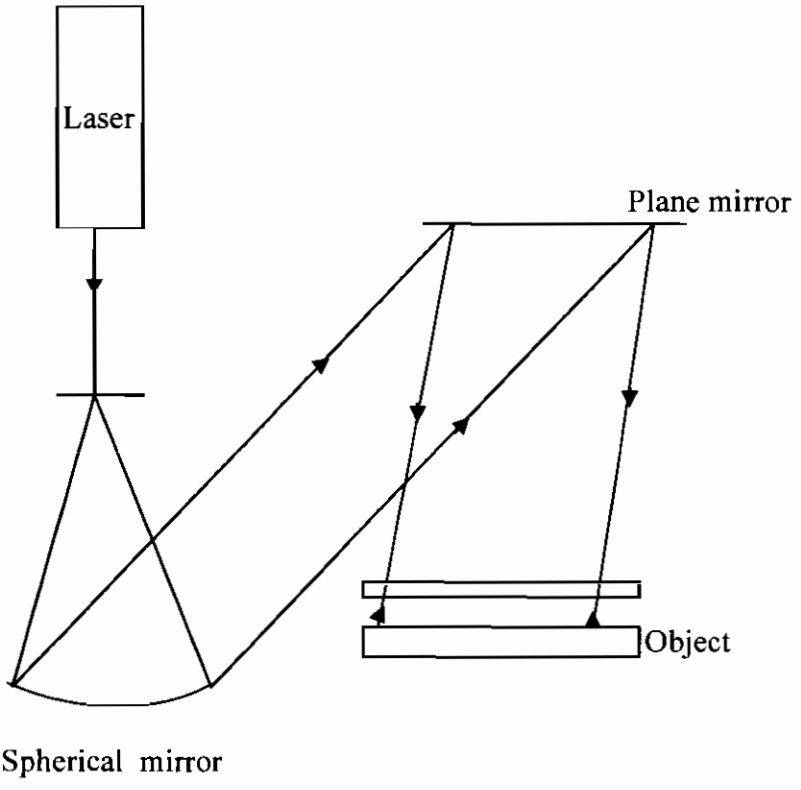

Figure 7.1 Reflection hologram recording setup

The spatially filtered laser light was made to fall on a spherical convex mirror. The reflected light from the spherical mirror was made to fall on a plane mirror (20 cm × 20 cm) placed at a height of approximately 70 cm above the table. The plane mirror was clamped in such way that the light reflected from it was directed onto the table. A square aluminum plate 10 cm × 10 cm was used as an object. The plate was coated with matt white paint for better reflection. The object was placed on the table and clamped

tightly in a purpose made mechanical holder to avoid mechanical vibrations. The distance between the object and the recording plate was approximately 1 cm. The recording plate was also firmly fixed. Exposure energy density of 1 mJ/cm^2 was used for recording [1]. At the recording plane a total intensity of 0.0033 mW/cm^2 was used with an exposure time of 300 seconds. Longer exposure times were used because of the low intensity laser power available. After processing, the image was reconstructed from the hologram and displayed on the monitor using the CCD camera. The image reconstruction from the hologram is shown in Figure 7.2.

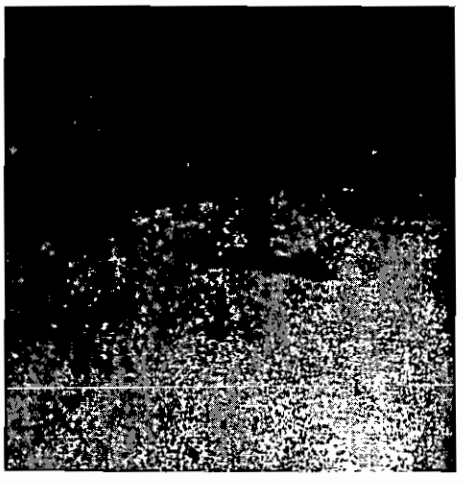

Figure 7.2 Photograph of image reconstructed from the hologram

7.6 Reflection HOE based ESPI system

The laser illuminates the holographic optical element and the CCD camera is placed in front of the HOE to capture the reconstructed image; at the same time the camera images the test object through the HOE.

The geometry of a reflection HOE based ESPI system is shown in Figure 7.3. The diverging beam of light from the laser illuminates the HOE; the light transmitted through the hologram falls on the surface of the object under test. The path length imbalance in the interferometer can be varied by varying the distance between the object and the holographic optical element. The laser is positioned in such a way that

the angle between the camera axis and laser beam axis is approximately 30 degrees. The angle is chosen in order for the CCD camera to be able to view the object normally through the HOE while avoiding the influence of reflected light from the HOE.

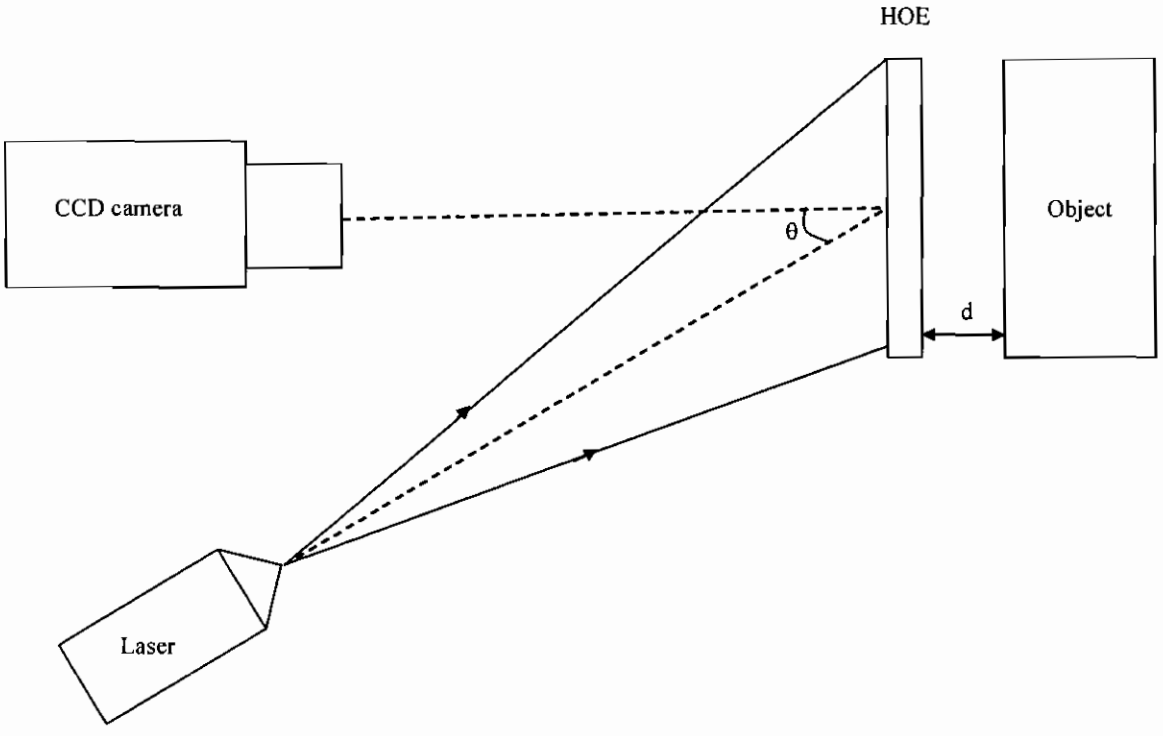

Figure 7.3 Reflection HOE based ESPI system

7.7 Reconstruction of Hologram at 784nm

Holograms were recorded on HP-650 plates using the He-Ne laser. A reflection hologram recorded at the visible wavelength can be reconstructed at 784 nm by swelling the holographic emulsion [5]. In order to find the optimum swelling time for maximum intensity in the reconstructed image, six holograms were recorded using the He-Ne laser with similar exposure energy and time of exposure. Developed holograms were immersed in swelling solution (prepared at CLOSPI) for different times ranging from 30 minutes to 3 hours. It was found that the holograms swelled for 150 minutes have good efficiency. Swelling procedures are already well established at CLOSPI and they

were used to enable the hologram to be reconstructed at 784 nm by changing the thickness of the emulsions [1, 5]. Swollen holograms are practically insensitive to humidity and there is no need to seal the hologram [5].

Before using the holographic optical element in the laser diode based ESPI system, it was tested using the He-Ne laser based ESPI system before swelling the hologram. The out-of-plane displacement of duraluminium plate, clamped around its periphery and connected to a vacuum chamber and pressurized uniformly, was studied. This exercise was carried out to make sure that the HOE was working satisfactorily. A typical fringe pattern obtained is shown in Figure 7.4.

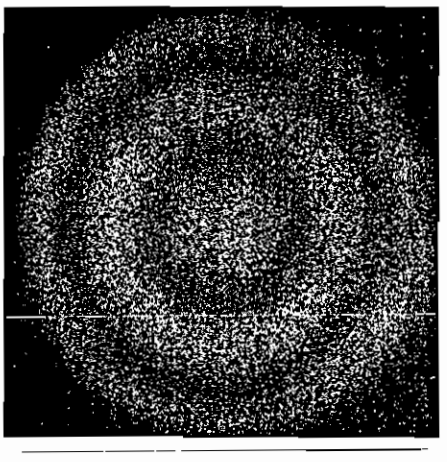

Figure 7.4 ESPI fringe pattern obtained using He-Ne Laser

Quantitative data from the ESPI fringes can be extracted by implementing phase shifting techniques in the interferometer [7]. In the present ESPI system phase shifting was implemented by varying the laser diode current in steps. The 5 frame phase shifting algorithm was used and the phase shifting errors can be minimized using this algorithm. Phase steps can differ from $\pi/2$ as long as they are equal [8]. From the experimental data, the phase step can be correctly calculated and used for correct phase map calculation. At the minimal current increments, experimentally estimated for this set-up, the influence of diode laser power variations could be neglected. The phase is calculated by using 5-frame algorithm given in equation 6.16.

Modulation of the diode laser current introduces a phase difference between the reference beam, (in this ESPI system which is, in fact, the reconstructed beam from the HOE) and the reflected beam from the object surface.

Suppose the geometrical path difference in the ESPI interferometer with a reflection HOE is d (approximately. twice the distance between reflection hologram and object). Then the phase difference is given by (2π d/ λ), where λ is the wavelength of the laser.

If the laser wavelength is changed by $\delta\lambda$ the phase difference in the interferometer changes by ($-2\pi\ \delta\lambda\ d\ /\lambda^2$) [9]. The value of diode current required to shift one full fringe was determined accurately by observing the ESPI fringes on the computer monitor. This value was divided into 4 equal steps to obtain five drive current values corresponding to phases of 0, 90^0, 180^0, 270^0 and 360^0.

7.8 Experimental

The experimental arrangement using the diode laser and HOE is shown in Figure 7.3. The test specimen was a circular duraluminium plate of 1.5 mm thickness with a diameter of 46 mm. The plate was clamped around the periphery, connected to a vacuum chamber and uniformly pressurized; approximately 0.1×10^5 N/m^2 of pressure was applied. The test object is shown in Figure 7.5. ESPITest software [10] was used to generate ESPI fringe patterns.

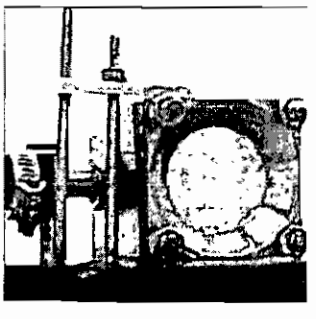

Figure 7.5 Photograph showing the test object

A Pulnix monochrome CCD camera with 0.75 cm interline transfer CCD and imager size of 752(H) × 582(V) was used to capture the fringe patterns. The camera has a resolution of 470 horizontal television lines. Five frames with a constant $\pi/2$ phase shift between each of them were obtained by changing the diode laser drive current. The laser diode current change required to shift one full fringe was measured and divided into four equal increments to obtain five drive current values corresponding to phases of 0, 90^0, 180^0, 270^0 and 360^0. Fringe patterns were obtained at each of the diode current settings and are shown in Figures 7.6 (a) to (e).

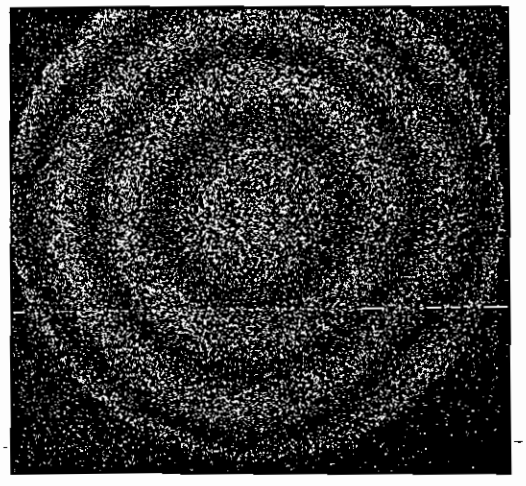

(a) 0°

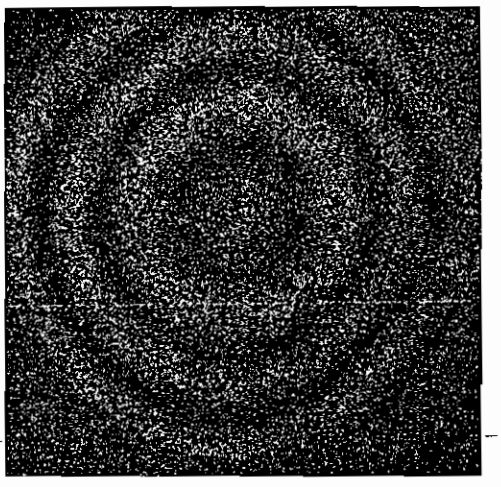

(b) 90°

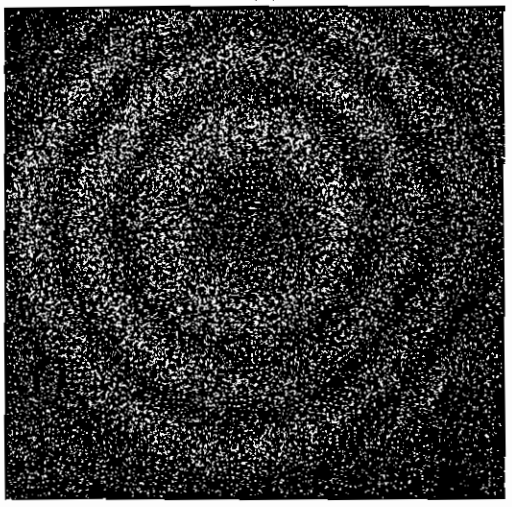

(c) 180°

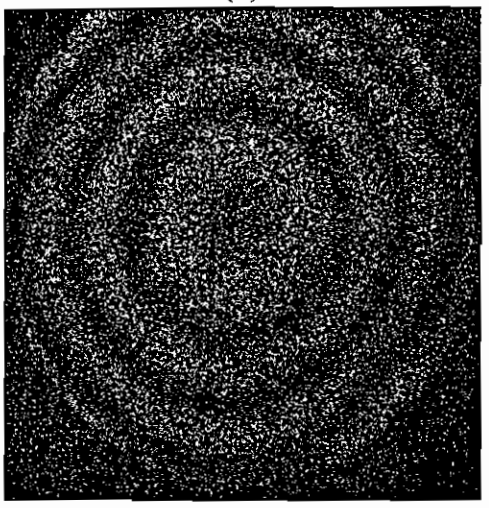

(d) 270°

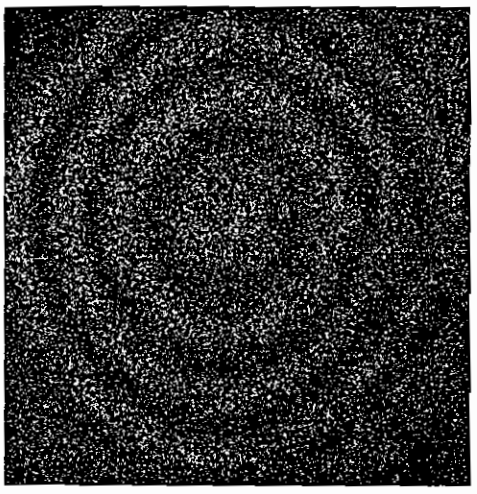

(e) 360°

Figure 7.6 Fringe patterns phase shifted by (a) 0° (b) 90° (c) 180° (d) 270° (e) 360°

The 5-frame algorithm with phase shift not equal to $\frac{\pi}{2}$[11] was used to minimize calibration error. The 2π ambiguities were removed by an adaptive unwrapping method [12] applied to the calculated phase map. The wrapped and unwrapped phase maps are shown in Figures 7.7 and 7.8.

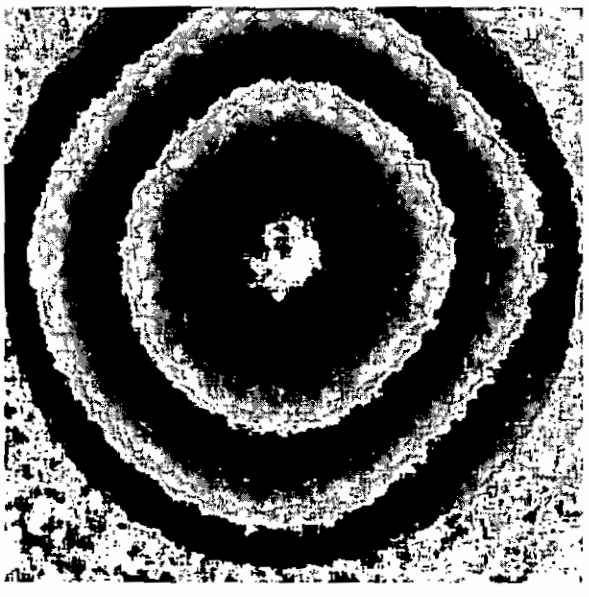

Figure 7.7 Wrapped phase map obtained using 5-frame algorithm

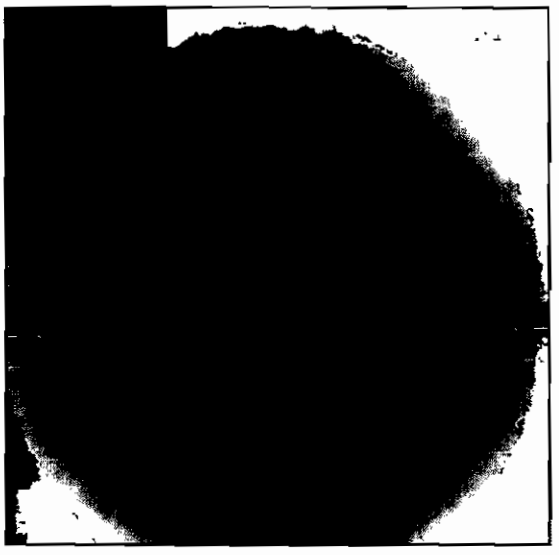

Figure 7.8 Unwrapped phase map

Mean value filtration with a 31 × 31 window was applied to reduce noise. In mean value filtration 31 × 31 pixels were averaged and the result is placed in the mid-window pixel. A 3D displacement map of the object was obtained using MATLAB and is shown in Figure 7.9. The out of plane displacement was found to be 1.26 μm.

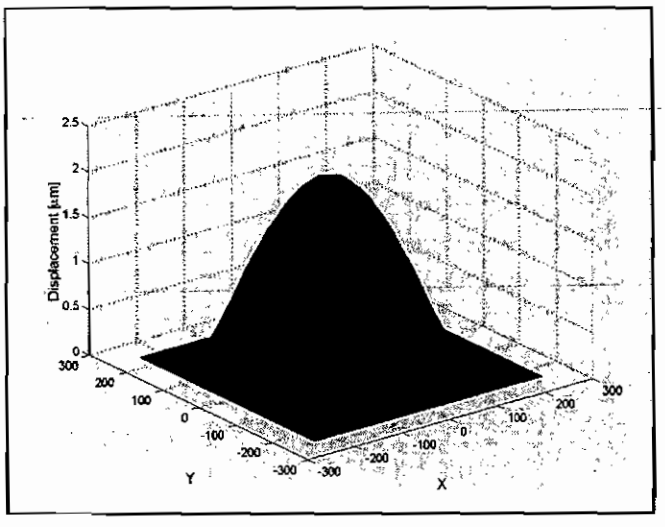

Figure 7.9 3D displacement map of the object deformation obtained from Figure 7.8 using MATLAB

Digital phase shifting for static loading has been implemented in a simple reflection HOE based ESPI system by modulating the drive current of the laser diode. In the next section vibration modes of objects are studied using the simple ESPI system.

7.9 Vibration studies

Electronic speckle pattern interferometry is a valuable tool for vibration analysis [13, 14, 15]. It possesses the unique advantages such as whole field, real time, fast and non-contact when compared with the conventional transducer based technologies used for vibration analysis. The quality of the interferogram obtained using ESPI is not good when compared to that of its chief competitor, holographic interferometry. This is due to the low resolution of the TV system. But for practical applications this drawback is outweighed by the high sampling rate of the TV system. A new interferogram is recorded every 1/25 s. Stetson and Powell gave a detailed explanation of time-averaged holographic recording of an object undergoing sinusoidal vibration [15]. The same explanation is valid for ESPI as well. Demand for non-contact measurement tools such as ESPI is growing, especially in industry, for vibration analysis. Even though it has got good application potential in industry its use is limited due to the requirement of extremely stable environment and complicated optical alignment. The second requirement can be overcome by using the compact system described in section 7.6 (Figure 7.3). When using the system (described in Figure 7.3), tedious chemical development is required to produce the reflection HOE which can be reconstructed at near infrared wavelength. A new improvement was made to produce the reflection HOE by recording the HOE with the diode laser (784 nm) to eliminate the swelling procedures. This step minimizes the chemical development procedures involved to produce the near infrared HOE.

7.9.1 Near infrared reflection HOE

The hologram was recorded using the diode laser operating at 784 nm. But the HP-650 plates have maximum sensitivity at ~650 nm and are almost insensitive at 784 nm. To record holograms at 784 nm HP-690 plates were used, having a different grain size. These emulsions have maximum absorption at 690 nm. To get the maximum diffraction efficiency 2 J/cm^2 of exposure energy was required at 784 nm. This value is more than 1000 times higher when compared with the exposure energies required by the normal HP-650 emulsions (for maximum diffraction efficiency the exposure is ~1 mJ/cm^2 at 633 nm wavelength). Under extremely stable conditions reflection holograms were recorded on HP-690 emulsions using a near IR laser diode with exposure times ranging from 5 to 30 minutes. Holograms were recorded using the experimental setup discussed in section 7.5 (Figure 7.1). This avoids half of the chemical development procedures by eliminating the swelling procedures.

7.10 Time average ESPI

The basic concept of time average ESPI is that a sinusoidally vibrating object will phase modulate light reflected from it to an extent that is proportional to the vibration amplitude.

Consider a test object whose surface is sinusoidally vibrating. The out-of-plane displacement of the object is described by

$$A = a_o e^{i(\omega t + \phi_v)} \quad \text{.....7.1}$$

Where a_0 is the amplitude, ω is the angular frequency, ϕ_v is the phase of the vibration.

For simplicity normal observation and normal illumination is used. The phase change due to the object vibration is

$$\phi(t) = \left(\frac{4\pi}{\lambda}\right) a_0 \cos(\omega t + \phi_v) \quad \text{.....7.2}$$

The object is vibrating out-of-plane in an out-of-plane sensitive ESPI system and the intensity distribution at the image plane of the CCD camera is given by (from equation 6.2)

$$\begin{aligned} I(x,y) &= I_1 + I_2 + 2\sqrt{I_1 I_2}\,\frac{1}{T}\int_0^T \cos\phi(t)dt \\ &= I_1 + I_2 + 2\sqrt{I_1 I_2}\,\frac{1}{T}\int_0^T \cos\left[\left(\frac{4\pi}{\lambda}\right) a_0 \cos(\omega t + \phi_v)\right]dt \end{aligned} \quad \text{.....7.3}$$

Applying a high pass filter removes the background intensity and with rectification equation 7.3 becomes

$$4I_1 I_2 \left\{\frac{1}{T}\int_0^T \cos\left[\left(\frac{4\pi}{\lambda}\right) a_0 \cos(\omega t + \phi_v)\right]dt\right\}^2 \quad \text{.....7.4}$$

Using the Bessel-function definitions, the interference term contains the information about the object vibration amplitude in the following form

$$4I_1 I_2 J_0^2\left(\frac{4\pi}{\lambda} a_0\right) \quad \text{.....7.5}$$

The time averaged interference term contains useful information about the vibration amplitude (a_o). The fringe pattern is different in appearance from the fringe pattern produced with static deformation. From the characteristics of the J_0^2 function it is seen that the brightest fringe corresponds to an argument of zero. The brightest fringe corresponds to the nodes of the motion. The brightness of the fringes decreases with increased amplitude of vibration. Time-average fringes themselves do not give information about the vibration phase of the object. The phase is completely lost because the averaging process during the exposure covers many vibration cycles [16]. The phase of the object vibration is obtained by modulating the reference beam in the

interferometer [17-22]. The reference beam can be reflected at a mirror vibrating with the same frequency as the object, with an amplitude a_r and phase ϕ_r. The Bessel component of the intensity distribution of the time averaged interferogram displayed on the monitor, is [23],

$$J_0^2\left\{\left(\frac{4\pi}{\lambda}\right)[a_0^2 + a_r^2 - 2a_0 a_r \cos(\phi_v - \phi_r]\right\}^{\frac{1}{2}} \quad \text{.....7.6}$$

where a_r, ϕ_r are the amplitude and phase of the reference beam path modulation.

The argument of the Bessel function originally contained the amplitude of the object vibration; with reference beam modulation the argument is replaced by the vectorial difference between the object and reference movement vectors.

The Bessel function will have maximum value when $a_o = a_r, \phi_v = \phi_r$.

With this condition, the fringe attains the maximum brightness. It is easy to detect the zero order fringe in the interferogram as its intensity is much higher than that of other order fringes. The significant intensity difference between the zero order and higher order fringes make it easy to assign the phase and amplitude to the points on the interferogram [23].

The zero order fringe can be shifted to any desired location on the object by changing the amplitude of the reference beam modulation. In this case the zero order fringe no longer represents the areas with zero amplitude of vibration but the areas vibrating with the same amplitude as that of the optical path difference in the interferometer. The phase of the vibration can be mapped by setting the amplitude of vibration of the object a_0 at a constant value and the region of maximum brightness is noted by varying ϕ_r. The fringes with maximum brightness represent the areas with the phase of the path difference modulation.

7.11 Comparison between transmission and reflection HOE based ESPI systems for vibration studies

A reflection HOE based ESPI system was used for mapping the phase and amplitude of vibration modes. A compact reflection HOE based ESPI system (Figure 7.3) was used for vibration analysis except that the HOE in the system was recorded at 784 nm.

Before describing the experimental work done on vibration analysis using the reflection HOE based ESPI system, comparison of the two systems (reflection & transmission) is made by introducing a transmission HOE based ESPI system with the piezoelectric transducer.

The geometry of the transmission HOE based ESPI system is shown in Figure 7.10. The laser beam is split into two using a beam splitter. Transmitted beam is deflected onto mirror M3 through M1 and M2. M3 is mounted on a piezoelectric device to produce the phase shift in the interferometer. Reflected beam from mirror M4 illuminates the test object. Reflected light from the piezo driven mirror M3 illuminates the transmission HOE to produce a speckle reference image. Object beam (1) scattered from test object and the speckle reference beam (2) are imaged using the CCD camera. When the test object is subjected to vibration, the vibration modes are seen on the computer monitor. This system is more complex than the transmission HOE based ESPI system used for static measurements (Figure 6.5), because of the incorporation of the piezoelectric transducer for phase mapping of the vibration modes.

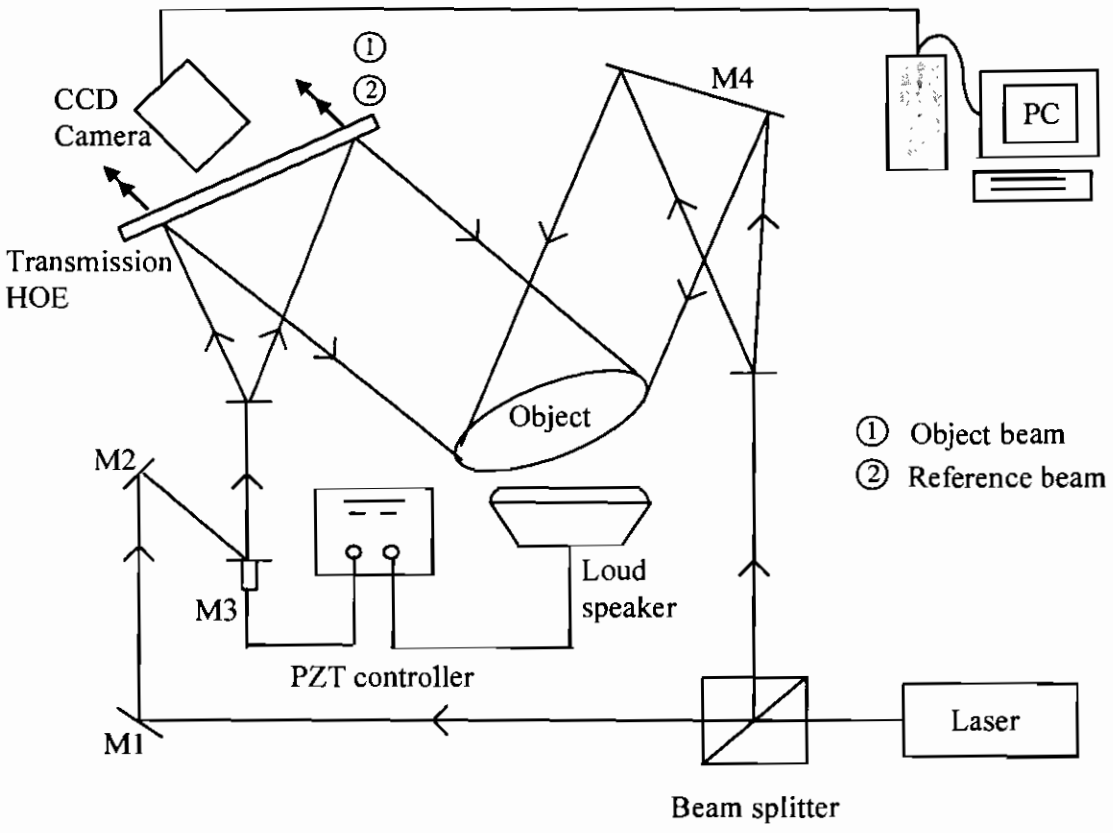

Figure 7.10 Transmission HOE based ESPI system for vibration measurements

The transmission HOE based ESPI system consists of the following optics: Mirrors (M1, M2, M3, M4) and a beam splitter. A He-Ne laser 632 nm wavelength with maximum power output of 25 mW was used in this experiment. The experimental setup is shown in Figure 7.11.

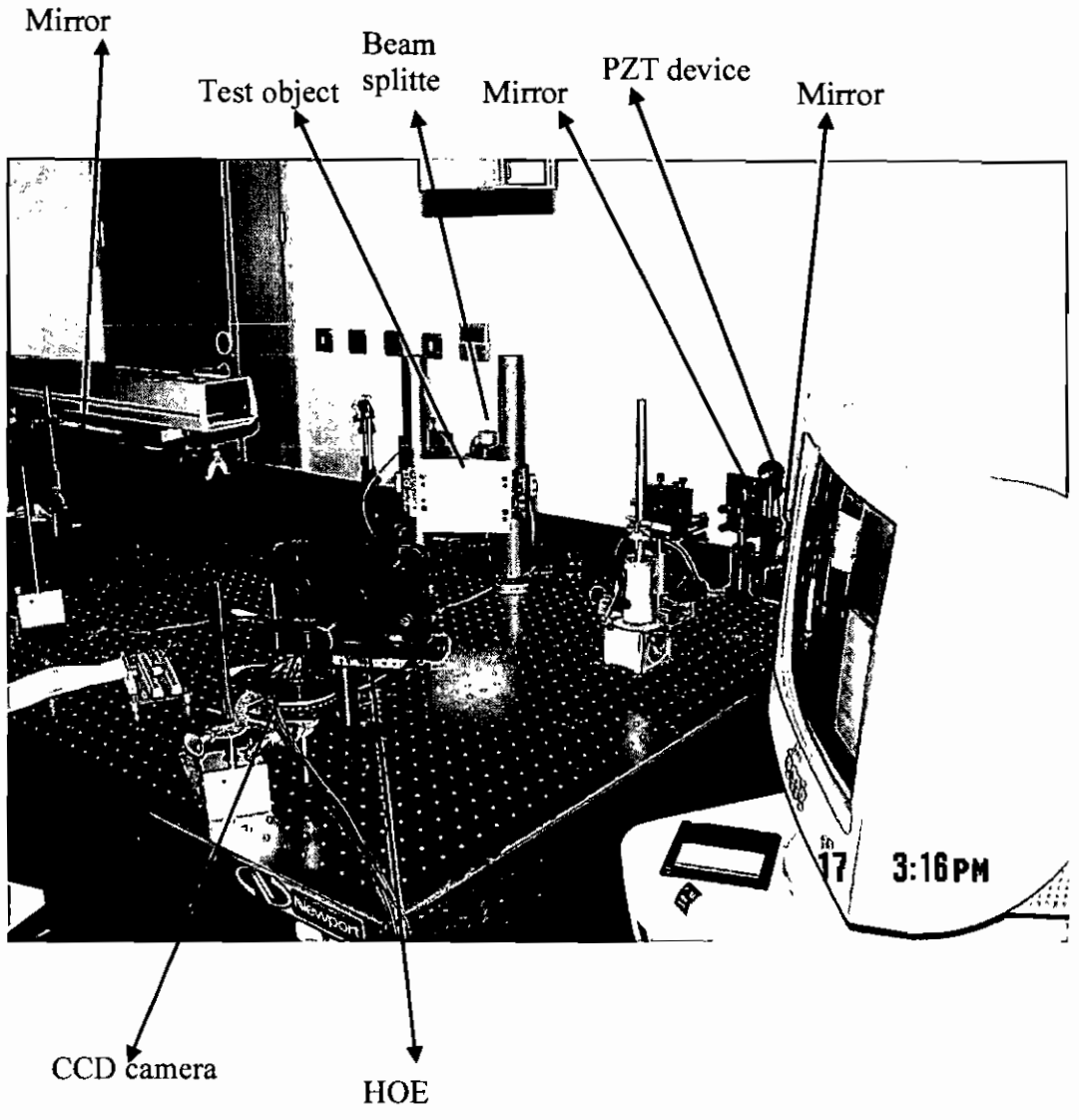

Figure 7.11 Transmission HOE based ESPI system - experimental setup

Vibration mode patterns of thin aluminium circular sheet clamped around its edges excited with a loud speaker were studied using the setup shown in Figure 7.11. Vibration mode patterns at frequencies 2950 Hz, 4400 Hz and 5500 Hz are shown in Figure 7.12. No image processing filters were used. The brightest areas in the fringe pattern represent the areas on the object surface which are not moving and are the nodal areas.

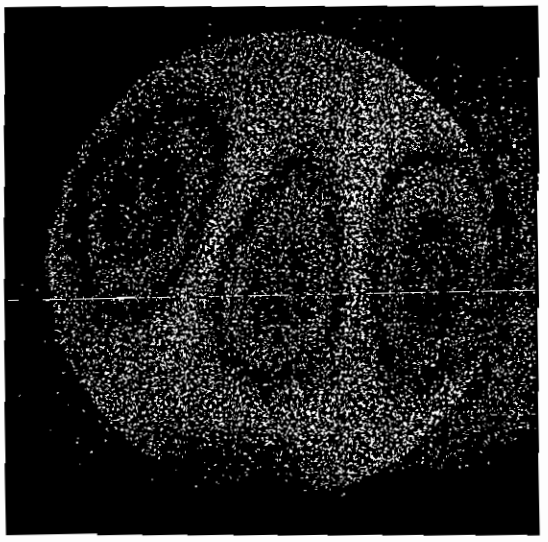

(a) 2950 Hz

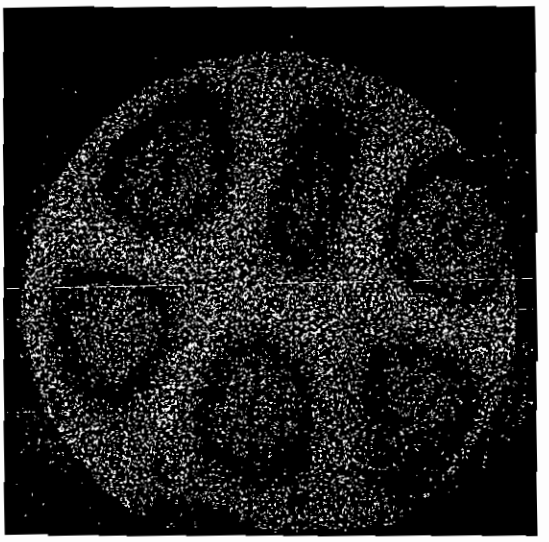

(b) 4400 Hz

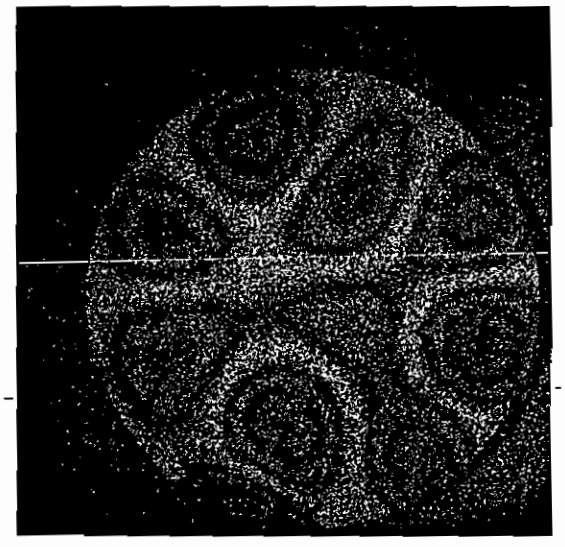

(c) 5500 Hz

Figure 7.12 Vibration mode patterns of thin aluminium circular sheet clamped around its edges excited with a loud speaker obtained using transmission HOE based ESPI system a) 2950 Hz, b) 4400 Hz, c) 5500 Hz

The above results were obtained using a transmission HOE based ESPI system. These results show that the vibration modes can be studied using the transmission HOE based ESPI system but the system is complex due to the incorporation of the

piezoelectric transducer to implement phase shifting. The aim of the work is to make the system simple and compact without affecting the performance. Preliminary results (section 6.5.3) indicated that in a reflection HOE based ESPI system phase shifting can be implemented by modulating the current in the laser. To study the amplitude and phase of the vibration modes a reflection HOE based ESPI system is used with a current modulated laser diode.

The reflection HOE based ESPI system only has four elements; HOE, CCD camera, the laser and test object. The path length can be varied in a reflection HOE based ESPI system by moving the test object towards or away from the HOE thus allowing easy implementation of phase shifting. The experimental setup of the reflection HOE based ESPI system is shown in Figure 7.13. Compared to the system in Figure 7.11 this system is simpler. This system was used for mapping the amplitude and phase of the vibration modes, phase shifting is done by modulating the current of the laser diode (described in the following section 7.12).

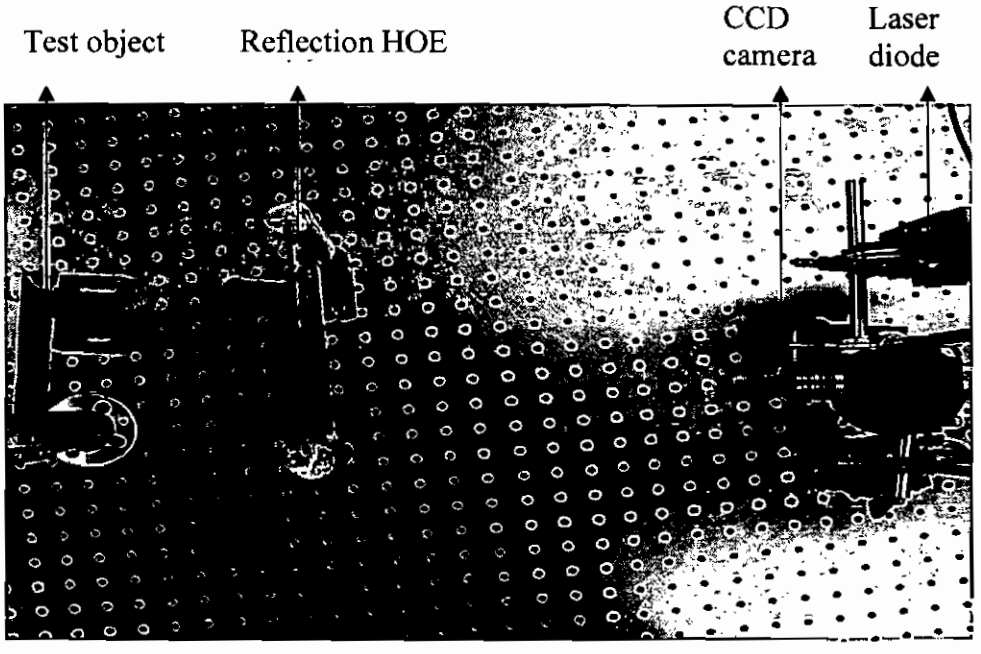

Figure 7.13 Reflection HOE based ESPI system for vibration studies

7.12 Experimental work using reflection HOE based ESPI system

Phase shifting techniques [5, 9] were used to get the information about the amplitude and phase of the vibration. Phase shifting was implemented by direct modulation of the diode laser wavelength at the vibration mode frequency. The laser diode frequency response was studied using a Michelson interferometer; this tells us the upper limit of vibration frequency that could be mapped using this technique. The laser drive modulation voltage needed to shift one full fringe for a particular path length difference in the interferometer was also measured.

The theory of laser diode current modulation in phase stepping interferometry has been reported elsewhere [24-28]. Wavelength modulation of a laser diode source via injection current modulation has been used in a speckle shearing interferometer for vibration analysis [29].

The following are the two important conditions used to map the amplitude and phase of the vibration modes.

Amplitude mapping of the mode pattern:

The amplitude of vibration of the object can be mapped by applying the following condition (equation 7.6) in the interferometer.

Fix $\phi_{ref} = \phi_{obj}$ and vary the amplitude of reference beam modulation; in this case the brightest fringe visible is where the object vibration amplitude equals the amplitude of oscillation of the optical path difference in the interferometer.

Phase mapping of the vibration:

The amplitude modulation of the path difference is fixed and the phase difference between object and reference beam is varied in steps. The brightest fringe in

the interferogram has the phase of the difference of phase between the object and reference beam paths.

7.12.1 Laser diode calibration

The laser diode was calibrated using a Michelson interferometer. The change in drive current need to shift one complete fringe was measured. Different path length imbalances (ranging from 5 cm to 20 cm) in the interferometer were used. It is very important to employ a laser diode with a flat frequency response including the vibration frequencies of interest. The laser diode frequency response was also obtained by using the Michelson interferometer. The experimental arrangement used for laser diode calibration is shown in Figure 7.14.

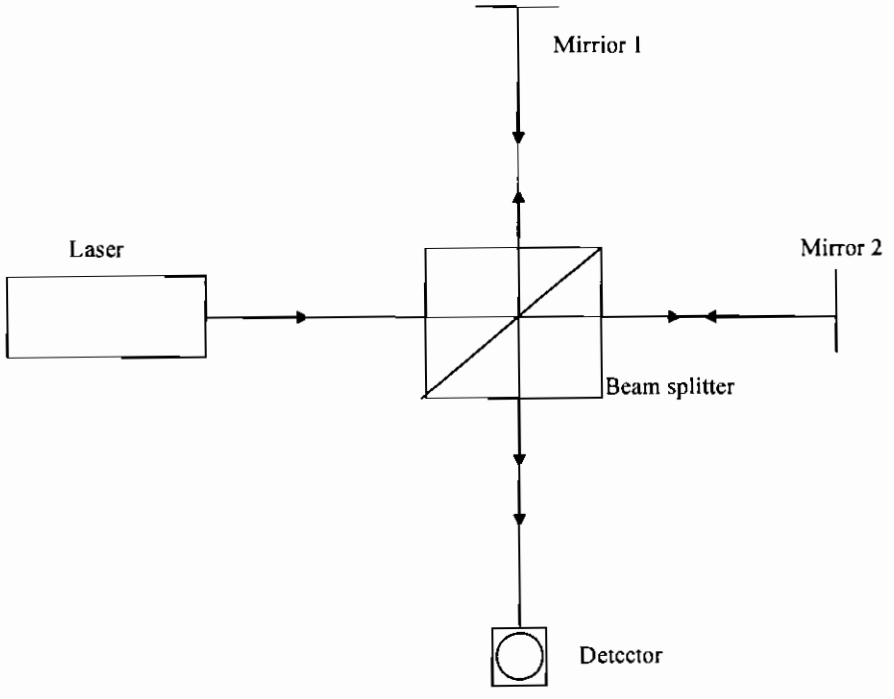

Figure 7.14 Laser diode calibration using a Michelson interferometer

The diode is operated at low power levels to avoid saturation in the images. The laser light is split using a beam splitter with beam ratio 1:1. The length of one arm of the interferometer is fixed and the other arm path length varied by changing the position of the mirror 2. The Michelson interference fringes are projected onto a screen using a 20X

microscopic objective and imaged using a CCD camera (Figure 7.15). A plot of the fringe order Vs modulation voltage is shown in Figure 7.16. There is a linear relationship between the fringe order and modulation voltage for each path length difference in the interferometer.

The experimental setup is slightly altered and one of the mirrors in the interferometer is replaced with a piezoelectrically driven mirror to study the frequency response of the diode laser. The voltage of the modulation signal applied to the diode laser is chosen such that the amplitude of oscillation of the optical path difference does not exceed one fringe order. A Texas instruments TSL 250 photodiode was used to detect the interference signal. It has the peak spectral response at 800 nm with frequency response of 10 MHz. A plot of photodiode voltage vs frequency of the drive signal was obtained. The laser exhibits a flat frequency response up to 1200 Hz and after that its frequency response decays, see Figure 7.17. Vibration modes of the object up to 1.2 kHz can therefore be studied.

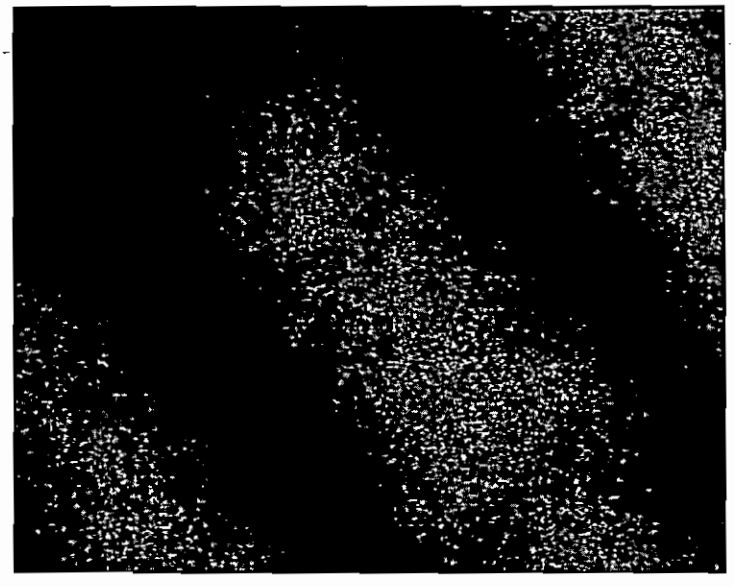

Figure 7.15 Photograph of Michelson interference fringes obtained using laser diode

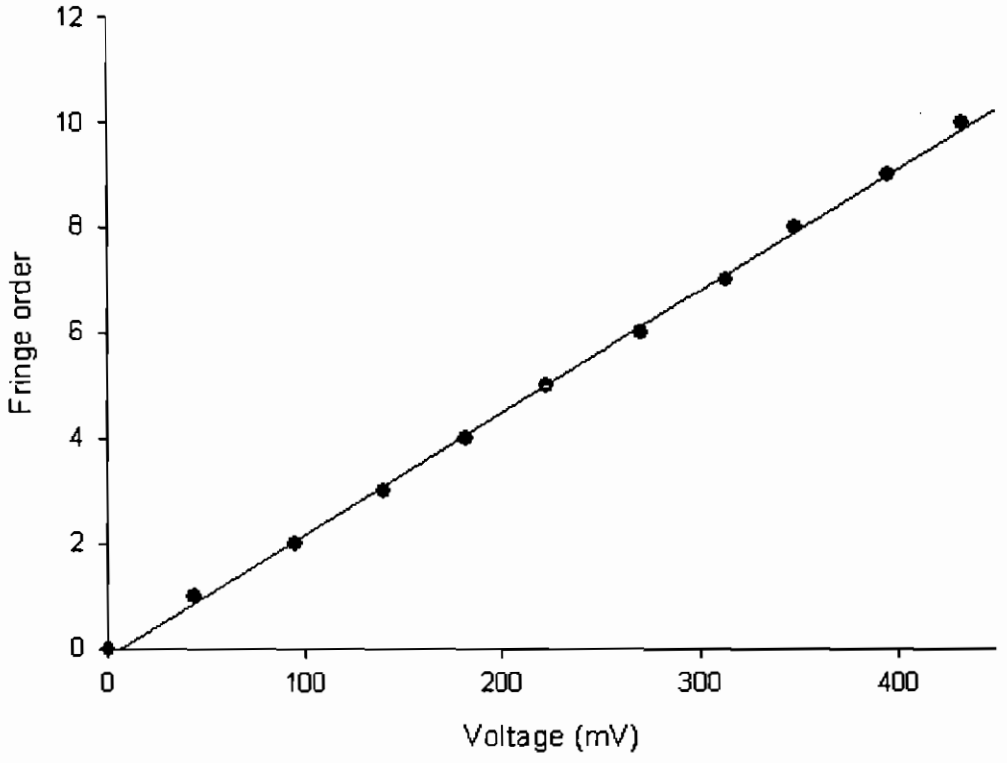

Figure 7.16 Plot of fringe order vs modulation voltage for an optical path difference of 10 cm

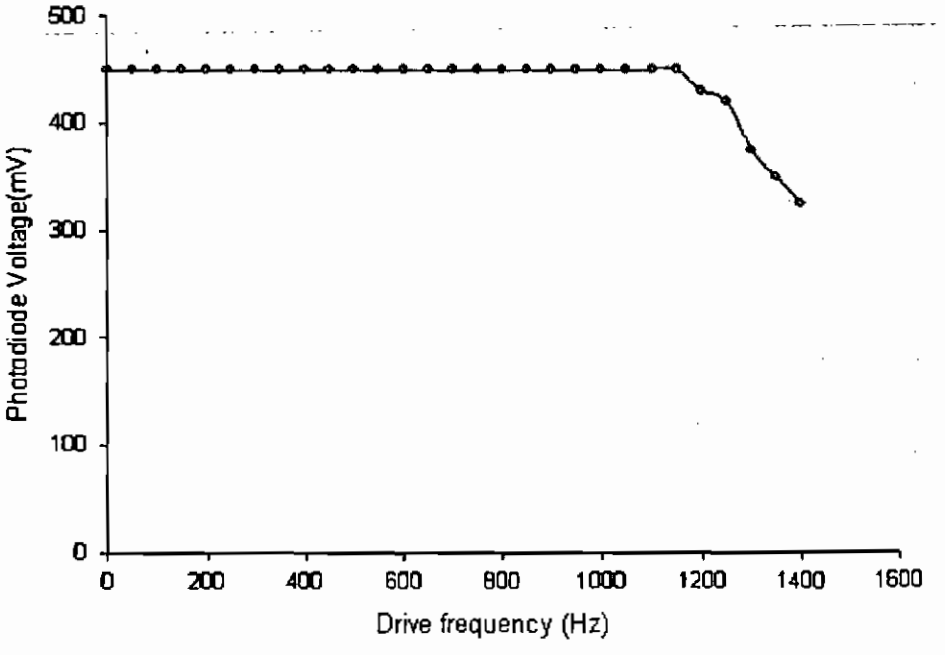

Figure 7.17 Frequency response of diode laser

7.12.2 Vibration mode pattern studies using HOE based ESPI system

The HOE based ESPI system shown in Figure 7.13 was used to map the amplitude and phase of the vibration mode patterns. The interferometer was setup on a Newport vibration isolated table. A 20X microscope objective was used to expand the beam of light. The laser beam fell on the HOE, which diffracted a speckle reference beam to the CCD and the light transmitted through the HOE illuminated the test object. The light reflected by the object was transmitted through the HOE to the CCD. The test object was a square brass metal sheet, 1 mm thick, firmly attached to a square shaped Mylar cone loudspeaker of 100 mm × 100 mm. The front face of the metal sheet was coated with matt white paint to improve reflection. A National Instruments frame grabber card IMAQ-1407 was used. A LabVIEW program was used for subtraction of specklegrams of two time averaged specklegrams from one another. A second LabVIEW program was developed to generate two ac signals from the computer by using the National Instrument's PCI-1200. The amplitude of each signal can be altered independently and there is a provision to introduce a predefined phase between the two signals. One of the signals is used to drive the loud speaker and the second is used to modulate the laser drive current.

Initially the distance between the HOE and test object was set at 10 cm, which gave an effective path difference of 20 cm in the interferometer. From the calibration curve of the diode laser it is known that modulating the laser diode by 43 mV modulation voltage produces 1.5 fringe shift. The amplitude of vibration of the object can be obtained from the fringe pattern. Initially the brightest regions on the image are the areas where the object vibration amplitude is zero. The bright fringe region on the surface of the object can be moved to different locations by increasing the modulation voltage. The phase mapping of the vibration modes can be done by introducing a phase

difference between the two signals. The amplitude and phase maps of the vibration mode at 975 Hz are shown in Figure 7.18. The brightest fringe represents zero amplitude of the vibration when there is no modulation in the interferometer. The time average fringe pattern with zero modulation of the path difference in the interferometer is shown in Figure 7.18(a). The brightest fringe has moved to edges of the test surface with a laser modulation voltage of 23mV in (7.18(b)).

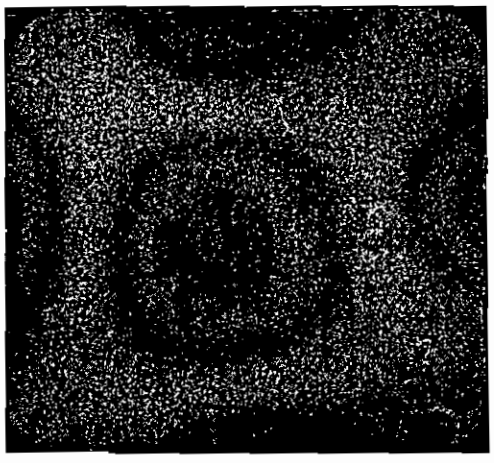

a) modulation voltage 0 mV

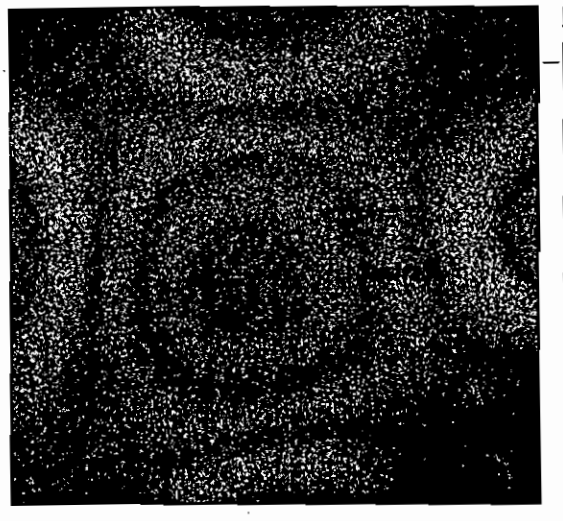

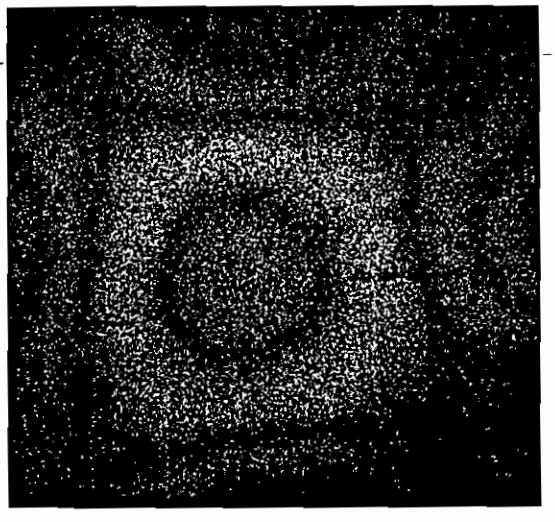

(b) modulation voltage 23 mV (c) 180^{o} phase

A phase difference of 180 degree exists between 7.18(b) and 7.18(c). The brightest fringe in Figure 7.18(b) is vibrating with zero degrees phase. It was shifted towards the centre of the object by applying a phase of 180 degrees between the two

signals driving the loud speaker and the laser diode. The bright fringe in Figure 7.18(c) is vibrating with 180 degree phase. The phase difference between the two signals was varied to 90 and 270 degrees.

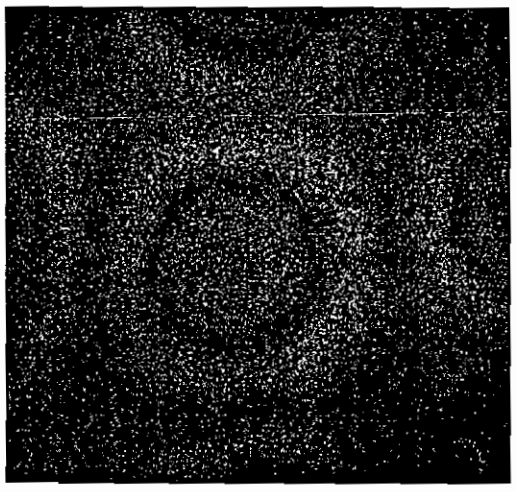

d) 90° phase

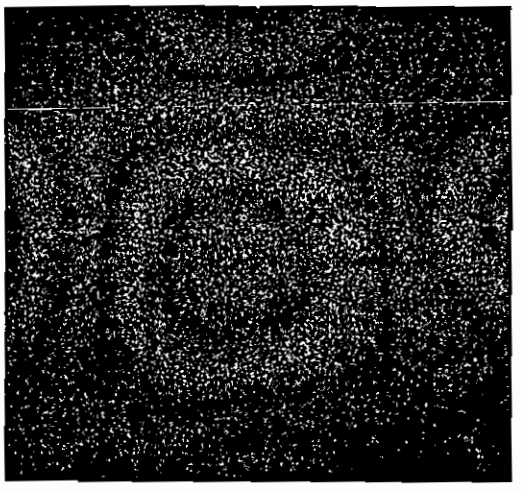

e) 270° phase

Figure 7.18 Vibration mode patterns obtained at a) 0mV modulation, b) 23 mV and 0° phase, c) 23 mV and 180° phase, d) 23 mV and 90° phase, e) 23 mV and 270° phase

The bright fringe, located at the center of the fringe pattern in 7.18(d) is vibrating with 90 degree phase and with 270 degree in 7.18(e).

The amplitude of the vibration was calculated from the roots of Bessel function (equation 7.5).

$$J_0(\frac{4\pi a_v}{\lambda}) = R_v \quad \text{.....7.7}$$

The first root of R_v for $J_0(R_v)$ is equal to 3.9624.

The amplitude of vibration is evaluated using the equation

$$a_v = \frac{\lambda R_v}{4\pi} \quad \text{.....7.8}$$

The brightest fringe (Figure 7.18(b)) is vibrating with amplitude of 0.247 μm.

The amplitude map of the time averaged ESPI fringe pattern of a circular thin aluminium sheet of diameter 10 cm clamped around its periphery vibrating at 500 Hz is shown in Figure 7.19. Initially the brightest fringe is at the periphery with no modulation voltage, which is shown in Figure 7.19(a). The brightest fringe moved across the object as the modulation voltage was increased. Fringe patterns obtained with modulation voltages of 43, 86, 129 mV are shown in Figures 7.19(b) to 7.19(d) respectively. With 129 mV of modulation voltage applied to the diode laser the brightest fringe was brought to the centre from the periphery.

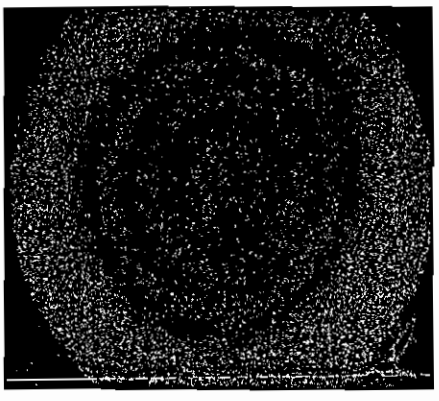

a) 0 modulation voltage

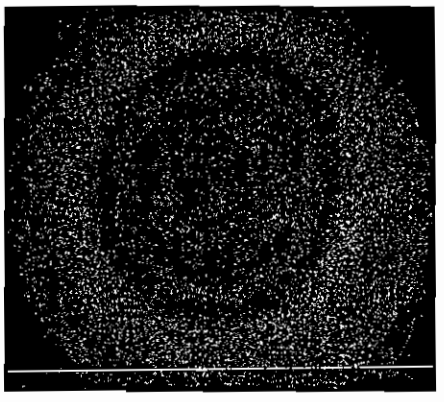

b) modulation voltage 43 mV

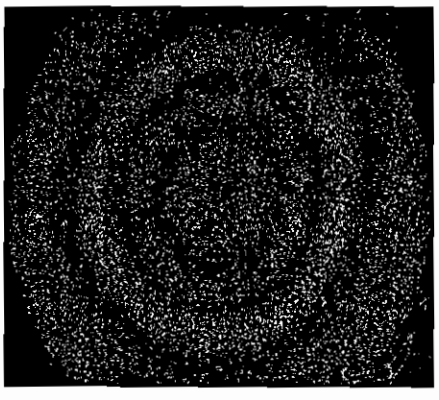

c) modulation voltage 86 mV

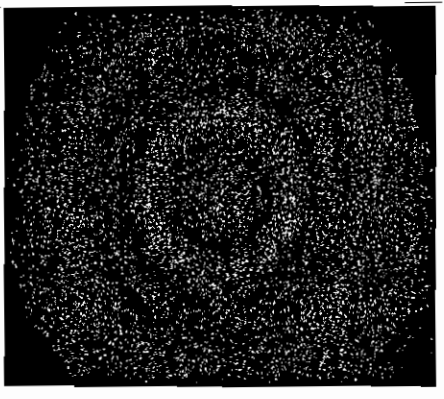

d) modulation voltage 129 mV

Figure 7.19 Amplitude map of the vibrating object a) modulation voltage 0 mV, b) modulation voltage 43 mV, c) modulation voltage 86 mV, d) modulation voltage 129 mV

7.13 Conclusions

A simple and compact phase shifting ESPI system that has good potential for practical applications is reported. The HP series silver halide emulsions are of particular interest because they are able to produce HOEs with good diffraction efficiency at near infrared wavelength when swollen. This compact ESPI system, which has the phase shifting facility, is possible with an infrared reflection HOE. When compared with a transmission HOE based ESPI system (described in chapter 6) using a reflection HOE produces the most simple system. Use of a plane mirror (Figure 6.6) is eliminated. The major concern with this system is that recording HOEs on silver halide emulsions requires tedious chemical processing during the development and the swelling procedure involves more chemical processing. Advantages of the simple and compact system are partly outweighed by the tedious procedures of development.

To minimize the chemical development involved, the HOEs were recorded using a near infrared laser diode (784 nm) with long exposure times. This eliminates the swelling procedures. The tedious chemical development still exists during HOE fabrication and it is a drawback associated with this system. This drawback can be overcome by using materials, which do not require chemical processing for hologram recording. The materials with self processing ability are a possible alternative to overcome this difficulty. At the same time it is more challenging and difficult to develop photopolymer materials which possesses high spatial frequency response to record reflection HOEs.

A simple ESPI system using a reflection HOE has been tested in static and dynamic loading conditions. The results are encouraging but the problem with silver halide recording materials is that they require chemical processing. This problem is eliminated by using a photopolymer recording material to fabricate reflection HOE.

Research is still in progress to improve the photopolymer material spatial frequency response for reflection holography and significant advances have been made [30]. In the next chapter use of a reflection photopolymer HOE in an ESPI system is discussed and preliminary results are presented.

References

1. V. C. Sainov, "Basic Characteristics and applications of reflection holograms," Proceedings of the International symposium on display holography, Holography workshops, Lake Forest College, Lake Forest, lllions, Volumel, July12-16, (1982).
2. H. Bjelkhagen, "Silver Halide Recording Materials for Holography and their Processing," Chapter 3.6.1, Springer-Verlag, v.66, (1995).
3. A. Katsev, M. Mazakova, M. Pancheva, N. Pangelova, T. Petrova, V. Razsolkov, "Silver light sensitive plates HP-490 and Developer FHP-3 for Holographic Applications," Jour of Signal AM, 9(2), 107-111, (1981).
4. T. Petrova, P. Popov, E. Jordanova, S. Sainov, "Holographic emulsion for the near-infrared region", Opt. Mat., 5, 193-195, (1996).
5. S. Jivkova, S. Shurulinkov, M. Kavehrad, "Holographic Parabolic Mirror as a Receiver Optical Front End for Wireless Infrared Communications: Experimental Study," Appl. Opt, 41 28, 5860, (2002).
6. S. Jikova, M. Kavehard, "Holographic optical receiver front-end for wireless infrared indoor communications," Appl. Opt, 40, 2828-2835, (2001).
7. P. K. Rastogi, "Holographic Interferometry Principles and Methods," Chapter 5, Springer series in optical sciences, Vol 68, Springer-Verlag Berlin, (1994).
8. K. Larkin, B. Oreb, "Design and assessment of symmetrical phase-shifting algorithms," J. Opt. Soc. Am. A, 9, 1740-1748, (1992).

9. K. D. Hinsch, H. Joost, P. Meinlschmidt, F. Schluter, "Modulation of laser diode parameters for special performance electronic speckle pattern interferometry (ESPI)," Opt. Comm, 144, 12-16, (1997).

10. ESPITest software, Andreas Langhoff, Milan, Portions Copyright © European Commission, Joint Research Centre, Ispra, Italy, (1998).

11. G. Stoilov, T. Dragostinov, "Phase-Stepping Interferometry: Five-frame Algorithm with an arbitrary step," Optics and Lasers in Engineering, 28, 61 - 69, (1997).

12. G. Stoilov, "Method for Adaptive Unwrapping Using a Criterion for Maximum Probability of The Information Reliability," in Proceedings of 2nd International Workshop on Automatic Processing of Fringe Patterns, W. Juptner, W. Osten, ed., Akademie Verlag - Berlin, Physical Research V.19, pp. 182-187 (1993).

13. O. J. Lokberg, "ESPI-The ultimate holographic tool for vibration analysis," J. Acou. Soc. of Am, 75, 1783-1791, (1984).

14. O. J. Lokberg, "Electronic speckle pattern interferometry," Phys. Tech, 11, 16-22, (1980).

15. K. A. Stetson, R. L. Powell, "Interferometric hologram evaluation and real-time vibration analysis of diffuse objects," J. Opt. Soc. Am, 55, 1694-1695, (1965).

16. O. J. Lokberg. "Use of chopped laser light in electronic speckle pattern interferometry," Appl. Opt, 18, 2377-2384, (1979).

17. O. J. Lokberg, K. Hogmoen, "Use of modulated reference wave in electronic speckle pattern interferometry," J. Phys. E: Sci. Instruments, 9, 847-851, (1976)

18. K. Hogmoen, O. J. Lokberg, "Detection and measurement of small vibrations using electronic speckle pattern interferometry," Appl. Opt, 16, 1869-1875, (1976)

19. O. J. Lokberg, K. Hogmoen, "Vibration phase mapping using electronic speckle pattern interferometry," App. Opt, 15, 2701-2704, (1976).

20. S. Ellingsrud, O. J. Lokberg, "Full field amplitude and phase measurement of loudspeakers by using TV-holography and digital image processing," J. Sound. Vibration, 168, 193-208, (1993).

21. K. Creath, "Phase shifting speckle interferometry," Appl. Opt, 24, 3053, (1985).

22. S. Nakadate, "Vibration measurement using phase-shifting speckle-pattern interferometry," Appl. Opt, 25, 4162-4167, (1986).

23. A. P. M. Hurden, "Vibration mode analysis using electronic speckle pattern interferometry," Opt. Laser. Tech, 14, 21-25, (1982).

24. K. Tatsuno, Y. Tsunoda, "Diode laser direct modulation heterodyne interferometer," Appl. Opt, 26, 37-40, (1987).

25. K. D. Hinsch, H. Joost, P. Meinlschmidt, F. Schluter, "Modulation of laser diode parameters for special performance electronic speckle pattern interferometry (ESPI)," Opt. Comm, 144, 12-16, (1997).

26. A. Valentin, C. Nicolas, L. Henry, A. W. Mantz, "Tunable diode laser control by a stepping Michelson interferometer," Appl. Opt, 26, 41-46, (1987).

27. L. R. Watkins, M. D. Hoogerland, "Interferometric ellipsometer with wavelength-modulated laser diode source," Appl. Opt, 43, 4362-4366, (2004).

28. P. Hariharan, "Phase-stepping interferometry with laser diodes: effect of changes in laser power output wavelength," Appl. Opt, 28, 27-29, (1989).

29. J. R. Huang, H. D. Ford, R. P. Tatam, "Heterodyning of speckle shearing interferometers by laser diode wavelength modulation," Meas. Sci. Technol, 7, 1721-1727, (1996).

30. J. Raghavendra, "Optimization of an acrylamide based photopolymer for reflection holographic recording," Dublin Institute of Technology, Dublin, October, (2005).

8. ESPI system using a photopolymer reflection HOE

8.1 Photopolymer reflection HOE

Reflection HOEs recorded in silver halide emulsions were used in the ESPI system (chapter 7). The most compact ESPI system was used to measure the out-of-plane deformation of an object in a static loading condition and to map the amplitude and phase of vibrating object under dynamic loading. Phase shifting was implemented using current modulation of the diode laser.

Acrylamide based photopolymer material was used to fabricate reflection holographic optical elements [1, 2, 3, 4]. Work is under progress at the Centre for Industrial and Engineering Optics to improve the spatial frequency response of the photopolymer to record reflection holograms. The material's spatial frequency response has been increased and the material is now capable of recording reflection holograms. The details about the material characteristics have yet to be published by the other members of the group. In this chapter the reflection holographic characteristics are not discussed in detail. The material was used to fabricate the reflection HOE.

8.2 Experimental work using photopolymer reflection HOE

A reflection HOE was recorded in acrylamide based photopolymer layers using an Nd-YVO_4 laser at 532 nm. The photopolymer layer preparation procedure was explained in section 5.4.1. The experiment was carried out on a Newport vibration isolation table. The schematic of the HOE recording is shown in Figure 8.1. The laser was switched on and allowed to run for 1 hour before recording the hologram, which enables the laser to thermally stabilise. The laser light was spatially filtered. A lens of 2.5 cm diameter with focal length of 25 cm was used to collimate the laser light.

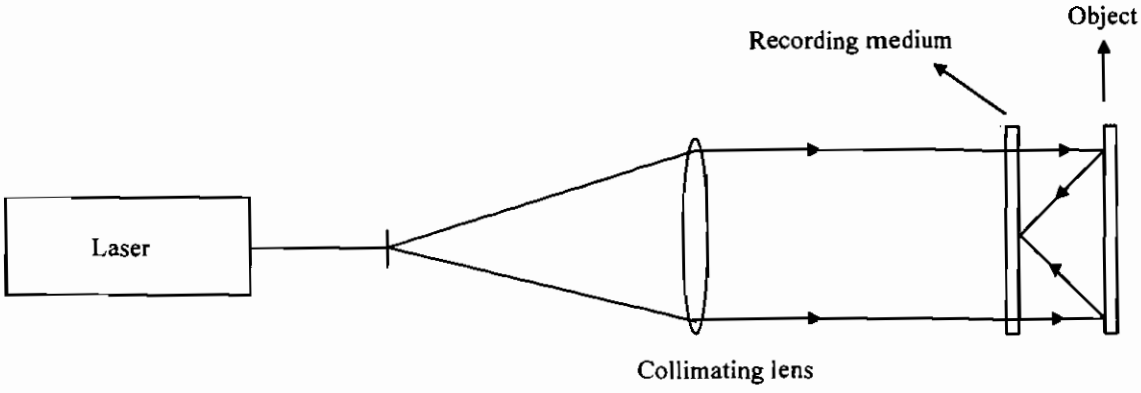

Figure 8.1 Reflection HOE recording geometry

A hologram of a 5 cm × 5 cm thick aluminium plate was recorded with the plate placed 1 cm apart from the recording medium. Light intensity of 40 mW/cm^2 with an exposure time of 60 seconds was used in fabricating the HOE.

The vibration mode patterns of a thin circular sheet of aluminium of 4 cm diameter attached to a paper cone loud speaker 4 cm in diameter were studied. The HOE was mounted on a rotational stage and illuminated by 532 nm laser light. The HOE was rotated and positioned in such a way that a bright reconstructed image of the original object was imaged with a CCD camera. The test object was placed behind the HOE. The CCD camera viewed the test object through the HOE. A LabVIEW program was used for subtraction of two time averaged specklegrams from one another [5]. The vibration mode patterns at frequencies 1000 Hz, 2600 Hz, 6400 Hz are shown in Figure 8.2.

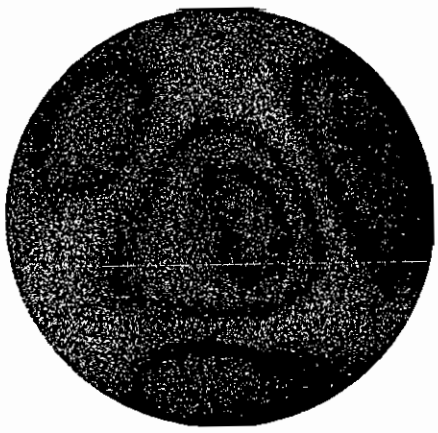

(a) 1000 Hz

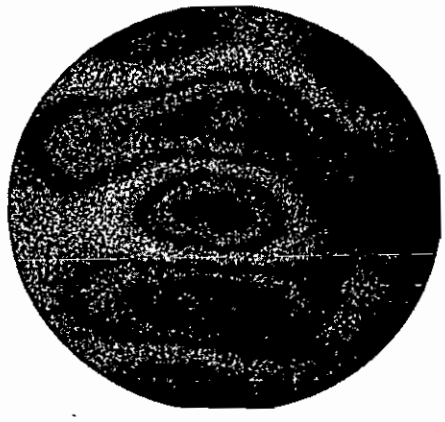

(b) 2600 Hz

(c) 6400 Hz

Figure 8.2 Time averaged vibration mode pattern

8.3 Conclusions

A photopolymer reflection HOE was used in the ESPI system. Fabrication of HOEs in the photopolymer has eliminated the cumbersome and lengthy development procedures usually required by the other conventional recording materials such as silver halide emulsions. For the first time, a reflection HOE recorded in photopolymer was used as the sole optical component in a compact ESPI system.

References

1. S. Martin, "A new photopolymer recording material for holographic applications: photochemical and holographic studies towards an optimized system," PhD Thesis, Trinity College, Dublin, August, (1995).

2. S. Martin, C. A. Feely, V. Toal, V., "Holographic Characteristics of an Acrylamide Based Recording Material," Appl, Opt, Vol. 36, 5757-5769, (1997).

3. S. Martin, P. Leclere, Y. Renotte, V. Toal, Y. Lion, "Characterisation of an acrylamide-based dry photopolymer holographic recording material" Opt. Engg, 33, 3942-3946, (1995).

4. I. Naydenova, R. Jallapuram, S. Martin, R. Howard, V.Toal, "Investigation of the diffusion processes in self-processing acrylamide-based photopolymer system," Appl. Opt, 43, 2900-2905, (2004).

5. P. K. Rastogi, "Digital speckle pattern interferometry and related techniques," John Wiley Sons Ltd, New York, (2001).

Conclusions

The purpose of this research work was to develop a simple and compact electronic speckle pattern interferometer using holographic optical elements. Photopolymers and silver halide emulsions were used to record the holographic optical elements. The self processing ability of the acrylamide based photopolymer was exploited in holographic interferometry and the chemical processing of holograms was eliminated.

The self processing capability of the recording material also reduces the time required for testing. The material is inexpensive and easy to prepare. The radial strain of a thick walled polyvinyl chloride pipe closed at both ends and vertically supported when pressurized was measured using holographic interferometry. Young's modulus of elasticity of the material (PVC pipe) was measured and it was in good agreement with the manufacturer's value.

A simple ESPI system was developed which incorporated a single HOE to generate a speckle reference wave. The final system does not contain any other optical components.

Use of transmission and reflection HOEs in the ESPI system was demonstrated. The radial strain of a thick PVC pipe was measured using the transmission HOE based ESPI system. Young's modulus of elasticity was measured. The results were compared with those obtained using holographic interferometry. Both were in good agreement with the manufacturer's value. For the first time both holographic interferometry and ESPI have been used in a single system. This is one of the key achievements in this work. The object can continue to be tested using ESPI when it is no longer possible to resolve the holographic interference fringes.

A HOE recorded at 532 nm was reconstructed using a near infrared diode laser operating at 784 nm. There are two advantages using a laser diode in an ESPI system; one is phase shifting by modulating the source wavelength and the second is the compactness of the laser diode. ESPITest software was used to generate the phase map of the thick PVC pipe. Young's modulus of elasticity of the pipe was in good agreement with the manufacturer's value.

An even simpler ESPI system was implemented by using a reflection HOE. The out-of-plane deformation of a circular thin duraluminium plate of 1.5 mm thickness with a diameter of 46 mm pressurized uniformly by connecting to a vacuum chamber was measured using this system. A 5-frame technique was used to calculate the phase. The amplitudes and phases of the vibration modes of an object were mapped by using direct modulation of the laser diode current in a near infrared reflection HOE based ESPI system.

The final ESPI system only contains the following components: laser diode, reflection HOE and CCD camera. This system has the disadvantage of tedious chemical development because the HOE was recorded in silver halide. .

This drawback was overcome by using materials, which does not require chemical processing. A reflection HOE was recorded in the photopolymer at 532 nm. Vibration mode patterns of a thin circular sheet of aluminium of 4cm diameter attached to a paper cone loudspeaker 4 cm in diameter were identified.

The following objectives can be considered for future work on reflection photopolymer HOEs in an ESPI system.

A HOE could be fabricated using a 532 nm diode laser whose current can be modulated. Alternatively the material spectral sensitivity could be extended to record

the HOE at near infrared wavelength because at these wavelengths, powerful laser diodes are available which can be current modulated.

As a final summary, incorporating a HOE in the ESPI system has the following unique advantages

1. A simple and compact system
2. No need of expensive optical components.
3. Minimal alignment procedures.
4. Easy to match the intensities of object and reference beams.
5. Complexity involved with conventional phase shifting devices is eliminated by modulating the source wavelength.

Due to the above advantages this type of system is ideal for use in industrial applications.

Appendix - Publications

Journal Publications

- S. R. Guntaka, V. Toal, S. Martin, "Holographic and Electronic Speckle-Pattern Interferometry using a Photopolymer Recording Material," Strain, 40(2), 79-81, (2004).
- E. Mihaylova, B. Potelon, S. Reddy, V. Toal, C. Smith "Mechanical characterization of unplasticised polyvinyl chloride thick pipes by optical methods," Opt. Lasers. Engg, 41, 889-900, (2004).
- S. R. Guntaka, V. Toal, S. Martin, "Holographically recorded diffractive optical elements for holographic and electronic speckle pattern interferometry," Appl. Opt, 41, 7475-7479, (2002).

Conference Proceedings

- S. R. Guntaka, J. Raghavendra, V. Toal, I. Naydenova, S. Martin, S. Mintova, "A compact electronic speckle pattern interferometry using a photopolymer reflection holographic optical element," Proc. SPIE, 5856-18, Optical Metrology, Munich, 13-16 June, (2005).
- S. R. Guntaka, V. Toal, S. Martin, B. Bowe "Digital speckle pattern interferometry using wavelength modulated diode laser and holographic optical element (HOE)," International conference on laser applications & optical metrology-ICLAOM-2003, New Delhi, India. 1-4 December (2003).
- S. R. Guntaka, B. Bowe, V.Toal, S. Martin "Holographic optical elements for combined holographic and digital speckle pattern interferometry," Speckle Metrology 2003, Trondheim, Norway, Proc. SPIE vol. 4933, eds. K. Gastinger, O.J.Lokberg & S. Winther, 239-245,18-20 June (2003).

- S. R. Guntaka, V. Toal, S. Martin "Applications in holographic and electronic speckle pattern interferometry of a photopolymer recording material," Proc. SPIE vol. 4876, 984-993, (2002).

Poster Presentations

- S. R. Guntaka, V. Toal, S. Martin, "Holographically recorded photopolymer diffractive optical elements for holographic and electronic speckle pattern interferometry," IOP spring week end meeting, Physics research in Ireland, 11-13 April 2003.
- S. R. Guntaka, V. Toal, S. Martin, "Holographically recorded photopolymer optical elements for holographic and electronic speckle pattern interferometry," Postgraduate research conference, DIT, Dublin, Ireland, 9-11 September, 2003.